

“FEDERICO II” UNIVERSITY OF NAPLES



Ph.D. in Chemical Sciences – XXXII Cycle

**Regulation of biofilm development in
Gram-negative and Gram-positive bacteria:
New antimicrobial strategies**

Angela Di Somma

ADVISORS: Prof. Angela Duilio

EXAMINER: Prof. Angela Arciello

COORDINATOR: Prof. Angela Lombardi

Ai miei genitori...

Le mie radici...

Summary

Abstract	4
Chapter 1	8
Introduction	8
<i>1. A Brief History of Biofilms</i>	9
<i>1.1 Biofilm Matrix</i>	11
<i>1.2 Biofilm Formation in static and dynamic conditions</i>	13
<i>1.3 Biofilm and antimicrobial resistance</i>	17
<i>2. Antimicrobial Peptides: the Achilles' Heel of Antibiotic Resistance?</i>	21
<i>2.1 Classification and mechanism of action of AMPs against planktonic and biofilm bacteria</i>	24
<i>2.2 Synergy between conventional antibiotics and AMPs to enhance the efficacy against drug resistance strains</i>	29
Chapter 2	36
Differential proteomic approaches in study of biofilm formation under alkylation stress	36
Exposure to DNA-methylating agents impairs biofilm formation and invasion of eukaryotic cells via down regulation of the N-acetylneuraminase lyase NanA	38
<i>DIGE Experiment</i>	39
<i>Biological network and functional annotation analysis</i>	45
<i>Western blot analysis upon methylation stress</i>	46
<i>Expression levels of nanA gene in the presence and in the absence of MMS</i>	47

<i>Effect of methylation stress on biofilm formation and adhesion capability of nonpathogenic E. coli</i>	50
<i>Investigation of NanA role in E. coli biofilm formation</i>	52
<i>Effect of methylating agent on adhesion/invasion capabilities of pathogenic E.coli</i>	55
<i>Experimental section</i>	57
The bifunctional protein GlmU is a key factor in biofilm formation induced by alkylating stress in <i>Mycobacterium smegmatis</i>	67
<i>MMS effect on M. smegmatis cells</i>	68
<i>MMS on M. tuberculosis clinical strains</i>	70
<i>Comparative proteomic analysis</i>	72
<i>Biological networks and functional annotation analysis</i>	76
<i>Effect of methylation stress on biofilm formation in M. smegmatis</i>	77
<i>GlmU is essential for biofilm formation in M. smegmatis</i>	78
<i>GlmU inhibition and biofilm formation in M. smegmatis.</i>	84
<i>Experimental section</i>	86
Chapter 3	93
Functional proteomic approaches in the study of the mechanism of action of antimicrobial peptides	93
The antimicrobial peptide Temporin L impairs E. coli cell division by interacting with FtsZ and the divisome complex	95
<i>Effect of Temporin L on E. coli cell growth</i>	96
<i>Pull Down experiment</i>	97
<i>Docking experiments</i>	101
	2

<i>Binding experiments</i>	102
<i>Enzymatic assays</i>	103
<i>Optical microscopy and TEM analyses</i>	104
<i>Scattering Measurements</i>	106
<i>Experimental section</i>	109
A deeper understanding of Magainin-2 mechanism of action	118
<i>Pull-Down experiment</i>	119
<i>Magainin-2 – BamA molecular docking</i>	123
<i>Experimental section</i>	126
Investigation of the antimicrobial activity of Temporin-L and Magainin-2 on different pathogenic strains	129
<i>Determination of the Minimum Inhibit Concentration and Minimum Bactericidal Concentrations values on EUCAST reference strain of TL and Mag-2.</i>	130
<i>Transmission electron microscopy</i>	132
<i>Differential proteomic experiment</i>	134
<i>Experimental section</i>	148
Chapter 4	153
Discussion	153
Bibliography	159

Abstract

During evolution, microorganisms developed different forms and organizations according to needs. They can be found in planktonic form or as sessile aggregates anchored to biotic or abiotic surfaces. This phenotype is known as biofilm, an ensemble of microbial cells irreversibly associated to a surface and enclosed in an essentially self-produced matrix (1). This articulated and complex matrix organization can be called “house of biofilm cells” (2), because biofilm protects bacteria cells allowing them to survive in hostile environments. This condition significantly contributes to the onset of diseases, encouraging the adhesion to host cells and preventing access to antimicrobial agents.

Currently, any drug targeting crucial processes for bacterial life will inevitably lead to the development of resistant strains. On the other hand, the development of potential molecules designed to prevent biofilm formation and the identification of target proteins involved in biofilm formation will leave pathogens exposed to antibiotic treatments. In the search for new drugs, increasing attention has been devoted to AntiMicrobialPeptides (AMPs), small molecules composed of 10-100 amino acid residues produced by all organisms. AMPs are attractive candidates for the design of new antibiotics because of their specific characteristics and a low propensity for the development of resistance.

My PhD project focused on the investigation of biofilm formation under stress conditions and the definition of the mechanism of action of antimicrobial peptides.¶ Two enzymes deeply involved in biofilm formation in *E.coli* and *M. smeg*, the N-acetylneuraminate lyase NanA and the Bifunctional protein GlmU, respectively, were identified. When these enzymes are impaired by either inhibitors or genetic deletion,

biofilm formation decreases confirming their key role in the process. Since they are present in prokaryotic and not in eukaryotics they represent promising targets for the development of new drugs.

The possible development of AMPs as new antibiotics is strictly dependent on the definition of their lethal effect at the molecular level. Our attention has been focused on the elucidation of the mechanism of action of Temporin-L by functional proteomics approaches and the evaluation of its antibacterial and antibiofilm properties. The results showed that Temporin-L (TL) interacts with several proteins belonging to the divisome and elongasome complexes, impairing the natural formation of the septal peptidoglycan and affecting the cell division process. We demonstrated that Temporin-L is able to affect bacterial cell division by inhibiting FtsZ a protein involved in the crucial step of Z-ring formation at the beginning of the division process. Moreover, we studied the mechanism of action of Magainin-2, another peptide deriving from frog skin. Preliminary results showed that a large number of the overexpressed proteins in the presence of the peptide are involved in porin activity and protein insertion into the outer membrane. The antimicrobial activities of Temporin-L and Magainin-2 on the EUCAST panel for susceptibility testing have also been evaluated. Magainin-2 did not exhibit a significant effect on the bacterial strains, while TL showed a strong activity on *S. aureus*, *E. coli* and *S. pneumonia* showing different effects as revealed by TEM microscopy. A differential proteomic experiment has been performed on *S. aureus*, which suggests that TL treatment might stimulate the synthesis of proteins involved in membrane extroflexion

and this phenomenon seems to reduce bacterial pathogenesis as shown by the down regulation of proteins involved in pathogenesis and cell adhesion.

Chapter 1

Introduction

Microorganisms have the extraordinary ability to live in almost all environments and to protect themselves from external agents through sophisticated survival mechanisms. They can be found in planktonic form or, in specific conditions, they grow as sessile aggregates on surfaces in order to defend themselves against hostile environments through sophisticated survival mechanisms such as biofilms. Biofilms consist of an ensemble of microbial cells irreversibly associated to a surface and enclosed in an essentially self-produced matrix ⁽¹⁾. This articulated and complex matrix organization can metaphorically be called “house of biofilm cells” ⁽²⁾, because biofilm protects bacteria cells underneath allowing them to survive in hostile environments.

Although their global organization and form are almost similar in all bacteria, the chemical composition of biofilms depends on the microbial species and on the environment where it develops.

1. A Brief History of Biofilms

The first description of biofilms occurred a few centuries before their relevance to the persistence of disease was realized. In 1684, a Dutch scientist, Antonie van Leeuwenhoek, observed a dental plaque using his self-constructed primitive microscope and he saw "delicious animalcules" aggregated in the “scurf of the teeth” and from “particles scraped off his tongues” ⁽³⁾. During the early part of the 20th century many scientists reported that most bacteria were not free-floating but were

attached to surfaces, such as the bottom of lakes ⁽⁴⁾. Arthur Henrici wrote, for example, "It is quite evident that for the most part the water bacteria are not free floating organisms, but grow on submerged surfaces; they are of the benthos rather than the plancton." ⁽⁵⁾. In a 1940 issue of *Journal of Bacteriology*, H. Heukelekian and A. Heller wrote "Surfaces enable bacteria to develop in substrates otherwise too dilute for growth. Development takes place either as bacterial slime or colonial growth attached to surfaces." In other words, when bacteria of all sorts can congregate in a colony as they attach to some surface, they begin to exhibit different properties than they do as individuals floating in isolation in solution. Zobell reported that the growth of bacteria attached to the surface of bottles was increased compared to planktonic bacteria ⁽⁶⁾. Scientists began to realize that some sessile bacteria were directly related to disease in 1977 when an aggregation of *Pseudomonas aeruginosa* was found in sputum from the lungs of infected cystic fibrosis patients. In 1978, Clark reported that an important component of *Streptococcus mutans* biofilm, polysaccharide glycocalyx formed on teeth ⁽⁷⁾. The term 'biofilm' was formally introduced in 1978 by Costerton ⁽⁸⁾ that described biofilms formation, suggesting that their morphologies and composition depend on the constituent bacteria as well as the conditions under which the biofilm was formed.

1.1 Biofilm Matrix

Biofilms are ubiquitous in nature, on the hulls of ships, inside pipes where they cause severe problems and on medical devices, such as catheters or implant where usually they cause chronic infections that are difficult to treat. Matrix biofilm consists of one or more extracellular polysaccharides (EPS), DNA and proteins ⁽⁹⁾. Channels in the biofilm allow water, air and nutrients to reach any part of the structure.

The EPS provide a scaffold for other carbohydrates, proteins, nucleic acids and lipids to adhere. The components, structures and properties of the exopolysaccharides differ from one another and depend on growth conditions, medium, and substrates. In some forms of biofilm, mannose, galactose and glucose are the most abundant carbohydrates, followed by N-acetyl-glucosamine, galacturonic acid, arabinose, fucose, rhamnose and xylose as it occurs in biofilm matrix from *E. faecalis*, *S. aureus*, *K. pneumoniae*, *A. baumannii*, *P. aeruginosa* ⁽¹⁰⁾. Most EPS are not biofilm specific, but their production increases as a result of a stress response, such as colanic acid production in *Escherichia coli* ⁽¹¹⁾ and alginate synthesis in *P. aeruginosa* ⁽⁷⁾.

Different bacterial biofilms were used as model to study biofilm formation, for example *S.aureus* (Gram-positive bacteria) uses a polymer of N-acetyl glucosamine (PNAG) also referred to as polysaccharide intercellular adhesin (PIA), to form biofilms⁽¹²⁾; *P.Aeruginosa* (Gram-negative bacteria) produces three distinct EPS to form biofilm: alginate, Pel, and Psl. The importance and contribution of each EPS to the matrix depend on the strain ^(13;14). For example, alginate is produced by mucoid strains of *P.Aeruginosa* that are often isolated from lungs of cystic fibrosis patients.

The *pel* gene cluster, encoding a glucose-rich polymer termed PEL, is found in most of the strains analyzed to date, but its expression strongly varies among strains ⁽¹⁰⁾. Extracellular proteins are another important component of biofilm matrix and play diverse roles in biofilm formation and dissolution. In biofilm formation, some proteins are attached to cell surfaces and polysaccharides in order to help the biofilm formation and its three-dimensional architectures. One example are the Gbls proteins that link bacteria and EPS, amyloid proteins such as TasA and Fap that increase biofilm formation and resistance to disruption force, LecA, LecB, Bap and CdrA involved in biofilm formation and infection process and BslA that forms a layer on the surface of biofilms that confers hydrophobicity to the biofilm.

Other proteins are able to dissolve biofilm matrix through an enzymatic degradation of polysaccharides, proteins, and nucleic acids as glycosyl-hydrolase-dispersin B that hydrolyzes polysaccharides, proteases that target matrix proteins and DNases that degrade extracellular nucleic acids thus facilitating either biofilm matrix reorganization or biofilm degradation and dispersal ⁽¹⁵⁾.

Extracellular DNA (eDNA) is an important biofilm component that was recently discovered. It was initially described in *P.aeruginosa*, *Streptococcus mutans*, then in *Enterococcus faecalis* and *Staphylococcus aureus*. Based on the strain, eDNA is originated by autolysis of bacteria under control of quorum sensing system or under process similar to necrosis of eukaryotic cells ⁽¹⁶⁾. Recently, it was demonstrated that eDNA is not only originated from lysed cells but can also be actively secreted; in *Neisseria gonorrhoeae* biofilm a large amount of extracellular DNA is secreted by the

type IV secretion system (T4SS) directly into the medium and facilitates initial biofilm formation ⁽¹⁷⁾.

1.2 Biofilm Formation in static and dynamic conditions

Biofilm formation was originally thought to require three stages: attachment of cells to a solid substrate, followed by cell-cell adhesion, growth and detachment.

Recently, four stages of biofilm development have been proposed (see **Fig.1**):

- 1) Attachment. This phase is divided into two stages: a reversible adhesion that constitutes the first stage of biofilm formation and consists in the contact of microorganisms with surfaces (adsorption). In this stage, some weak interactions such as Van der Waals forces, electrostatic forces and hydrophobic interactions between the molecules present on the surface of microbial cells and those occurring on the surface are established. This is followed by an irreversible adhesion phase in which covalent interactions and production of exopolysaccharides by microorganisms take place.
- 2) Adhesion on surface. Production of extracellular polysaccharides by microorganisms or by cellular organelles such as pili and fimbriae that constituted a viscous layer (glycocalyx) to protect the initial micro-colonies, allowing their survival. Flagella are important in interactions between cells and surface; type IV pili-mediated twitching motilities enable attached cells to aggregate and form microcolonies.

- 3) Maturation and development of biofilm. The colony grows and acquires a mushroom-like architecture and bacteria undergo further adaptation to life in a biofilm. Two properties are often associated with surface-attached bacteria: increased synthesis of EPS and the development of antibiotic resistance. These features appear to create a protective environment and cause biofilms to be a tenacious clinical problem.
- 4) Detachment and return to the planktonic growth. The biofilm is capable to release part of its colonies into the environment and the cells may start entering another biofilm cycle in appropriate conditions to further colonize distant surfaces.

Each stage of the biofilm formation process depends on the microbial genera, species, characteristics of the attachment surface, environmental conditions and physiological status of the microorganism ⁽¹⁸⁾.

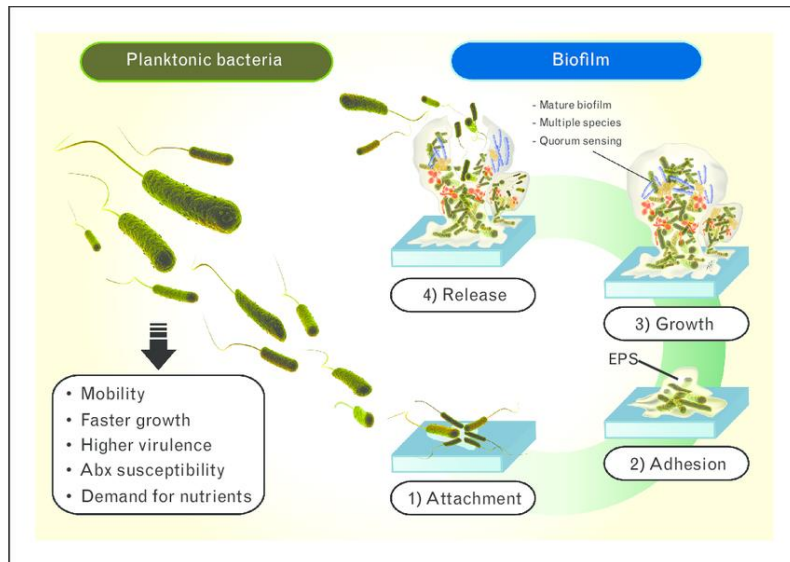


Figure 1. Four stages of biofilm formation.

Study of biofilm formation is normally performed in static condition, an artificial state motivated by the need to unveil the molecular and cellular mechanisms underlying biofilm formation. This approach has clarified many aspects of biofilm formation and allowed researchers to standardize experimental conditions in the absence of environmental complexities. However, static conditions are usually very far from reality because in the majority of cases, biofilm forms under fluid flow with the flow playing a significant role in the production, composition and architecture of the biofilm ⁽¹⁹⁾.

The ocean environment is a prime example of such dynamic conditions, as the ship hull is highly colonized by biofilm. On the other hand, in biomedical field, medical devices like catheter, prosthesis and heart valves are often attacked by biofilm due to the continuous flow of intracellular fluids originating frequent infections ⁽²⁰⁾.

The advent of new technologies, specially microfluidics, has rapidly attracted a growing interest as they might give the opportunity to investigate biological phenomena in real-life conditions as vasculature of living hosts, quiet river flows, medical devices etc. In microfluidic experiments, an unprecedented control might be exerted on flow conditions, providing identical and reproducible culture conditions, as well as real-time observations ⁽²¹⁾.

A fundamental parameter to be considered during biofilm formation in dynamic conditions is the hydrodynamic force. The fluid flow directly affects microbial interaction with surfaces for the presence of gradients in the fluid velocity, known as hydrodynamic shear. Shear, always generated near a solid surface, affect also the direction of cells swimming as recently demonstrated for *Bacillus subtilis* and *Pseudomonas aeruginosa*. In the absence of flow, the spatial distribution of cells in a dilute suspension was uniform, whereas in the presence of flow, a large decrease in cell concentration was observed at the centre of the channel (the region of low shear) with an accumulation occurring in the proximity of surfaces (the regions of high shear)⁽²²⁾.

In addition, fluid shear also influences physical properties of biofilms such as density and strength. A study by Liu & Tay found that biofilms grown at higher shear were smoother and denser than those grown at low shear ⁽²³⁾. Stoodley et al. reported

that *Desulfovibrio spp.* (an anaerobic sulphate-reducing bacteria) and *P. aeruginosa* biofilms grown at higher shear were more rigid and stronger than those grown at lower shear. It is still unclear whether the increased density and strength of biofilms exposed to higher shear are regulated at the genetic level or are determined by purely physical mechanisms but it appears that EPS are fundamental for both the structure and cohesive strength of biofilms ⁽²⁴⁾.

Zhang et al. designed a microfluidic gradient mixer to monitor biofilm development as a response to defined calcium and nitrate gradients. These studies demonstrate that the microfluidic device coupled with a microscope is an effective tool for *in situ* analysis and quantification of biofilm formation and transport in porous media at pore scale ⁽²⁵⁾.

1.3 Biofilm and antimicrobial resistance

Today, the increase and spread of antibiotic resistance among microorganisms (bacteria, fungi, viruses, and parasites) represents one of the greatest emergencies for human health worldwide ⁽²⁶⁾. The generation of bacteria resistance is based on difference genetic mechanisms developed to counteract the effect of the antibiotics thus allowing bacteria survival. This can be accomplished by either change in the genetic material or acquisition of new genetic material or combination of the two:

- ❖ Modification of the antibiotic. One of the most successful bacterial strategy to cope with the presence of antibiotics is to produce enzymes that inactivate

the drug by adding specific chemical groups as acetylation, phosphorylation or adenylation to the compound or by degradation of the molecule, as the β -lactamases, thus preventing the interaction between the antibiotic and its target(s) ⁽²⁷⁾.

- ❖ Modification of Antibiotic target. Bacteria can generate systems of drug secretion by producing protein excretion pumps as in *Escherichia coli* and *Neisseria gonorrhoeae* impairing the antibiotic from reaching its target. Alternatively, they may lack classic permeability systems as *Pseudomonas aeruginosa*, being constitutively resistant to various types of antibiotics ^(28,29).
- ❖ Limiting access to the antibiotic target. The biofilm matrix constitutes a stubborn source that protects bacteria from a variety of physical, chemical and biological stresses. Biofilms limit molecules diffusion, either by transport limitation (the inability of the antimicrobial molecules to spread through the polymer matrix) or inactivation of the antimicrobial molecule by the matrix material.

Nutrient and antimicrobial molecules must diffuse through the biofilm matrix before reaching microbial cells and entering the microorganisms. Therefore, bacteria growing beneath biofilms are more resistant to antibiotics representing a microbial threat for the onset of prolonged or chronic infections ^(30,31). The increased antimicrobial resistance of microorganisms in biofilms has long been investigated. Costerton et al. observed that when *P. aeruginosa* biofilm and planktonic cells were treated with tobramycin, planktonic cells could not survive a concentration greater

than 50 µg/mL, but biofilm cells could tolerate up to 1 mg/mL ⁽³²⁾. Similarly, Abee et al. reported that the effective inhibitory concentrations of two different disinfectants, benzalkonium chloride and the oxidizing agent sodium hypochlorite, on *S. aureus* biofilms were 50- and 600-times higher than planktonic cells, respectively ⁽³³⁾.

The reasons for increased antibiotic resistance by bacteria in biofilms are not yet fully understood. However, it is clear that many factors varying from organism to organism play an active role in this mechanism y:

a) The thick EPS matrix covers and protects bacteria that become more resistant to the clearance of host immune system, to adverse environmental conditions and to antimicrobial agents penetration;

b) Nutrient and oxygen depletion within the biofilm causes some bacteria to enter a stationary state, in which they are less sensitive to growth-dependent antimicrobial molecules;

c) Mutation or acquisition of a new genes via genetic exchange ⁽³⁴⁾. D'agostino et al. speculated that association of bacteria with a surface during biofilm formation caused a number of physiologic responses because of the repression or induction of genes. They demonstrated that a specific gene was induced by surface associated bacterial cells but this induction did not occur in liquid media. This finding would support the idea of a tactile receptor in bacteria and could have implications for a wide spectrum of phenotypic characteristics in biofilm bacteria, including traits that might confer resistance ⁽³⁵⁾.

Based on these characteristics, biofilm play crucial roles in human as well as non-human infections and represents the most important adaptive mechanism closely related to pathogenicity.

2. Antimicrobial Peptides: the Achilles' Heel of Antibiotic Resistance?

The rapid emergence of resistant bacteria is occurring worldwide, hampering the efficacy of antibiotics, which transformed medicine and saved millions of lives. Many decades after the first patients were treated with antibiotics, bacterial infections have again become a threat. The antibiotic resistance crisis has been attributed to the abuse and misuse of these drugs that created a selection pressure for bacteria to develop resistant strains ⁽³⁶⁾.

However, the development of new antibiotics has slowed down after its mid-20th century peak. Most of them were discovered by empirical screening of fermentation products and chemicals for bacterial growth inhibition. Although knowledge and technology have improved since then to ameliorate screening methods and to focus onto rationally target-based screening, only a few molecules have made the way to the clinic. An overview of the discovery of antibiotics and the onset of antibiotic resistance is shown in **Fig. 2**. Other new products have been derived from existing antibiotics, improving the spectrum of action, the ease of use, the safety or avoiding resistance mechanisms.

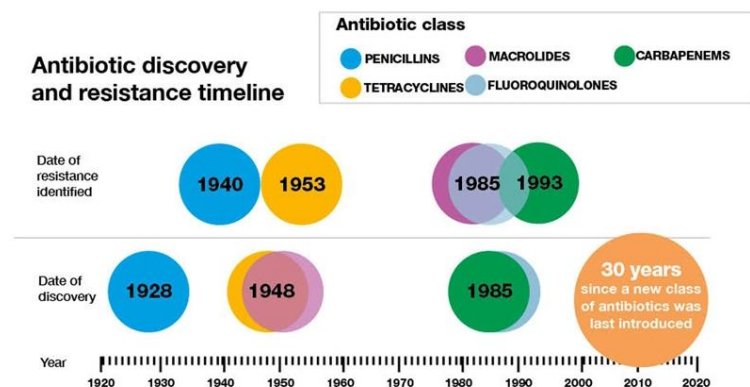


Figure 2. Timeline of modern antibiotic discovery and subsequent resistance.

The golden era of antibiotics is about to end and the development of new therapeutic agents to fight bacterial infections should be prioritized. The need for new antibiotics has stimulated interest in the development of AntiMicrobialPeptides (AMPs) as new possible human therapeutics, alone or in combination with current antibiotics in order to enhance antibacterial properties of common antibiotics while also possibly impairing resistance.

Antimicrobial peptides are small molecules composed of 10-100 amino acid residues produced by all organisms and constitute a class of compounds particularly interesting as new alternative therapeutic agents for their rapid bactericidal activity, their broad spectrum of action on both Gram-positive and Gram-negative bacteria, fungi and viruses, and their immunomodulatory activity.

The existence of AMPs has been known since 1939, when the first class of antimicrobial peptides, the gramicidins, was isolated, from *Bacillus brevis* ⁽³⁷⁾. Gramicidins were also the first AMP to be tested clinically but were found not suitable for systemic application due to their high toxicity ⁽³⁸⁾. To date, research in the field of AMP discovery is thriving and more than 2000 AMPs have been characterised according to the ADP3 database ⁽³⁹⁾.

Usually AMPs are synthesized as pro-forms before being processed to the active, mature peptides ⁽⁴⁰⁾. Most AMPs are cationic (cationic AMPs, CAMPs), show pronounced amphipathy and their structure includes both hydrophobic and hydrophilic moieties with a highly positive net charge (+2 to +9). They can be effective on a wide spectrum of microorganisms and can display powerful antimicrobial activities against antibiotic-resistant strains.

AMPs are produced by several tissues and cell types in a variety of plants and in animal species like insects, amphibians and vertebrate. Initially, they were extensively studied in insects and other non-vertebrate organisms; then a variety of AMPs were found in the secretion of amphibian skin and fully characterized ⁽⁴¹⁾. AMPs are secreted by amphibian skin in an holocrine manner, often in very high concentration, following a cellular stress or damage, in response to infection or environmental stress, acting as the first defense against the invasion of pathogens ⁽⁴²⁾. In this way animals as well as plants defend themselves against invading pathogenic microorganisms because AMPs rapidly kill various microbes without exerting toxicity against the host.

The importance of this class of molecules has made it an important object of study, leading to the production of thousands of synthetic variant peptides in addition to the natural occurring peptides.

2.1 Classification and mechanism of action of AMPs against planktonic and biofilm bacteria

According to the secondary structure, AMPs can be classified into 3 classes: i) α -helix peptides without cysteine residues; ii) β -sheet peptides with globular structure and disulfide bridges; iii) linear peptides ⁽⁴³⁾.

The modes of action of AMPs are not fully understood but most of the AMPs act at the level of bacterial cell membranes with a variety of mechanisms depending on the molecular properties of the peptides themselves and on the lipid composition of the membranes, different from those of common drugs, thus not allowing the development of resistance mechanisms ⁽⁴⁴⁾.

A further classification of AMPs was then performed according to their mechanism of action:

a) Membranolytic mechanism. AMPs can lead to bacterial cell lysis by three different processes of peptide-membrane interaction, barrel-stave, toroidal and carpet mechanisms ⁽⁴⁵⁾.

Barrel-stave and toroidal models are the simplest although fundamentally different models of membrane permeation by AMPs involving the formation of trans bilayer pores or channels through the membrane as shown in **Fig. 3A**. In the barrel stave pore model, AMPs interact laterally with one another to form a specific structure that is reminiscent of a membrane protein ion channel. In the toroidal pore model, specific peptide-peptide interactions are not present, but peptides affect the local curvature of the lipid bilayer in a cooperative manner such that a toroid of high curvature forms⁽⁴⁶⁾.

In addition to the pore models described above, in the carpet model AMPs do not insert into the membrane but accumulated on the surface inducing local weaknesses of the lipid bilayers into specific areas. This alteration leads to a local disturbance in the membrane stability, causing the formation of large cracks, leakage of cytoplasmic components, disruption of the membrane potential and, ultimately, degradation of the entire membrane⁽⁴⁷⁾.

b) Non-membranolytic mechanism. Recently, increasing evidence have been reported showing that AMPs may also interact with intracellular targets as shown in **Fig 3B**. Although the formation of ion channels, transmembrane pores and extensive membrane rupture eventually lead to microbial cells lysis, there is increasing speculation that these effects are not the only mechanisms of microbial killing. Some observations revealed that there are alternative sites of antimicrobial peptide activity targeting a number of intracellular processes by interacting with practically all classes of macromolecules. These mechanisms include inhibition of cell wall synthesis by alteration of the synthesis and polymerization of peptidoglycan layer; binding to DNA

and RNA or inhibition of DNA replication, SOS induction, chromosome segregation and failure of septation process; inhibition of protein synthesis after binding to ribosome or by interrupting the protein-folding pathway and activation of hydrolytic enzymes such as autolysins that cleave peptidoglycan ⁽⁴⁸⁻⁴⁹⁾.

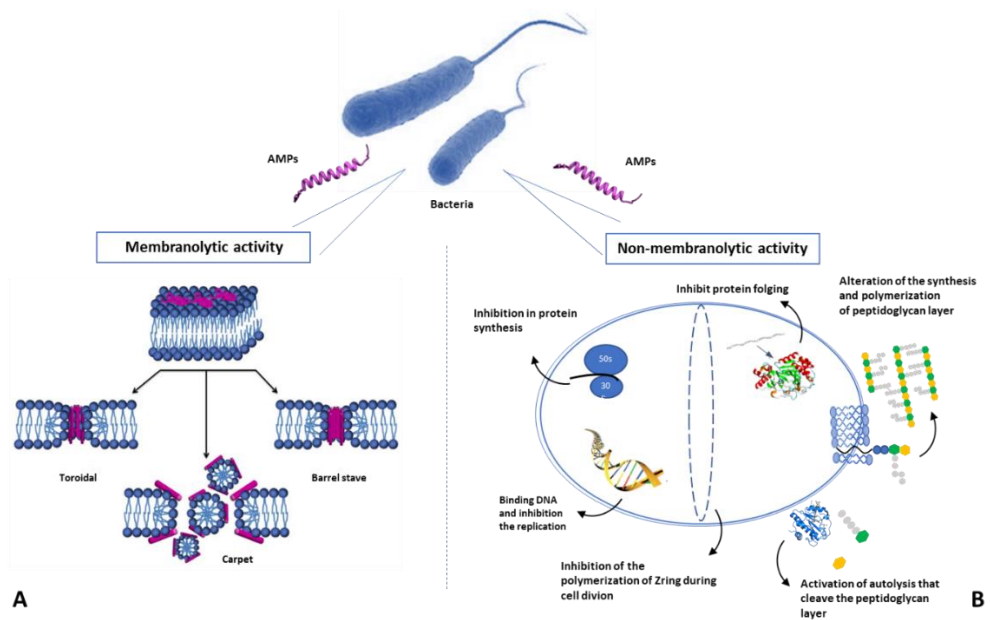


Figure 3. Mechanisms of action of AMPs: in panel A is show the destruction of membrane with tree different model. In panel B is show the intracellular target of AMPs that inhibit and altered cellular process.

In addition to the effects on planktonic bacteria, several anti-biofilm mechanisms of AMPs have also been reported in the literature. A PubMed survey on papers published since 2005 yielded 856 results using “antimicrobial peptides and biofilms” as keywords, while the number of the corresponding papers was only 107 in the previous decade ⁽⁵⁰⁾.

The main anti-biofilm mechanisms of AMPs reported so far (shown in **Fig.4**) are:

a) Disruption or degradation of the membrane potential of biofilm embedded cells.

According to the charge of biofilm EPS and the AMPs, the peptide may enter biofilm architecture and interact with cell membranes altering the membrane potential. In *P. aeruginosa* the AMP (CSA)-13 can quickly penetrate into biofilms and permeabilize bacterial cell membranes ⁽⁴⁵⁾. Membrane integrity is essential for the survival of bacteria irrespective of the metabolic stage of the cell. Thus, AMPs may have the ability to kill not only metabolically active cells but also slow growing, persisted cells and even bacteria released from the biofilm during the dispersal phase ⁽⁵⁰⁾.

b) Degradation of the polysaccharide and biofilm matrix.

AMPs were shown to alter and reduce the architecture of biofilm matrix by targeting polysaccharide intracellular adhesine (PIA) in *P.aeruginosa* or impairing the EPS production in *S.aureus*⁽⁵¹⁾. Moreover, the stimulation of specific enzymes expression (DNase I, α -amylase, and dispersin B) could inhibit the destruction and detachment of biofilm ⁽⁵²⁾.

c) Interruption of bacterial cell signalling systems.

Communication among bacterial cells within the biofilm and coordination of their behaviour occur through the secretion of particular signal molecules, an event known as Quorum Sensing (QS) ⁽⁵³⁾. AMPs can interfere with QS signalling thus preventing biofilm formation in different bacteria ⁽⁵⁰⁾, or can also interfere with the second messenger nucleotides signal, which is important in host-microbe interaction and biofilm formation ⁽⁵⁴⁾. A further mechanism consists in the increasing twitching motility in bacteria through stimulation of the expression of specific proteins involved in motility as type IV pili ⁽⁵¹⁾.

d) Downregulation of genes responsible for biofilm formation and transportation of adhesion proteins.

AMPs can inhibit genes controlling the mobility of extrachromosomal elements and the transport of adhesion proteins or the expression of genes encoding proteins involved in cell-to-surface and cell-to-cell interactions and biofilm formation such as ABC transporter and ATP-binding proteins.

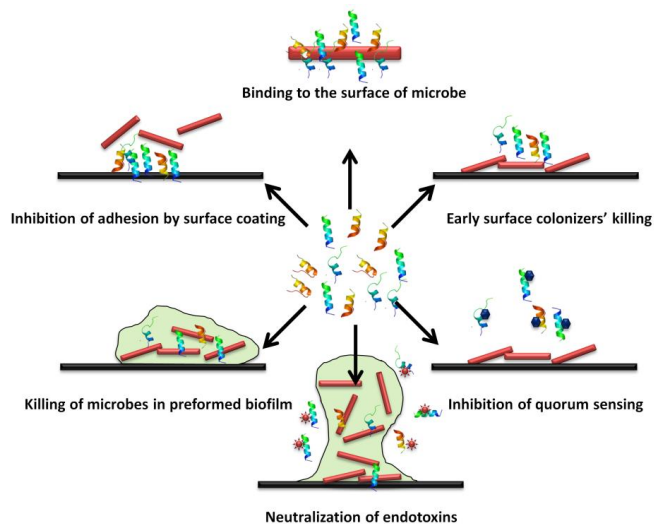


Figure 4 . AMPs can inhibit multiple steps independently including quorum sensing, inhibition of cell adhesion to the other cells and surfaces, activation of genes responsible for motility, down-regulation of genes responsible for production of EPS and causing direct bacterial killing.

2.2 Synergy between conventional antibiotics and AMPs to enhance the efficacy against drug resistance strains

The synergy of various AMPs with different antibiotics drug resistance strains has been reported in numerous papers ⁽⁵⁵⁾. Combined use of antimicrobial agents, in particular those with different targets, and antibiotics is a known strategy to overcome multiple drug resistance. Such synergy is believed to play a key role in fighting the

various resistance mechanisms evolved by pathogenic bacteria during their long coexistence with the immune system of the host. Therefore, the combined use of AMPs with other antimicrobials such as conventional antibiotics definitely has the potential to increase the effectiveness of both groups of compounds⁽⁵⁶⁾. The lantibiotic Nisin, a the polycyclic antibacterial peptide produced by *Lactococcus lactis* and occurring in nature in five variants originated by amino acidic substitutions, was shown to be active again *S.aureus* and *C. difficile*. Nisin has promising potential for clinical application with its Generally Regarded As Safe (GRAS) status and was approved by the World Health Organisation (WHO) and the US Federal Food and Drug Administration (FDA) for the use in food preservation.

Lewies et all. demonstrated that the Nisin Z variant was more selective against bacterial cells than Mellitin (a different natural AMPs) and has a great potential for the use as adjuvant in combination with conventional antibiotics as novobiocin for dermal applications towards *S. aureus* and *S. epidermidis* commonly found on the skin surface⁽⁵⁷⁾.

Recently Geitani et all. evaluated the synergy effects of four CAMPs in combination with colistin on clinical and laboratory *S.aureus* and *P.aeruginosa* strains. Results suggested that a great synergic effect occurred with two of this CAMPs, LL-37 and CAMA (cecropin (1–7)-melittin A(2–9) amide) on all tested strains. The negligible cytotoxic effects and their reduced tendency to develop resistance makes these AMPs interesting alternative drugs, exhibiting strong and rapid antibacterial activity either alone or in combination with antibiotics. CAMPs may then

represent potential future therapeutic solutions for infectious diseases associated to multi-resistant bacteria ⁽⁵⁸⁾.

2.3 Bacterial strategies of resistance to antimicrobial peptides

Microorganisms developed the ability to defend themselves against external agents triggering sophisticated resistance mechanisms. As the development of resistance to antimicrobial compounds represents one of the most serious problem for healthcare systems, the research of new antibacterial molecules is of the utmost importance. In this scenario, AMPs have often been suggested as potential novel antimicrobial compounds for their commonly bactericidal mode of action that makes them potential candidates.

However, AMPs therapeutic potential might be limited by the observation that they constitute an essential part of the innate immune system of humans and many other organisms. Therefore, during their co-evolution with humans bacteria have developed some AMPs resistance mechanisms ⁽⁵⁹⁾.

The mechanisms of bacterial resistance against AMPs may be grouped into three classes as illustrated in **Fig. 5**:

a) Extracellular proteins. Secreted bacterial proteins, such as proteases, are the first bacterial defence mechanisms encountered by AMPs when interacting with bacteria.

Proteolytic degradation of AMPs by extracellular enzymes represents a simple, yet effective mechanism of AMPs resistance. *Streptococci* produced metalloproteases such as SepA or SpeB that degrade or fragment many host AMPs, including LL-37 and beta-defensins ^(60,61). One of the most intensively studied group of proteases in Gram-negative bacteria is the omptin family, a group of aspartate proteases found in the enterobacterial outer membrane (OM). OmpT in *E. coli*, PgtE in *S. enterica* serotype and *S. typhimurium* and Pla in *Y. pestis* are representative members of this class of proteases and have been demonstrated to cleave AMPs including LL-37, the homologous murine cathelicidin-related antimicrobial peptide (CRAMP) and protamine ⁽⁴⁰⁾.

b) Surface modification. Cationic AMPs are attracted by the negatively charged bacteria outer membrane or cell wall, but these, in turn, can reduce their surface charge and increase surface density to limit peptide adhesion. Since Gram-negative and Gram-positive bacteria have different cell envelope structures, they developed different strategies to reduce peptide adhesion. In Gram-positive bacteria, such as *Staphylococcus*, *Streptococcus* and *Clostridium*, D-alanylation of wall teichoic and lipoteichoic acids typically mediated by the products of the *dlt* operon, reduces the net negative charge and confers relative protection against AMPs ⁽⁶²⁻⁶³⁾. Similar to Gram-positive, Gram-negative bacteria can regulate their surface charge by modification of the lipopolysaccharides, which are part of their outer membrane, by reduced phosphorylation, sugar substitution or lipid addition reducing the fluidity of the outer

membrane ⁽⁶⁴⁾. As an example, in *P. aeruginosa* and *S. typhimurium* an aminoarabinose is linked to a phosphate group in lipid A ⁽⁶⁵⁾.

c) Efflux pump. Even when AMPs have already entered the cytoplasmic membrane, bacteria can still remove them through specific efflux pumps, similar to those used to resist traditional antibiotics. A large number of AMP-exporting efflux pumps in bacteria have been described including ATP-binding cassette (ABC) transporters, specific designed for the secretion of newly synthesized AMPs and the nodulation cell-division efflux pumps ⁽⁴⁶⁾. Recently, Cheung et al., have demonstrated that the *Staphylococcus aureus* Pmt ABC transporter is able to defend bacteria from the lethal effect of several human AMPs and to survive elimination by human neutrophils ⁽⁵⁹⁾

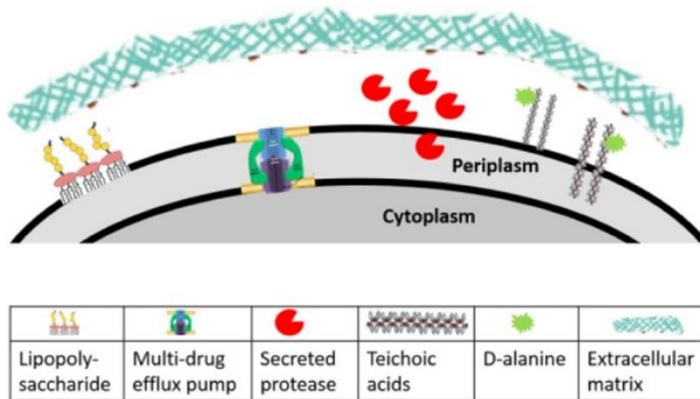


Figure 5. The mechanisms of bacterial resistance against AMPs. Bacterial resistance strategy against antimicrobial peptides were devise into secretion extracellular protein, surface modification as addition of lipopolysaccharide, teichoic acids and D-alanine end efflux pump.

2.4 The skin frog peptide: Temporin L and Magainin-2

The vast majority of AMPs are isolated from frog skin. They are synthesized and stored in the granular glands of the dermal layer of the skin and following stress or injuries are released on the skin surface. AMPs confer a strong advantage against different microorganisms (bacteria, protozoa, yeasts, and fungi) ⁽⁶⁶⁾. Normally, there are no conserved structural motifs among AMPs that can be responsible for activity although more than 50% are cationic. The AMPs used in this PhD thesis are Temporin L (TL) and Magainin-2, whose primary and secondary structures are shown in **Fig 6A and 6B**.

TL, a natural peptide secreted from the skin of the European frog *Rana temporaria*, is active against Gram-positive and Gram-negative bacteria. TL is a polycationic peptide with a positive net charge of +3 and its amino acid sequence consists of 13 residues. CD studies demonstrated that in aqueous buffer TL does not show a regular conformation while the peptide assumes an α -helix conformation when transferred into a membrane-like environment such as SDS and DPC. NMR studies revealed that TL assembles into an amphipathic antiparallel dimer in the presence of *E. coli* LPS and the helical structure is maintained upon interaction with *E. coli* cells ^(67,68).

Magainin-2 has been isolated from the skin of the African clawed frog *Xenopus laevis*, and belongs to the class of magainins. Magainin-2 is a polycationic peptide with

a positive net charge of +3, due to the presence of lysine and arginine residues and its amino acid sequence consists of 23 residues.

Magainin-2 in aqueous solution shows a disordered structure, as occurs for TL, whereas in the presence of SDS micelles or *E.coli* cells assumes an amphipathic α -helical conformation with a slight bend centered at residues 12 and 13⁽⁶⁹⁾.

A

Temporin-L	FVQWFSKFLGRIL
Magainin-2	GIGKFLHSAKKFGKAFVGEIMNS

B

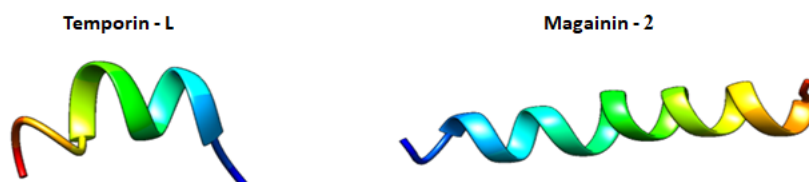


Figure 6 (A) Sequences of the peptides used in this study. (B) NMR structure of Temporin L in SDS micelles (PDB code 6GS5) and Magainin-2 in DPC micelles (PDB code 2MAG). The images were generated using the program CHIMERA.

Chapter 2

Differential proteomic approaches in study of biofilm formation under alkylation stress

The new era of eukariotics and procariotics genomes sequencing allowed the study of biological processes with new advanced dynamic approaches, in contrast to the static concept of genome. Proteins have a dynamic behaviour as their expression greatly changes following different stimuli, both external or internal to the cell. The number of proteins present in a given moment in the cell also changes according to the type of cell, wild type or mutated.

In this scenario, the differential proteomics approaches were focused on the study of changes in the expression of the proteome of a biological system, in response to specific stimuli or simply during the development of the system in different conditions.

Caterino et al. analysed the proteome of Methylmalonic acidemia (MMA) using liver specimens from donors and MMA patients that received elective liver or combined liver-kidney transplantation to identify deregulated proteins. Using differential proteomics they identified protein targets for new therapies designed to alleviate the symptoms of the disease ⁽⁷⁰⁾.

Moreover, Vertommer et al. characterize the role of chaperone SarA in *Escherichia coli* during the folding and insertion of β -barrel protein in Outer Membrane, comparison wild type and *surA* deletion mutant ⁽⁷¹⁾.

A large number of reports confirmed the great importance of the differential proteomics methodologies in the study of proteins expression levels whose impact in the biomedical field cannot be overestimated.

Exposure to DNA-methylating agents impairs biofilm formation
and invasion of eukaryotic cells via down regulation of the N-
acetylneuraminate lyase NanA

The work presented in this chapter has been published as:

Di Pasquale P, Caterino M, Di Somma A, Squillace M, Rossi E, Landini P, Iebba V, Schippa S, Papa S, Selan L, Artini M, Palamara A.T., and Duilio A.

“Exposure of E. coli to DNA-Methylating Agents Impairs Biofilm Formation and Invasion of Eukaryotic Cells via Down Regulation of the N-Acetylneuraminate Lyase NanA”.

Front Microbiol. 2016. doi: 10.3389/fmicb.2016.0014

DIGE Experiment

The global effect of alkylating stress in *E.coli* was investigated by a differential proteomic approach using the Differential in Gel Electrophoresis procedure (DIGE). Bacterial cells were grown in four replicates and each culture was divided into two aliquots, one of them was treated with 0.04% MMS and the other one was kept untreated and used as control. Bacterial cells were lysates from MMS treated and negative control and the protein extracts submitted to bidimensional electrophoresis using a 3-10 pH gradient. The relative quantitative analysis was performed so that only proteins up or down expressed in all four treated cell samples versus control were considered (**Fig 7A**). The corresponding preparative gel is reported in **Fig7B**, where differently expressed proteins in the presence of MMS are labeled and were submitted to the identification procedure.

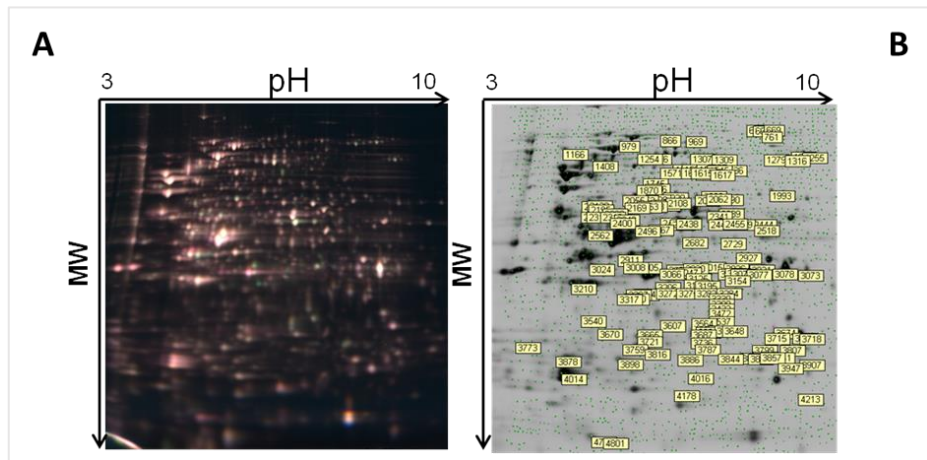


Figure 7. Differential proteomic analysis of MMS treated MV1161 *E.coli*. (A) Differential in Gel Electrophoresis (DIGE) of protein extracts from MV1161 *E.coli* in the absence and in the presence of MMS. Super imposed images of the individual fluorescent scans of analytical gels for the four analysed biological replicates. Adapted with permission from Di Pasquale et al 2016.

The spots of interest were picked, *in situ* hydrolysed with trypsin and the resulting peptide mixtures analysed by LC-MS/MS. Mass spectral data were used to search a non-redundant protein database by Mascot software. A total of 69 differentially expressed proteins were identified in MMS treated *E.coli* cells compared to controls, 61 down- and 8 up-regulated, and are listed in **Table1**. For each protein, the fold change, spot number, p-value, protein description, gene official symbol and Swiss-Prot code are reported.

Fold Change (2^x)	n SPOT	p-value	Protein description	Gene Symbol	Swiss Prot
METABOLIC PATHWAYS					
-2.76	1545	0.0018	Transketolase 2	tktB	P33570
-1.82	1530	0.0049	Fumarate reductase flavoprotein subunit	frdA	P00363
-1.73	2441	0.0042	Bifunctional protein GlmU	glmU	P0ACC7
-1.67	3025	0.0023	Dihydroorotase	pyrC	P05020
-1.62	3317	0.0068	Cytidine deaminase	cdd	P0ABF6
-1.62	2006	0.0032	Fumarate hydratase class I, anaerobic	fumB	P14407
-1.56	2314	0.0039	aspartate ammonia-lyase	aspA	P0AC38
-1.53	3125	0.0028	PTS system mannose-specific EIIAB component	manX	P69797
-1.53	2041	0.0014	Bifunctional purine biosynthesis protein PurH	purH	P15639
-1.53	3125	0.0028	L-threonine dehydratase catabolic TdcB	tdcB	P0AGF6
-1.51	2562	0.0061	Thymidine phosphorylase	deoA	P07650
-1.39	3005	0.0041	Aspartate-ammonia ligase	asnA	P00963
-1.30	1408	0.0029	Catalase-peroxidase	katG	P13029
-1.30	2055	0.0057	3-octaprenyl-4-hydroxybenzoate carboxy-lyase	ubiD	P0AAB4
-1.30	2055	0.0057	Malate synthase A	aceB	P08997
-1.26	3070	0.0094	UDP-glucose 4-epimerase	galE	P09147
-1.25	2348	0.00189	Glycerol kinase	glpK	P0A6F3
-1.21	2467	0.0089	Bifunctional protein FolC	folC	P08192
Fold Change (2^x)	n SPOT	p-value	Protein description	Gene Symbol	Swiss Prot
-1.15	3787	0.0027	2,3-bisphosphoglycerate-dependent phosphoglycerate mutase	gpmA	P62707

+1.09	2400	0.0063	Glutamate decarboxylase beta	gadB	P69910
+1.09	2400	0.0063	Bifunctional protein HldE	hldE	P76658
-1.52	2050	0.00081	Phosphoenolpyruvate carboxykinase	pck	P22259
-1.40	1870	0.0015	Trehalose-6-phosphate hydrolase	treC	P28904
-1.79	3026	0.0012	Galactitol-1-phosphate dehydrogenase	gatD	P0A9S4
-1.65	2131	0.0032	2,3-bisphosphoglycerate-independent phosphoglycerate mutase	gpml	P37689
-1.30	2055	0.0057	Phosphoenolpyruvate carboxykinase [ATP]	pckA	P22259
+1.37	2105	0.0091	6-phospho-beta-glucosidase A	bglA	P24240

GLYCOLYSIS/GLUCONEOGENESIS

-1.65	2131	0.0032	2,3-bisphosphoglycerate-independent phosphoglycerate mutase	gpml	P37689
-1.52	2050	0.00081	Phosphoenolpyruvate carboxykinase	pck	P22259
-1.51	2562	0.0061	6-phosphogluconate dehydrogenase	gnd	P00350
-1.48	3030	0.0068	Aldehyde reductase, NADPH-dependent	yqhD	Q46856
-1.41	3078	0.0024	Glyceraldehyde-3-phosphate dehydrogenase A	gapA	P0A9B2
-1.30	1408	0.0029	Dihydrolipoyllysine-residue acetyltransferase component of pyruvate dehydrogenase complex	aceF	P06959
-1.21	2467	0.0089	D-tagatose-1,6-bisphosphate aldolase subunit GatZ	gatZ	POC8J8
-1.20	3721	0.0024	Deoxyribose-phosphate aldolase	deoC	P0A6L0
-1.15	3787	0.0027	2,3-bisphosphoglycerate-dependent phosphoglycerate mutase	gpmA	P62707
-1.12	2062	0.0069	Pyruvate kinase I	pykF	P0AD61
+1.24	2169	0.0053	Phosphoglucomutase	pgm	P36938

Fold Change (2^x)	n SPOT	p-value	Protein description	Gene Symbol	Swiss Prot
AMINOACYL-tRNA BIOSYNTHESIS					
-1.69	3047	0.0044	Phenylalanine tRNA synthetase, alpha subunit	pheS	P08312
-1.27	1307	0.0004	Threonine-tRNA ligase	thrS	POA8M3
-1.19	3031	0.0071	tRNA-dihydrouridine synthase A	dusA	P32695
-1.17	2425	0.005	Histidine-tRNA ligase	hisS	P60906
+1.20	1571	0.0017	Methionine-tRNA ligase	metG	P00959
MICROBIAL METABOLISM IN DIVERSE ENVIRONMENTS					
-2.76	1545	0.0018	Transketolase 2	tktB	P33570
-1.85	761	0.0062	Formate dehydrogenase, nitrate-inducible, major subunit	fdnG	P24183
-1.56	2314	0.0039	Aldehyde dehydrogenase A, NAD-linked	aldA	P2555
BIOSYNTHESIS OF SECONDARY METABOLITES					
-5.78	3272	0.00024	N-acetylneuraminate lyase	nanA	POA6L4
-1.68	3674	0.000046	Glucosamine-6-phosphate deaminase	nagB	POA760
-1.72	2441	0.0042	Tryptophanase	tnaA	POA853
-1.30	1408	0.0029	Polyribonucleotide nucleotidyltransferase	pnp	P05055
+1.09	2400	0.0063	Glutamate decarboxylase beta	gadB	P69910
GLYCEROPHOSPHOLIPID METABOLISM					
-1.65	2131	0.0032	Aerobic glycerol-3-phosphate dehydrogenase	glpD	P13035
-1.49	1963	0.0055	Anaerobic glycerol-3-phosphate dehydrogenase subunit A	glpA	POA9C0

TRANSPORTERS					
-1.67	3025	0.0023	Oligopeptide transport ATP-binding protein OppD	oppD	P76027
-1.12	2062	0.0069	Ribose import ATP-binding protein RbsA	rbsA	P04983
+1.37	2105	0.0091	Potassium transporter peripheral membrane protein	trkA	P0AGI8
BACTERIAL CHEMOTAXIS AND MOTILITY					
-1.32	3008	0.0066	Flagellar motor switch protein FliM	fliM	P06974
OTHER					
-1.62	3317	0.0068	Probable deferrochelataase/peroxidase YfeX	yfeX	P76536
-1.53	2041	0.0014	Ribonuclease G	rng	P0A9J0
-1.53	2041	0.0014	Transcriptional regulatory protein TyrR	tyrR	P07604
-1.38	3005	0.0041	Uncharacterized oxidoreductase YdgJ	ydgJ	P77376
-1.32	3008	0.0066	Aminomethyltransferase	gcvT	P27248
-1.32	3206	0.0033	Probable acrylyl-CoA reductase AcuI	acuI	P26646
-1.30	2055	0.0057	Uncharacterized sulfatase YdeN	ydeN	P77318
-1.26	3073	0.0072	HTH-type transcriptional regulator CysB	cysB	P0A9F3
-1.26	979	0.0049	Elongation factor G	fusA	P0A6M8
-1.26	979	0.0049	Chaperone protein ClpB	clpB	P63284
+1.51	2148	0.0031	Alkyl hydroperoxide reductase	ahpF	Q8XBT4

Table 1. Differentially expressed proteins. Adapted with permission from Di Pasquale et al 2016.

Biological network and functional annotation analysis

The network distributions of the 69 differentially expressed proteins were explored using the STRING software. Stronger associations are represented by thicker lines (Fig 8). The top-ranked networks were in Metabolic Pathways with a p -value of $3.45E-10$, Glycolysis/Gluconeogenesis (p -value = $5.87E-8$) and Microbial metabolism in diverse environments (p -value = $2.11E-7$).

Interestingly, most of the identified proteins belonging to metabolic processes were down regulated, as expected by the inhibition of cell growth by methylating agents, as previously observed⁽⁷²⁾. Among these, the most intriguing result in the presence of MMS was the strong decrease in the expression of the N-acetylneuraminase lyase (NanA), an enzyme involved in sialic acid metabolism. The expression level of NanA protein was reduced by a factor of 2^6 , which corresponds to about 60 times decrease in protein concentration.

NanA is the first enzyme of the canonical pathway of sialic acid catabolism including *nanA*, *nanK*, *nanE*, *nagA* and *nagB* and catalyzes the aldolic cleavage of N-acetylneuraminic acid (sialic acid) to form pyruvate and N-acetyl-D-mannosamine⁽⁷³⁾. Since sialic acid was widely recognized as a signaling molecule in biofilm formation and cell-cell interactions, we then investigated the biological role of NanA in biofilm formation.

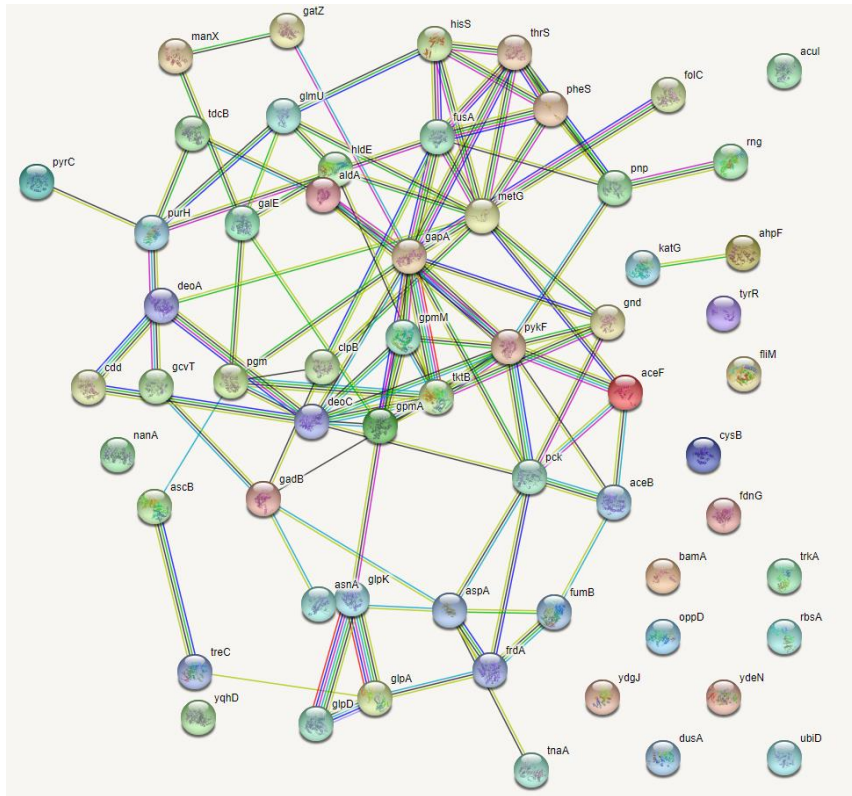


Figure 8. The network distribution of the 61 differentially expressed proteins according to STRING software. Adapted with permission from Di Pasquale et al 2016.

Western blot analysis upon methylation stress

Proteomic data were independently confirmed by western blot analysis.

Recombinant NanA protein fused with N-terminal His tag was cloned and produced in *E.coli* and purified by metal affinity chromatography. The purified of recombinant protein was analyzed by SDS-PAGE (12,5%). Its primary structure was characterized by MALDI mapping, the secondary structure by Circular Dichroism analysis and the quaternary structure by gel filtration. (data not shown).

Specific anti NanA antibodies were then produced in rabbit, tested using different amounts of *E.coli* extracts and used to assess the expression of NanA under methylation stress conditions. Figure 9A shows the western blot analysis of protein extracts from *E.coli* grown in the absence and in the presence of 0.04% MMS. Protein content was normalis ed by using the Maltose Binding Proteins that was demonstrated to be unaffected by methylation stress by DIGE analysis. A strong decrease in the amount of NanA was clearly detected upon methylation stress, thus confirming proteomic results.

Expression levels of nanA gene in the presence and in the absence of MMS

The significant down regulation of NanA was further investigated at mRNA level to assess whether a transcriptional or translational control was elicited by methylation stress leading to the low expression of the protein. Total RNA was extracted from 0.04%. MMS treated and untreated *E.coli* cells. The RNA quality was verified by denaturing agarose electrophoresis showing the presence of the three typical bacterial

bands (23S, 16S and 5S) and by evaluating the absorbance ratio A260/A280 that was included in the range 2.1 and 2.3 demonstrating a high-quality product.

Total RNA was reverse transcribed to obtain cDNA. Real time PCR assays were carried out to detect *nanA* gene expression levels in both MMS treated and untreated *E.coli* cells. Melting point curves displayed a single peak and any amplification of non-specific targets or primer dimers was not observed demonstrating the specificity of amplification. *rpoA* was used as housekeeping gene to normalize the threshold cycle values (Ct). The relative difference of *nanA* expression levels between treated and untreated conditions was calculated by using $2^{-\Delta\Delta Ct}$ method. Analyses were performed in triplicate.

The results of PCR amplification are shown in Fig. 9B. Transcription of *nanA* gene was unaffected by MMS treatment showing a RNA amount almost similar to the untreated cells being the difference shown in Fig. 9B not significant. Altogether these data suggested the occurrence of a negative translational control of *nanA* exerted by an unknown cellular mechanism in the presence of methylation stress.

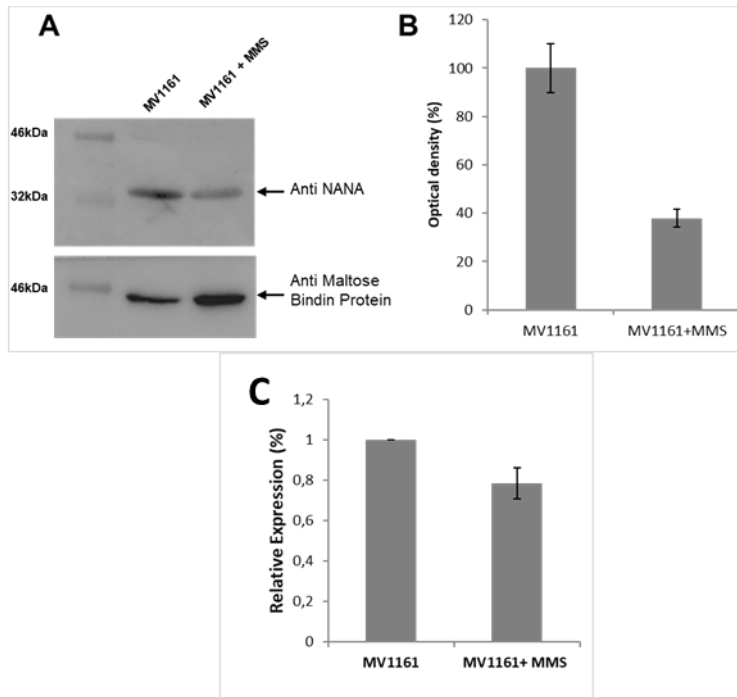


Figure 9. Effect of fmethylation stress on expression levels of NanA. (A) Western blot analysis of protein extracts from *E. coli* in the absence and in the presence of 0.04% MMS. (B) Densitometric analysis of the immunoblot. Protein content was normalized using the Maltose Binding Protein. Data are expressed as the percentage of relative expression and represent the mean \pm SD of three replicates. (C) *nanA* gene expression levels measured by real-time PCR assays in both MMS treated and untreated *E. coli* cells. Data are expressed as the percentage of relative expression and represent the mean \pm SD of three replicates. Adapted with permission from Di Pasquale et al 2016.

Effect of methylation stress on biofilm formation and adhesion capability of nonpathogenic *E. coli*

Sialic acid was reported to play a pivotal role in molecular recognition and, particularly in sialidase negative bacteria like *E.coli*, this amino sugar and its metabolites could be a key signal in cell-cell interactions (Sohanpal, BK PNAS 2004). A correlation between sialic acid availability, biofilm formation and invasion of host cells in pathogenic bacteria has already been reported ⁽⁷⁴⁾.

On this ground, we explored the possibility that decreasing NanA levels upon exposure to methylating agents might also affect these processes in *E.coli*. Thus, we performed *in vitro* and *in vivo* assays addressed to evaluate biofilm formation and adhesion abilities of a non-pathogenic *E.coli* strain.

Cells were then grown in LB medium supplemented with 1% glucose, which promotes biofilm formation by ca. 5-fold (data not shown), either in the presence or in the absence of 0.04% MMS. As reported in **Fig. 10A**, methylation stress decreased biofilm formation by about 60% compared to negative control.

Since biofilm mechanisms are usually associated to cellular adhesion/invasion processes, we tested the effect of methylation stress on the capabilities of MV1161 to adhere to human HeLa cells. Following 0.04% MMS treatment, *E.coli* cells were subcultured and several different dilutions added to HeLa cells in order to establish the best bacterial/eukaryotic cells ratio. Analyses were performed in triplicate.

Data obtained for one of the three cellular dilutions are reported in **Fig. 10B** showing that *E.coli* adhesion on HeLa cells was drastically decreased in the presence

of 0.04% MMS, demonstrating a functional correlation between methylation stress and adhesive cellular properties.

Since NanA was heavily downregulated following MMS treatment, these data might suggest a possible involvement of this enzyme in the bacterial cohesive properties affecting the biological processes leading to biofilm formation.

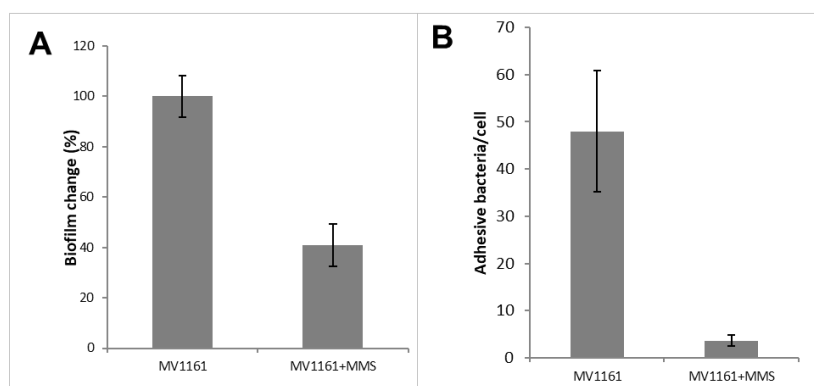


Figure 10. Biofilm formation and adhesion capability of MMS treated non pathogenic E.coli. (A) Biofilm formation of non pathogenic E.coli in the presence of MMS. Data are expressed as the percentage of crystal violet absorbance and represent the average of three independent experiments. **(B)** Adhesion capability of non-pathogenic E.coli to HeLa cells in the presence and in the absence of MMS. Data represent the average of three independent experiments. Adapted with permission from Di Pasquale et al 2016.

Investigation of NanA role in *E. coli* biofilm formation

To investigate whether the decrease in biofilm formation following MMS treatment was caused by loss of NanA expression, in collaboration with Professor Paolo Landini University “La Sapienza” in Roma, a null mutant was constructed.

Biofilm formation experiments were performed on a $\Delta nanA$ mutant in comparison with both untreated and MMS treated MV1161 strain as control.

As reported in **Fig. 11A** $\Delta nanA$ showed a phenotype nearly superimposable to MV1161 *E. coli* under methylation stress conditions.

Next, we checked the effect of MMS on the residual biofilm formation in the *nanA* mutant strain to investigate whether the decrease in adhesion in the MMS treated cells and in the *nanA* mutant strain are both due to loss of NanA. Biofilm formation experiments were performed on $\Delta nanA$ mutant under methylation stress conditions in comparison with untreated MV1161 strain as control. Treatment with MMS did not provide further decrease in the adhesive capabilities of the *nanA* mutant strain as shown in **Fig. 11B**, indicating that the two effects were not additive.

The biological implication of the lyase in biofilm formation was further supported by complementation assays. The $\Delta nanA$ mutant was then complemented with a plasmid vector bearing the *nanA* gene and the *nanA* restored *E. coli* strain was used in biofilm assays. The re-integration of the lyase NanA restored the ability of the mutant strain to adhere to abiotic surface, as biofilm formation was greatly increased in the complemented strain (**Fig. 11C**).

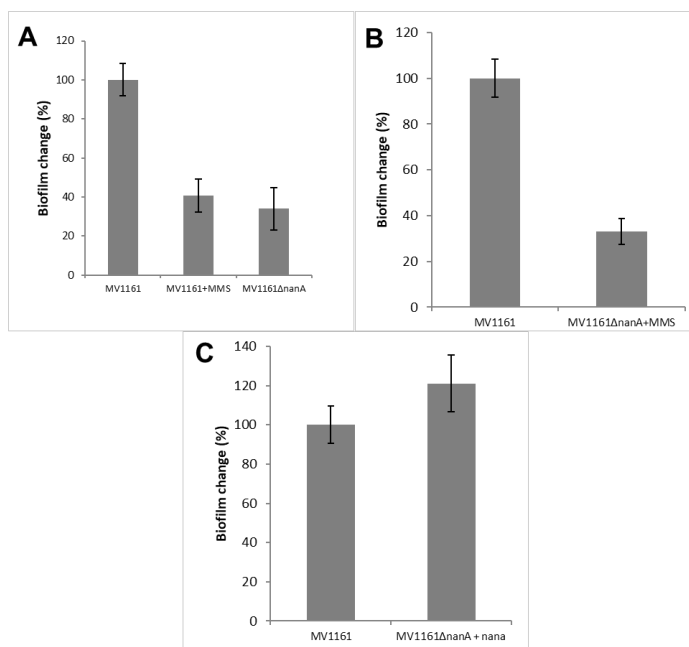


Figure 11. Biofilm formation in different condition. A) Biofilm formation of: MV1161 E.coli strain, MV1161 E.coli strain in presence of 0.04% MMS and MV1161 Δ nanA mutant strain. **B)** Biofilm formation of MV1161 E.coli strain and MV1161 Δ nanA mutant strain in presence of 0.04% MMS **C)** Biofilm formation of MV1161 E.coli strain and MV1161 Δ nanA mutant strain complemented with a nanA gene. Adapted with permission from Di Pasquale et al 2016.

NanA fundamental role in biofilm formation was finally assessed by performing biofilm experiments in the presence of a specific sialidase inhibitor, N-Acetyl-2,3-dehydro-2-deoxyneuraminic acid (DANA), a sialic acid analogue that specifically

inhibits neuraminidase activity. Biofilm formation was performed in the presence of increasing DANA concentrations ranging from 1 to 100 $\mu\text{g/mL}$. **Fig. 12** shows biofilm production of *E.coli* MV1161 strain in the absence and in the presence of 50 $\mu\text{g/mL}$ DANA inhibitor. Inhibition of sialidase activity greatly affected *E.coli* adhesive properties as demonstrated by the clear decrease in biofilm production to a level very similar to that observed following MMS incubation.

These results confirmed the hypothesis that the impairment of biofilm formation under methylation stress is mediated by downregulation of NanA and pointed out to the importance of the sialidase catalytic activity to promote/prevent cell-cell interactions.

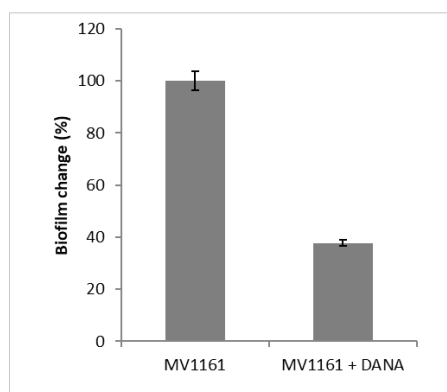


Figure 12. Biofilm formation of MV1161 *E.coli* strain and MV1161 *E.coli* strain in the presence of DANA inhibitor. Adapted with permission from Di Pasquale et al 2016.

Effect of methylating agent on adhesion/invasion capabilities of pathogenic *E.coli*

In order to verify if MMS could affect adhesive and invasive properties of a pathogenic *E.coli*, we used the LF82 strain, a prototype of the adherent-invasive *E.coli* (AIEC) pathogen⁽⁷⁵⁾. This strain showed strong adhesive and invasive capabilities in intestinal cells and prolonged intracellular survival in macrophages, leading to enhanced pro-inflammatory cytokines release⁽⁷⁶⁾.

As shown in **Fig. 13A**, upon 0.04% MMS treatment, LF82 strain showed a decreased steady state level in the growth curve ($OD_{600_{LF82}}=4.7$ vs $OD_{600_{LF82+MMS}}=1.6$), a different mid-point ($t_{mid-point_{LF82}}=5.9h$ vs $t_{mid-point_{LF82+MMS}}=3.8h$), and a diminished intrinsic growth rate in the logarithmic phase ($r_{LF82}=0.76$ vs $r_{LF82+MMS}=0.37$). This result revealed that MMS affected LF82 growth, leading to the hypothesis of a parallel alteration in its adhesive and invasive properties.

To assess this point, we performed adhesion and invasion assays upon 4 hours of LF82 infection on Caco-2 cells in the presence of MMS at concentrations of 0.04%, which did not affect the viability of the pathogenic strain (**Fig. 13B**). Results showed that adhesion was diminished by 60.2% (Mann-Whitney, p -value = 0.0238), while invasion by 53.5% (Mann-Whitney, p -value= 0.0353) (**Fig. 12C**). Interestingly, MMS treatment led also to a diminished aggregative behavior of LF82, which usually aggregates within cell-to-cell junctions on Caco-2 monolayers (data not shown).

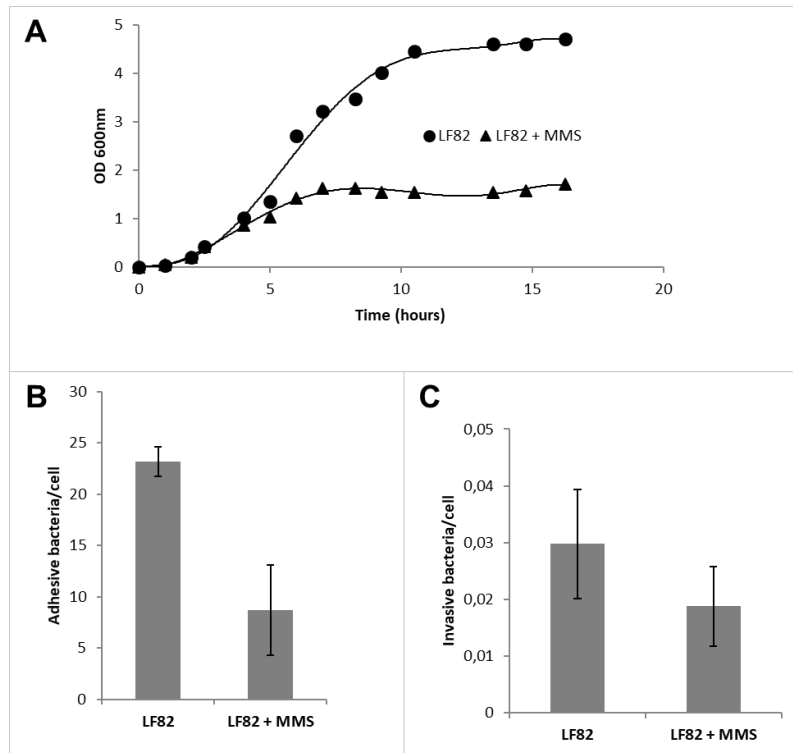


Figure 13. Effect of methylation stress on pathogenic *E. coli* strain LF82 (AIEC). **A)** Growth curves of AIEC strain LF82 in presence (triangle) and in absence (circles) of MMS. Superimposed to data points, for each growth curve, is the 4-parameter logistic regression following the formula $y = y_0 + a/[1+(x/x_0)^b]$, where y_0 is the intercept with y-axis, a is the maximum value of y , x_0 is the mid-point, and b is the curvature coefficient. **B)** Adhesion indexes of LF82 strain on Caco-2 cells after 4h infection, in presence and in absence of MMS, was measured. Values were reported as the mean adhesive bacteria (\pm standard error of the mean) per single Caco-2 cell. **C)** Invasion indexes of LF82 strain on Caco-2 cells after 4h infection, in presence and in absence of MMS, was measured. Values were reported as the mean adhesive bacteria (\pm standard error of the mean) per single Caco-2 cell. Adapted with permission from Di Pasquale et al 2016.

Experimental section

E. coli strains

E. coli MV1161, a derivative of the standard laboratory strain AB1157, was used as reference strain in this work. Isogenic *AnanA::kan* mutants was constructed using the λ Red technique⁽⁷⁷⁾. The MV1161 Δ *AnanA::kan* mutant was transformed with pMAL-c5x-*nanA* plasmid in order to complement neuraminidase activity. The strain LF82⁽⁷⁵⁾, a prototype adherent-invasive *E. coli* (AIEC) strain, was used in adhesion and invasion experiments with CaCo2 cells. LF82, was grown overnight in LB medium at 37°C, 180 rpm agitation, then used to inoculate 1:100 two different 250 mL flasks containing 100mL of pre-warmed LB, and underwent growth at 37°C, 180 rpm. Once reached an OD₆₀₀=0.5, MMS was added to one flask at 0.04%, and OD₆₀₀ measurements were taken every hour from both flasks.

Differential In Gel Electrophoresis (DIGE)

DIGE experiments were performed on four biological replicates of MMS treated and four biological replicates of MMS untreated *E.coli* as previously described⁽⁷⁸⁾ *E.coli* cells were homogenized in 0.5 ml of lysis buffer (7M urea, 2M thiourea, 4% chaps, 30mM Tris-HCl pH 7.5) using a Dounce homogenizer. The protein extract concentrations were determined and equal amounts of the protein lysates were then labeled *in vitro* using two different fluorescent cyanine minimal dyes (Cy3 and Cy5, respectively) differing in their excitation and emission wavelengths. A third cyanine dye (Cy2) was used to label a mixture of all samples as internal standard. The three differently labeled protein mixtures were pooled and subjected to isoelectric focusing

through a pH range of 3-10 over a length of 24 cm. The reducing and alkylating steps were performed between the first and the second electrophoretic step.

Acrylamide strips were then transferred to the top of a classical SDS PAGE gel for a second orthogonal electrophoresis analysis. The Cy2, Cy3 and Cy5 images were obtained by scanning each of the four DIGE gels at excitation/emission wavelength of 480/ 530 nm for Cy2, 520/590 nm for Cy3 and 620/680 nm for Cy5 using a Typhoon 9410 TM scanner (GE Healthcare). The semi-preparative gel, prepared in an identical fashion, was scanned with 480/633 nm wavelengths. After consecutive excitation at both wavelengths, the images from the preparative gel were overlaid and subtracted (normalized) from the samples, whereby only differences (up or down regulated proteins) between the two samples were visualized. By performing a high resolution image analysis on the six biological replicates, it was possible to visualize significant differences between numerous protein spots present on the gels. Differentially regulated spots were defined as having a variation higher than 1.2 ($p < 0.05$) per previously established methods ⁽⁷⁹⁾. The gels showed a high degree of similarity, with more than 80% of all spots superimposeable. The remaining 20% showed variation and were further studied.

Proteomic analysis

The spots of interest were excised, hydrolyzed and the peptide mixtures analyzed by MALDI-MS and LC-MSMS mass spectrometry, on a 4800 Plus MALDI TOF/TOF™ (Applied Biosystems, Framingham, MA, USA) and a LC/MSD Trap XCT Ultra (Agilent Technologies, Palo Alto, CA) equipped with a 1100 HPLC

system and a chip cube (Agilent Technologies) respectively. MALDI spectra were acquired in the positive ion reflector mode using delayed extraction in the 800 - 4000 Da mass range. LC-MS/MS analysis was performed using data-dependent acquisition of one MS scan followed by MS/MS scans of the three most abundant ions in each MS scan. Raw data analyses were converted into a Mascot format text to identify proteins using Matrix Science software. The protein search considered the following parameters: non-redundant protein sequence database (NCBI nr), specificity of the proteolytic enzyme used for the hydrolysis (trypsin), taxonomic category of the sample, up to one missed cleavage, cysteines as S-carbamidomethylcysteines, unmodified N- and C-terminal ends, methionines both unmodified and oxidized, putative pyro-Glu formation by Gln, precursor peptide maximum mass tolerance of 200 ppm, and a maximum fragment mass tolerance of 200 ppm.

Identified proteins were investigated to predict functional protein association networks for each entry using the STRING online database (<http://string-db.org>). Proteins were analyzed with the STRING software.

RNA extraction, Reverse transcription and Real-time PCR

Three *E. coli* culture replicates were grown at 37 °C in the presence and in the absence of 0.04% MMS according to proteomics experiments. In order to obtain an immediate stabilization of RNA, two volumes of RNA protect Bacteria Reagent (Qiagen) were added directly to one volume of bacterial culture (10 OD_{600nm}). Bacterial cells were harvested and pellet was stored at -20°C. Total RNA was extracted from culture using RNasy Midi Kit (Qiagen) according to the manufacturer's

instructions. The purity and integrity of total RNA was verified by both 1% denatured agarose electrophoresis and by evaluating the A260/A280 absorbance ratio within the range 2.1 - 2.3.

Total RNA (1 µg) was reverse transcribed in 40 µL final reaction volume using TaqMan Universal PCR Master Mix kit (Applied Biosystem) according to the manufacturer's instructions. The cDNA was synthesized at 48 °C for 60 min and then stored at -20 °C. Real-time PCR primer sequences were designed using Primer Express3.0 software. Quantitative real-time polymerase chain reaction (qRT-PCR) was performed using SYBR green PCR Master Mix (Applied Biosystems) according to the manufacturer's instructions to measure *nanA* gene expression. *rpoA* amplifications were used as normalization controls. Each sample was analyzed three times to obtain average data. Relative transcript levels were calculated using the $2^{-\Delta\Delta C_t}$ formula (Ct= threshold cycle) ⁽⁸⁰⁾.

Production of recombinant NanA protein and anti NanA antibodies.

E. coli MV1161 was amplified from host DNA by polymerase chain reaction (PCR) using the following primers: FW AGCGGATCCATGGCAACGAATTT; RW AATAAAGCTTTCACCCGCGCTCTT, where the recognition sites for BamHI and HindIII are underlined. To obtain the *nanA* gene, the PCR product was digested with the appropriate restriction enzyme and cloned into the BamHI and HindIII sites of the pET28a vector. The resulting plasmid contained the coding sequence for the recombinant NanA protein fused to a 6-histidine tag to facilitate protein purification.

The recombinant gene was expressed into the *E. coli* strain BL21. Cells were grown in LB medium at 37°C with 50µg/mL kanamicin to an optical density of ~ 0.5 at 600 nm, and 0.1 mM isopropyl-beta-D-thiogalactopyranoside (IPTG) was added. The culture was grown for 3 h at 37°C for NanA production. Cells were harvested by centrifugation at 5000 rpm for 15 min at 4°C. The cellular pellet was resuspended in equilibration buffer (20 mM Na₂HPO₄, pH 7.4, 500mM NaCl, 20 mM imidazole) containing 1mM PMSF and disrupted by passage through a French Press.

The cell extract was centrifuged at 13 000 rpm for 20 min at 4°C, to remove cell debris and the supernatant was filtered with a syringe-driven filter (0.22 µm) before protein purification. Soluble cell extract was loaded onto a His-Select Nickel Affinity Gel equilibrated with equilibration buffer and the bound protein was eluted with 500 mM imidazole in 50mM phosphate buffer pH 7.4, 500mM NaCl.

Protein concentration was estimated with Bradford reagent (Bio-Rad protein assay), protein purity was assessed by SDS-polyacrilamide gel electrophoresis (SDS-PAGE) and its primary structure verified by MALDI mapping strategy. Purified NanA protein was used to produce antiNanA antibodies by rabbit immunization (PRIMM, Milano, Italy).

Western Blot

E. coli culture were grown at 37 °C in the presence and in the absence of 0.04% MMS according to proteomics experiments. The cell pellets were lysed by French Press, the cell extract was centrifuged at 13 000 rpm for 20 min at 4°C, to remove the cell debris. The protein content of the samples was quantified with the Bio-Rad

(Hercules, CA, USA) protein assay. Protein samples (30 mg/sample loaded in each lane) were separated onto 12,5 % SDS-PAGE gels and transferred on to PVDF membrane, and probed with the antibodies against NanA (1:3000; Primm, Milano Italy) for 18h at 4 ° C under slow stirring. Blots were then incubated in horseradish peroxidase-conjugated secondary antibodies and target proteins were visualized by ECL detection (Pierce) using a computer-assisted imaging system (ChemiDoc; Biorad). Western blotting quantification was performed using Image Lab 4.0 software (Biorad) after normalization Anti-Maltose Binding Protein antibody (New England Biolabs) levels.

Static biofilm assays

2 mL of overnight bacterial cultures grown in LB + 1% glucose was added into 6-well flat bottomed polystyrene plate (Falcon). The plates were incubated at 37°C in aerobic conditions in the presence of 0.04% MMS. Growth was monitored by measuring the OD600, and after 24h incubation the ability of the *E.coli* strain to adhere to the polystyrene plates was tested. The liquid medium was removed and the wells washed with sterile distilled water. The plates were then stained with crystal violet for 5 min. Excess stain was rinsed off by placing the plate under running tap water. After the plates were air dried, the dye bound to the adherent cells was solubilized with 20% (v/v) glacial acetic acid and 80% (v/v) ethanol per well. The OD of each well was measured at 590 nm.

Biofilm assays on the complemented null NanA mutant strain were performed in the same conditions described above in the presence of 0.1mM IPTG.

Biofilm formation in the presence of sialidase inhibitor were carried out on *E.coli* MV1161 strain grown in sterile 6-well flat-bottomed polystyrene plates treated with different concentrations of N-Acetyl-2,3-dehydro-2-deoxyneuraminic acid (DANA) ranging from 1 to 100µg/mL. The plates were incubated aerobically at 37 °C for 24 hours and biofilm production was quantified as previously described.

Invasion assays

HeLa cells, cultured in 24-well plates, were infected with 0.05 mL of logarithmically grown bacteria in the presence or in the absence of MMS as above described. The entry of MMS was tested by infecting cells for 1 h at 37 °C at an MOI of about 10 bacteria per cell. After incubation, the monolayers were washed with PBS and 0.5 mL of fresh medium containing 200 mg/mL of gentamicin was added to each well and maintained for 1 h at 37 °C to kill extracellular bacteria. Cells were then lysed by the addition of 0.025% Triton X-100 and plated on LB to count viable intracellular bacteria.

Caco-2 intestinal cells were used for invasion assay with AIEC LF82 strain, using the gentamicin protection assay ⁽⁸¹⁾. Caco-2 cells were seeded in a 12-well plate at a density of 4×10^5 cells/well, let stand for 1 day, and medium (DMEM with low glucose supplemented with 10% FBS) replaced the day of infection. One mL of a 6 hours-old LF82 culture (logarithmic phase) was harvested, and MMS at 0.04% was added for 20 minutes in one tube, while another was left non-treated as a control. After the induction step, both tubes were centrifuged at 3000 rpm for 5 minutes, and bacterial pellets resuspended in PBS. Ten µL of resuspended pellets were added to each well

to obtain a MOI of bacteria/cells 10:1, and 12-well plates were incubated for 4 hours at 37°C, 5% of CO₂. After infection, cells were washed 3X with PBS, and 2 mL of pre-warmed culture medium supplemented with 400ug/mL of gentamicin were added to each well, then the plate was incubated for 2h at 37°C, 5% of CO₂. Gentamicin was then removed washing 3X with PBS, and 1 mL of Triton X-100 1% was added and left for 5 minutes during which the plates were gently swirled 3 times. Serial dilutions in PBS were performed till 10⁻⁶ and 100 µL of each dilution were plated onto TSA petri dishes (repeated three times). Colony-forming units (CFU) per mL were calculated, and invasion index was expressed as the number of invasive bacteria per single Caco-2 cell. Invasion assays were performed in triplicate in separate experiments, and results expressed as mean ± standard error of the mean.

Bacterial adhesion to Caco-2 cells

Bacteria from 18 h cultures in BHI broth, grown in the absence of MMS were further subcultured up to OD600 of 0.5 at 37 °C in BHI with or without MMS 0.04%. HeLa cells, cultured in 24-well plates (Falcon) to obtain semi-confluent monolayers (1x10⁵ cells/well) were then inoculated with 0.05 mL of bacterial suspensions in logarithmic-phase growth at a MOI of about 10 bacteria per cell. The adhesion assay was carried out by keeping cells and bacteria in contact for 1 h at 37 C. Loosely bound bacteria were removed from the cell monolayers by two washes with PBS. The cells were then lysed with 0.025% Triton X-100 and plated on LB agar to determine viable adherent bacteria. Adhesion efficiency was expressed as the percentage of the inoculated bacteria that adhered to HeLa cells.

Caco-2 intestinal cells were used for adhesion assay with AIEC LF82 strain. Caco-2 cells were seeded in a 12-well plate at a density of 4×10^5 cells/well, let stand for 1 day, and medium (DMEM with low glucose supplemented with 10% FBS) replaced the day of infection. One mL of a 6 hours-old LF82 culture (logarithmic phase) was harvested, and MMS at 0.04% was added for 20 minutes in one tube, while another was left non-treated as a control. After the induction step, both tubes were centrifuged at 3000 rpm for 5 minutes, and bacterial pellets resuspended in PBS. Ten μ L of resuspended pellets were added to each well to obtain a MOI of bacteria/cells 10:1, and 12-well plates were incubated for 4 hours at 37°C, 5% of CO₂. After infection, cells were washed 3X with PBS, and 1mL of Triton X-100 1% was added for 5min, during which the plates were gently swirled 3 times. This concentration of Triton X-100 had no effect on bacterial viability for at least 30 minutes. Serial dilutions in PBS were performed till 10^{-6} and 100 μ L of each dilution were plated onto TSA petri dishes (repeated three times). Colony-forming units (CFU) per mL were calculated, and adhesion index was expressed as the number of adhesive bacteria per single Caco-2 cell. Adhesion assays were performed in triplicate in separate experiments, and results expressed as mean \pm standard error of the mean.

The bifunctional protein GlmU is a key factor in biofilm formation
induced by alkylating stress in *Mycobacterium smegmatis*

The work presented in this chapter has been published as:
Di Somma A, Caterino M, Soni V, Agarwal M, di Pasquale P, Zanetti
S, Molicotti P, Cannas S, Nandicoori VK, Duilio A.
“The bifunctional protein GlmU is a key factor in biofilm formation induced by
alkylating stress in Mycobacterium smegmatis”.
Res Microbiol. 2019 Jun - Aug;170(4-5):171-181. doi:
10.1016/j.resmic.2019.03.00

MMS effect on *M. smegmatis* cells

Based on the data obtained in *E. coli*, preliminary experiments were carried out on *M. smegmatis* to examine the lowest amount of MMS clearly affecting cells growth. *M. smegmatis* cells were grown with and without different concentrations of MMS (0.01 to 0.07% w/v) and the bacterial cells viability was determined by measuring CFUs. **Fig. 14A** shows a decrease in number of CFU/mL in present of increasing doses of MMS. The concentration of 0.03% MMS led to a decrease of about 50% cell viability, confirmed by growth profile reported in **Fig 14B** and this concentration was used for further studies.

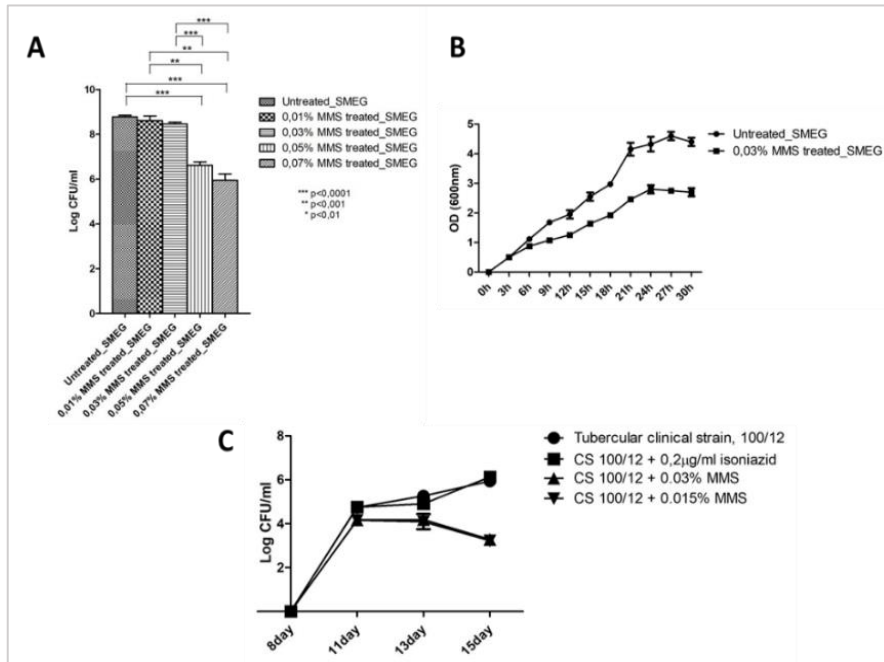


Figure 14. Cell viability and growth profile of *M. smegmatis* and *M. tuberculosis* clinical strain 100/12 at increasing doses of MMS. A) *M. smegmatis* wild type cells were grown at 37°C and treated with 0.01% (w/v), 0.03% (w/v), 0.05% (w/v), 0.07% (w/v) MMS in comparison with untreated cells. Cell viability was evaluated by enumerating CFUs after four days incubation. Experiments were run in triplicate and the error bars on the graphs stand for the standard deviation from the mean of the 3 experiments. One way ANOVA statistical test using Graph pad prism software was performed, $p < 0.0001$. **B:** Growth profiles of *M. smegmatis* cells in the absence (circle) and in the presence (square) of 0.03% MMS. Experiments were run in duplicate and the standard deviation is reported as error bars. **C:** Cell viability of *M. tuberculosis* clinical strain 100/12 resistant to isoniazid in the presence of isoniazid (square), 0.03% MMS (up triangle) and 0.015% MMS (down triangle). Circles refer to control cells. Cell viability was evaluated by enumerating CFUs on samples withdrawn from bacterial cultures at 11, 13 and 15 days after four days incubation. The error bars on the graph are represented as the standard deviation from the mean of 3 experiments. Adapted with permission from Di Somma et al 2019.

MMS on *M. tuberculosis* clinical strains

In collaboration with Prof.ssa Paola Mollicotti and his group in “University of Sassari, Department of Biomedical Science,” we have investigated the effects on *M.tuberculosis* (MTB) under alkylating stress to explore whether limited doses of MMS might also affect MTB cell viability. The experiments were performed on two reference (H37Rv and H37Ra) and 4 different tubercular strains of *M.tuberculosis* three of which had developed drug resistance (strain 100/12 resistant to isoniazid, strain 223/12 resistant to streptomycin and strain 1726/11 resistant to both isoniazid and rifampicin) and on 4 different species of mycobacterium (*M.gordonae*, *M. szulgai*, *M.xenopi* and *M. chelonae*). The Minimum Inhibitory Concentrations (MIC) of MMS for both reference strains were calculated by REMA assay⁽⁸²⁾ and resulted to be 0.10% and 0.05% for H37Rv and H37Ra respectively. Alkylation experiments were carried out in triplicate and cell viability was evaluated by numbering CFUs after 4 days incubation. When the bacteria cultures were exposed to MMS treatment (0.03% or 0.015% w/v), seven out of eight mycobacteria samples appeared sensitive to MMS showing decreased cell viability in these conditions. **Fig.15** shows the number of viable colonies of strain 100/12 resistant to isoniazid, following treatment with MMS in comparison with untreated cells or cells treated with isoniazid. The viability of strain 100/12 was affected by both MMS concentrations whereas the isoniazid treatment was clearly ineffective.

These results were confirmed by microscopy analysis of mycobacterial cells. **Fig. 15** shows the optical microscopy images of strain 100/12 in all conditions tested. In

the presence of both MMS concentrations (Panels C and D), a remarkable disappearance of the typical mycobacterial cells clusters was clearly detected with respect to control samples (Panel A) while isoniazid treated cells did not show significant differences compared with the control cells (Panels A and B).

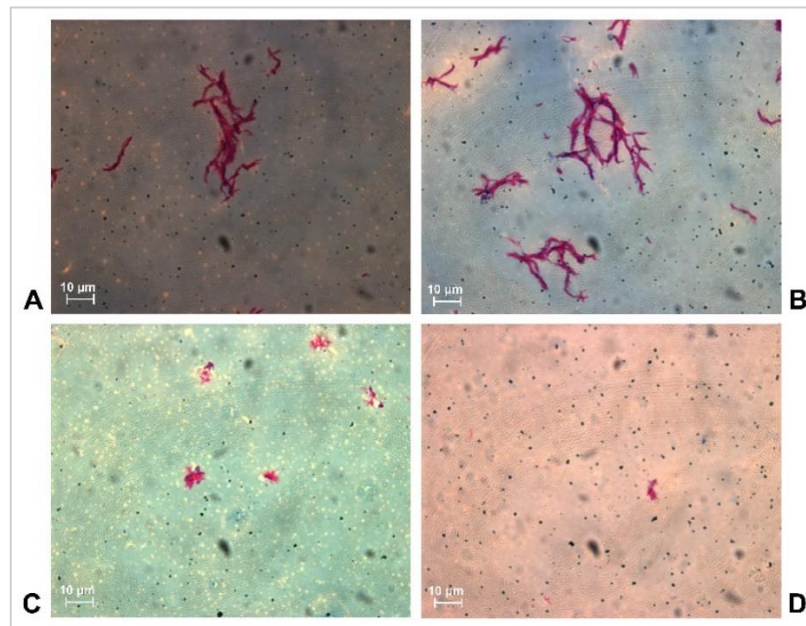


Figure 15. Microscopical observations of mycobacterial strain 100/12 cells. Optical microscopy images of the *M. tuberculosis* clinical strain 100/12 resistant to isoniazid observed following incubation with isoniazid (B) or in the presence of 0.015% MMS (C) or 0.03% MMS (D). Control cells images are reported in Panel A for comparison. Adapted with permission from Di Somma et al 2019.

Comparative proteomic analysis

The same approach used in *E.coli* was exploited to evaluate the response of *M. smegmatis* to alkylating stress. Four biological replicates of *M. smegmatis* were treated with 0.03% MMS and untreated cells were used as negative control. Following 3h incubation, protein extracts from MMS treated and untreated *M. smegmatis* cell cultures were labelled with fluorescence dyes and fractionated by 2D electrophoresis according to the DIGE technology ⁽⁸³⁾, using a 3-10 pH gradient (**Fig. 16A**). Comparative and quantitative analyses were performed and the up- or downregulated proteins with a statistically significant fold-change were defined. The MMS treated sample was then run on a preparative gel in the same conditions and stained with Sypro Ruby (**Fig. 16B**).

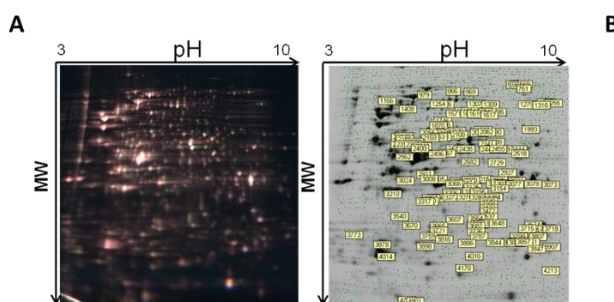


Figure 16 Differential in Gel Electrophoresis (DIGE) of protein extracts from MMS treated and untreated *M.smegmatis* cells. **A:** Superimposed images of the individual fluorescent scans of analytical gel. Equal amounts of protein lysates from four biological replicates were labeled in vitro using Cy3 (MMS treated) and Cy5 (MMS untreated) dyes. A third cyanine dye (Cy2) was used to label a mixture of the two samples used as internal standard. **B:** Semi-preparative 2D-Gel Electrophoresis of protein extracts from *M. smegmatis* cells. Adapted with permission from Di Somma et al 2019.

Stained spots matching the corresponding DIGE analytical gels were selected for identification by mass spectrometry and the mass spectral data were processed by an in-house version of the Mascot software. A total of 71 differentially expressed proteins were identified and the results are summarized in **Table 2**. For each protein, the fold change, spot number, protein description, Swiss-Prot code are reported.

Fold Change	n Spot	Protein Description	Swiss Prot	Score	Identified peptide
-2,34	1547	Alpha/beta hydrolase	A0QQP0	35	1(1)
-2,02	554	Phosphoenolpyruvate carboxylase	A0QWX4	182	10(8)
-2,02	554	Protein translocase subunit SecA 2	A0QYG9	560	17(20)
-1.90	1993	Piperidine-6-carboxylic acid dehydrogenase pcd	A0QT96	28	1(1)
-1.79	1551	Inosine-5'-monophosphate dehydrogenase	A0QSU3	395	10(17)
-1,74	2287	IcLR family transcriptional regulator	A0QXK4	28	1(2)
-1,61	998	Alpha-1,4-glucan:maltose-1-phosphate maltosyltransferase	Q9RP48	89	5(6)
-1,61	998	Acyl-CoA synthase fad32	A0R618	76	3(9)
-1.60	2441	Uroporphyrinogen decarboxylase	A0QW23	161	6(8)
-1,6	2441	Phospho-2-dehydro-3-deoxyheptonate aldolase	A0QW41	48	2(4)
-1,56	2404	Sulfate adenyltransferase subunit 2	A0R242	158	4(4)
-1,56	2404	6-phosphofructokinase PfkA	I7G6C4	158	10(15)
-1.55	802	Isocitrate dehydrogenase icd2	A0QSZ3	241	8(10)
-1,50	882	3-hydroxyacyl-CoA dehydrogenase fadB	A0R465	646	23(34)
-1,47	1950	IcLR family transcriptional regulator	A0QXK4	29	1(1)
-1,39	2664	IcLR family transcriptional regulator	A0QXK4	28	1(1)
-1.30	989	GTP-binding protein TypA	A0R2J0	362	14(27)
-1,28	1157	Alpha/beta hydrolase	A0QQP0	32	1(1)
-1,25	1162	Endopeptidase IV	A0QSH0	310	10(15)
-1,25	1162	Uroporphyrinogen-III synthase	0QR19	115	3(6)

-1.25	1162	1-deoxy-D-xylulose-5-phosphate synthase	A0QW19	394	10(12)
-1,17	2348	F420-dependent oxidoreductase	A0R461	96	2(4)
-1,17	2348	Adenosine deaminase	A0QT14	79	3(5)
-1.14	1339	DNA or RNA helicase of superfamily protein II	A0R451	294	12(16)
-1,14	1339	1-pyrroline-5-carboxylate dehydrogenase	A0R2H8	208	4(6)
-1,14	1339	Fumarate reductase	A0QT08	111	4(5)
-1,13	1849	IcIR family transcriptional regulator	A0QXK4	29	1(1)
-1,07	1067	Acyl-CoA oxidase	A0R0Q9	680	22(28)
1,03	2380	Adenosine deaminase	A0QT14	302	12(17)
1,03	2380	Putative phenylalanine aminotransferase	A0R5X8	195	9(9)
1,09	2986	ABC-type sugar transport system ATPase component	A0R505	28	1(2)
1,15	1276	Acyl-CoA synthase	A0R090	344	12(15)
1,15	1276	Fumarate reductase	A0QT08	167	7(10)
1,16	1387	Ribonuclease J rnj	A0QVT2	666	17(24)
1,28	1747	IcIR family transcriptional regulator	A0QXK4	36	1(3)
1,29	1361	Pyruvate dehydrogenase	A0QZB5	287	8(17)
1,29	1361	Ribonuclease J rnj	A0QVT2	127	3(7)
1,29	1361	60 kDa chaperonin 1	A0QQU5	116	5(8)
1,29	1947	IcIR family transcriptional regulator	A0QXK4	32	1(2)
1,30	1957	3-ketoacyl-CoA thiolase fadA2	A0QPE8	124	3(6)
1,32	3167	3-Hydroxyacyl-CoA dehydrogenase	A0R2P1	231	7(15)
1,33	1376	Carbohydrate kinase FGGY	I7F889	31	1(2)
1,35	1927	D-alanyl-D-alanine dipeptidase vanX	A0R4L7	28	1(1)
1,49	2221	Alanine dehydrogenase	A0QVQ8	201	9(15)
1,51	1655	Inosine-5'-monophosphate dehydrogenase	A0QSU3	45	2(6)
1,56	3246	IcIR family transcriptional regulator	A0QXK4	28	1(1)
1,58	2313	Inositol-3-phosphate synthase	A0R7G6	550	16(20)
1,63	840	DNA gyrase subunit B	A0QNE0	315	10(20)
1,67	1948	Divalent metal cation transporter MntH	A0R3T6	36	1(2)
1,68	1512	IcIR family transcriptional regulator	A0QXK4	29	1(1)

1,69	1692	Bifunctional protein GlmU	A0R3C7	35	1(5)
1,75	2399	Alkanal monooxygenase alpha chain	A0R293	95	3(5)
1,75	2399	4-hydroxy-2-oxovalerate aldolase 2 bbhI-2	A0R4S6	73	3(5)
1,78	902	Serine/threonine protein kinase	A0R3L2	144	4(6)
1,78	902	Ribonucleoside-diphosphate reductase subunit alpha 1	P0CG99	235	9(13)
1,78	902	LpqN	I7G7W9	153	4(6)
1,81	2258	Fructose-1,6-bisphosphatase	A0R2U7	187	6(8)
1,81	2258	Acetyl-CoA acetyltransferase fadA3	A0R2Y1	165	5(11)
1,81	2258	NADPH:quinone reductase	A0R2M2	121	5(7)
1,82	2408	Ribonucleoside-diphosphate reductase subunit alpha 1 (nrdE1)	P0CG99	29	1(2)
2,17	1249	Acyl-CoA ligase FadD31	I7G4U9	195	6(8)
2,17	1249	Acyl-CoA synthase	A0R090	72	1(3)
2,18	1320	Endopeptidase IV	A0QSH0	59	3(3)
2,32	1163	Chaperone protein DnaK	A0QQC8	72	2(6)
2,4	3511	3-isopropylmalate dehydratase small subunit leuD	A0QUZ0	76	3(3)
2,4	3511	Peptidyl-prolyl cis-trans isomerase ppiA	A0QNF6	63	2(2)
2,47	1572	D-ribose-binding periplasmic protein	A0QZW4	29	1(1)
3,33	532	Glycine dehydrogenase (decarboxylating)	A0QYF7	480	16(23)
3,33	532	DNA polymerase III gamma/tau subunit dnaX	A0R5R6	224	7(12)
3,33	532	Alanine--tRNA ligase	A0QWQ4	163	5(6)
4,61	1629	Conserved hypothetical proline and alanine rich protein	A0QNJ7	239	6(9)

Table 2. Differentially expressed proteins in MMS treated M.Smegmatis cells. Adapted with permission from Di Somma et al 2019.

Biological networks and functional annotation analysis

Bioinformatics Resources such as STRING functional protein interaction networks (<http://string-db.org/>) and DAVID (<https://david.ncifcrf.gov/>) were used to evaluate the network distribution of the 71 identified differentially expressed proteins.

Among the up-regulated proteins, the STRING analysis revealed a large network comprising most of the identified proteins (43 out of 71; number of edges 74, clustering coefficient 2.71 and enrichment p-value 4.38e-07). Data are reported in Supplementary Fig. 1. Stronger associations are represented by thicker lines. Within this network, a subcluster including 6 proteins, Chaperone protein DnaK (DnaK), DNA gyrase subunit B (GyrB), Peptidyl-prolylcis-trans isomerase (PpiA), 60 kDa chaperonin 1 (GroEL1), Alanine-tRNA ligase (AlaS) and Inosine-5'-monophosphate dehydrogenase (GuaB), was detected. All these proteins were reported to be involved in biofilm formation to varying degrees ^(84,85).

When the DAVID database ⁽⁸⁶⁾ was used to examine the identified upregulated proteins, 11 proteins were found involved in metabolic pathways gathering within the Glycan Biosynthesis and Metabolism area. Among these, the enzyme GlmU was reported to be involved in biofilm production of several pathogenic and nonpathogenic bacteria ^(87, 88, 89), whereas LeuD and VanX are involved at different levels in cell wall biosynthesis to produce peptidoglycan chain precursors ^(90,91). These results suggest that MMS treatment of *M. smegmatis* gave rise to an increase in the expression of proteins contributing to defence mechanisms involving cell wall architecture and biofilm formation.

Effect of methylation stress on biofilm formation in *M. smegmatis*

The hyper-expression of proteins involved in biofilm formation as a result of methylation stress prompted us to perform specific assays to evaluate the amount of biofilm formed by *M. smegmatis* with and without MMS.

Static growth conditions were preliminarily optimized in order to accurately measure biofilm formation. *M. smegmatis* was inoculated in wells and incubated at 30°C for 4 days in 7H9 medium. Cells were then treated with either 0.03% or 0.05% MMS and quantification of attached cells was determined after 24 h by crystal violet staining and subsequent measurement of absorbance at 590 nm. Experiments were performed in triplicate and the averaged data are reported in **Fig. 17**.

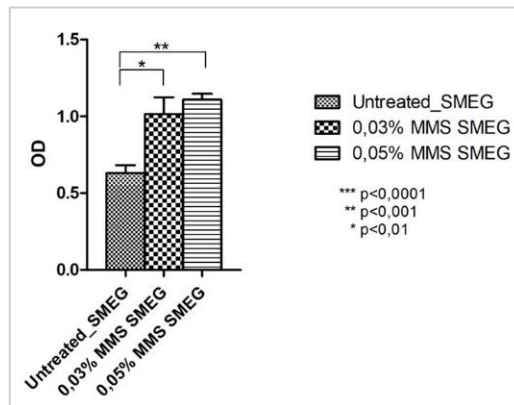


Figure 17 Biofilm formation in *M. smegmatis* under different conditions. The error bars on the graph stand for the standard deviation from the mean of 3 experiments. One way ANOVA statistical test using Graph pad prism software was performed, $p < 0.0001$. Adapted with permission from Di Somma et al 2019.

As report in **Fig17** methylation stress increased biofilm production compared to untreated cells in a dose-dependent manner. Cell viability was evaluated by CFUs measurements at both MMS concentrations according to Fig. 14A. This finding was in agreement with proteomic results suggesting that *M. smegmatis* response to damaging events led to increasing biofilm production mechanisms. It should be underlined that in the same conditions, MMS treatment strongly decreased biofilm formation in *E. coli*⁽⁹²⁾.

GlmU is essential for biofilm formation in *M. smegmatis*

Differential proteomics results suggested that MMS treatment of *M. smegmatis* increased the expression of proteins involved in biofilm formation. Among these, the expression of GlmU was upregulated by almost 50-fold under biofilm inducing conditions. Moreover, GlmU was reported to play a role in biofilm formation in *E. coli*, *S. epidermidis* and *S. aureus* being involved in the synthesis of an essential precursor required for biofilm production ^(87,88,89,93). On this ground, we pursued a detailed investigation to assess the putative role of GlmU in biofilm formation in *M. smegmatis*, if any.

Biofilm production in *M. smegmatis* was evaluated in the absence of GlmU. *glmU* is an essential gene and hence a mutant can only be generated in the presence of an inducible copy. In collaboration with prof Nandicoori (National Institute of

Immunology, International Centre for Genetic Engineering and Biotechnology, Aruna Asaf Ali Marg, New Delhi) we utilized a previously developed integrative construct in his group, pST-KirT-glmU, ^(94,95) where the expression of *glmU* is under the regulation of tetracylin inducible promoter ⁽⁹⁶⁾. This promoter is functional in the absence of anhydrotetracylin (ATc) and addition of ATc shuts off the expression of the enzyme. In order to generate *glmU* mutant in *M. smegmatis*, pST-KirT-glmU was electroporated to generate the merodiploid (**Fig. 18A**). The *glmU* at native locus was replaced with *hyg^r* marker and the recombination at the native locus was confirmed by PCR (**Fig. 18B**). Two independent recombinants were streaked along with *M. smegmatis* (*Ms*) and merodiploid (*Ms::glmU*) strains in the presence or absence of ATc (**Fig. 18C**). It is clear from the data that the recombinants failed to grow in the presence of ATc. Western blot analysis of wild type (*Ms*) and mutant (*Ms::glmU*) in the absence and presence of ATc showed that the growth defect observed was indeed due to the depletion of GlmU (**Fig. 18D**). Growth pattern analysis performed in the absence or presence of ATc was in agreement with the above data (**Fig. 18E**). SEM analysis, performed to evaluate the impact of GlmU depletion on morphology, showed presence of significant number of fused cells with wrinkled surface (**Fig. 18F**).

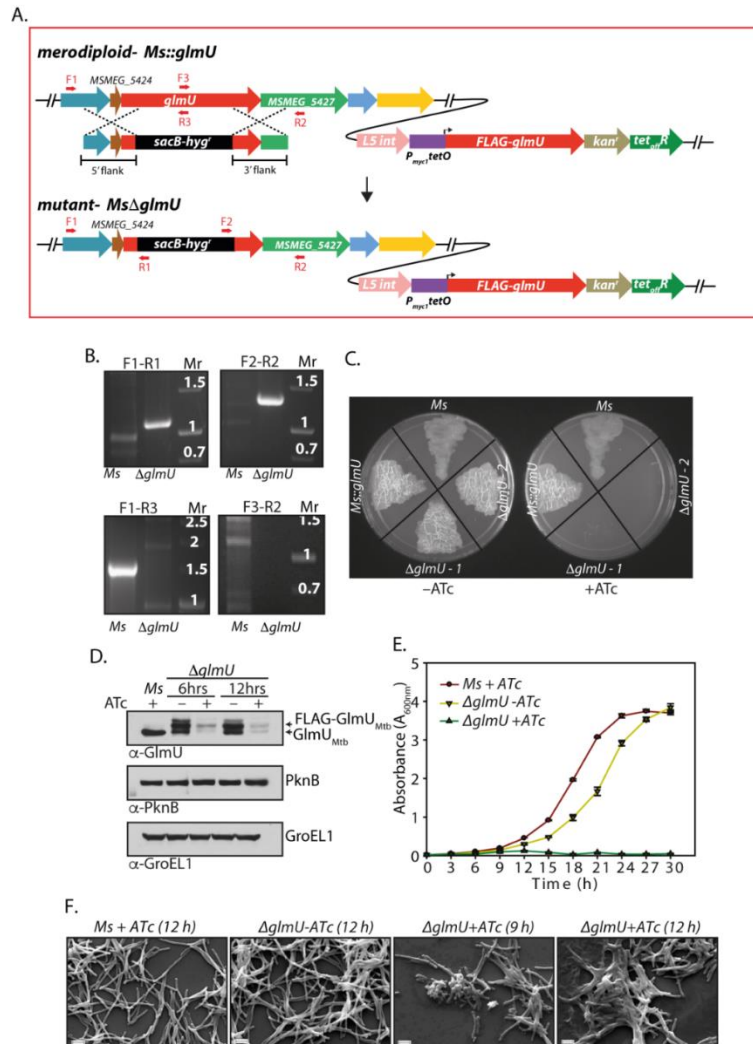


Figure 18. Generation of *glmU* mutant in *M. smegmatis*. **A)** Schematic diagram representing the genomic location of *glmU* (MSMEG_5426) and homologous recombination between flanking sequence

in the phagemid and the genomic locus. **B)** Agarose gel showing the PCR amplification of the *Ms* & putative Δ *glmU* mutant using specific primers. Primers F1 and R2 are beyond the flanks, R1 and F2 belongs to resolvase sites in *sacB/hygR* cassette and F3 and R3 binds to the native *glmU*. Amplification with F1-R1 or F2-R2 primers results in 1.08 kb or 1.29 kb size products with Δ *glmU* strain but none with the *Ms*. Whereas PCRs with F1-R3 or F3-R2 primers amplifies 1.6 kb or 1.26 kb band with the *Ms* and none with the Δ *glmU* mutant. **C)** *Ms*, *Ms::glmU* and Δ *glmU* cultures grown to an A600 of 0.8 OD and streaked on 7H11 agar plates with or without ATc. **D)** Western blots showing endogenous *GlmU* and FLAG-*GlmU* at 6 h & 12 h post ATc addition. For loading control *PknB* and *GroEL1* were probed. **E)** Growth curve analysis of *Ms* and Δ *glmU* in presence or absence of ATc up to 30 h. **F.** SEM images of *Ms* and Δ *glmU* at 9 h and 12 h after the addition of ATc. Scale bars 2 μ m. Adapted with permission from Di Somma et al 2019.

Next, we set out to evaluate the role of *GlmU* in biofilm production using the *Ms* Δ *glmU* mutant. *M. smegmatis* and *Ms* Δ *glmU* strains were grown at 30°C in triplicate in multiwell plate. Both biofilm formation and cell viability of the *Ms* Δ *glmU* mutant used as control were measured just before the addition of ATc and the corresponding values are shown in **Figs. 19A** and **B** (*Ms* Δ *glmU*-ATc, second bar in the figures). The expression of *GlmU* was then inhibited by adding 200 ng of ATc at different time points, 24, 48, 72 and 96 h, in different wells of *Ms* Δ *glmU*. ATc was shown to have no effect on wild type *M. smegmatis* culture (first bar in **Figs. 19A and B**).

As shown in Fig. 19A, when *Ms* Δ *glmU* cultures were treated with ATc after 24 or 48 h of growth, a decrease of about 82% or 68% respectively in biofilm formation was observed (**Fig. 19A**, third and fourth bars) suggesting that depletion of *GlmU* at the early phase of growth might impair biofilm production underlining a possible involvement of *GlmU* in this process. No significant differences in biofilm formation were detected when *GlmU* depletion was induced at late stage of cell growth (**Fig.**

19A, fifth and sixth bars), indicating that depletion of GlmU was ineffective when maximum biofilm production had already occurred.

Then, we performed a similar experiment and determined cell viability in *M. smegmatis* and the *MsΔglmU* mutant either in the absence (*MsΔglmU-ATc*) or in the presence (*MsΔglmU+ATc*) of ATc. **Fig. 19B** shows that following 24h ATc treatment a large decrease in cell viability of the *MsΔglmU* mutant was observed whereas no significant differences in cell density were observed between *MsΔglmU-ATc* and *MsΔglmU+ATc* cultures when ATc was added at 72 and 96 h (**Fig. 19B**, fifth and sixth bars). These data raised the question whether the reduced biofilm formation had to be ascribed to a decrease in the replication rate of *MsΔglmU* when the expression of GlmU was stopped as this enzyme is essential for growth, or to a specific role exerted by GlmU itself.

In an attempt to solve the question, we tested whether the overexpression of GlmU had an effect on biofilm formation. We used a newly developed integrative construct where the expression of *glmU* is under the control of isovaleronitrile (IVN) inducible promoter (*Ms.pNit-glmU*)⁽⁹⁶⁾. *M. Smegmatis* and *Ms.pNit-glmU* strains were grown at 30°C in triplicate in multiwall plate. Biofilm formation of the *Ms.pNit-glmU* mutant used as control was measured just before the addition of IVN and the corresponding values are shown in **Fig. 19C** (*Ms.pNit-glmU-IVN*, second bar in the figure).

The expression of GlmU was then induced at 48 h in the *Ms-pNit-glmU* mutant by treatment with 5μM IVN. At five days of growth, crystal violet assay was performed to measure the formation of biofilm and the cell density was determined by measuring the absorbance at 590 nm. As shown in **Fig. 19C**, following IVN stimulation at 48 h

Ms.pNit-glmU showed a 45% enhancement of biofilm formation (*Ms.pNit-glmU*+IVN, third bar in the figure), indicating that increasing amount of GlmU impacted biofilm production and suggesting a role of the enzyme in this process.

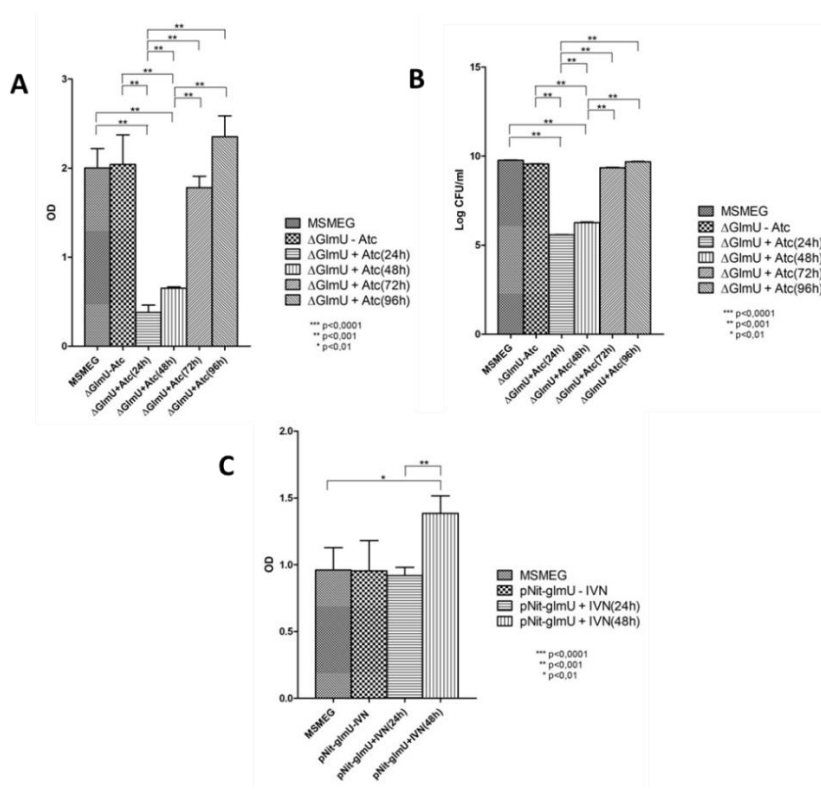


Figure 19. GlmU is required for biofilm formation in *M. smegmatis*. A) Formation of biofilm was measured after 24 h, 48 h, 72 h and 96 h in different wells for *Ms* Δ glmU conditional deletion mutant strains *M. smegmatis* culture. B) Colonies were counted and log₁₀CFU/ml values were calculated and plotted using graph pad prism software. C) Overexpression of GlmU in *Ms.pNit-glmU* overexpressing mutant strains increases biofilm formation. The error bars on the graphs stand for the standard deviation from the mean of 3 experiments. One way ANOVA statistical test using Graph pad prism software was performed, $p < 0.0001$. Adapted with permission from Di Somma et al 2019.

GlmU inhibition and biofilm formation in *M. smegmatis*.

To further define whether or not GlmU had a role in biofilm formation in *M. smegmatis*, we measured biofilm levels following inhibition of the acetyltransferase domain of GlmU. Several authors reported that inhibition of GlmU by thiol-specific reagents ^(87,93,97,98) or its reaction product N-acetylglucosamine-1-phosphate ^(88, 99,100,101,102) resulted in decrease of biofilm production in various microorganisms with only a slight effect on bacterial growth.

The amount of biofilm produced by *M. smegmatis* under methylation stress conditions was measured in the presence of different concentrations of iodoacetamide (IAA), a GlmU acetyltransferase domain inhibitor ^(88,97). **Fig. 20A** shows that inhibition of GlmU by 20 μ M IAA decreased biofilm levels induced by MMS treatment. The growth profiles of *M. smegmatis* in the presence of 20 μ M IAA was also evaluated indicating only a slight effect of the chemical agent on bacterial growth that in these conditions was still able to grow (**Fig. 20B**).

A further GlmU inhibition experiments was then performed in the presence of N-Acetylglucosamine-1-phosphate (GlcNAc-1P), a competitive inhibitor of GlmU ^(99,100,101). Biofilm formation was then measured following MMS treatment of *M. smegmatis* cells in the presence of 20mM GlcNAc-1P. Inhibition of GlmU enzymatic activity resulted in a clear decrease of biofilm formation as shown in **Fig. 20C**.

These data supported the results obtained with GlmU mutants, confirming the involvement of this enzyme in the defence mechanisms elicited by *M. smegmatis* upon alkylation stress.

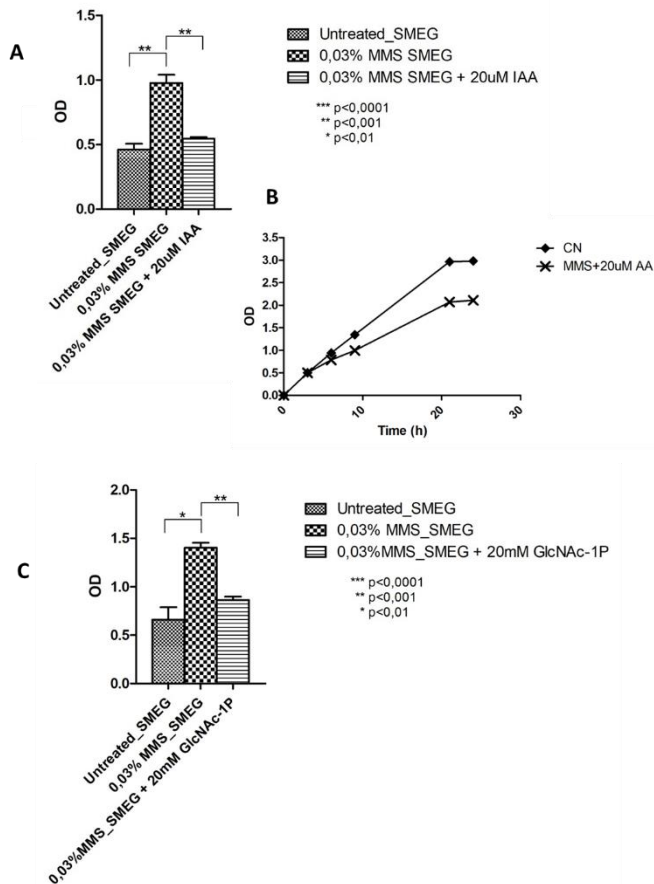


Figure 20. Biofilm formation in *M. smegmatis* in the presence of domain inhibitor. **A)** Biofilm production following treatment of *M. smegmatis* with 20 μ M iodoacetamide (IAA) for 24 h. **B)** Growth profiles of *M. smegmatis* cells in the presence of 0.03% MMS (square), or 0.03% MMS and 20 μ M IAA (triangle) in comparison with untreated cells (circle). **C)** Biofilm production in *M. smegmatis* in the presence of 20 mM N-acetyl glucosamine-1-phosphate for 24 h. The error bars on the graphs A, B and C stand for the standard deviation from the mean of 3 experiments. One way ANOVA statistical test using Graph pad prism software was performed. ***, $p < 0.0001$. Adapted with permission from Di Somma et al 2019.

Experimental section

M. smegmatis and MTB culture

M. smegmatis wild type cells were grown 3 days in 7H9 medium, supplemented with 10% ADC, containing 0.05% tween 80 at 37°C. Saturated *M. smegmatis* cultures were diluted to 0.05 OD in fresh medium; cells were divided in aliquots and treated with MMS in a 0.01-0.07% w/v range for 24 h. Bacterial cultures were serially diluted and incubated on 7H11 plate supplemented with 10% OADC at 37°C. Cell viability was determined by enumerating CFUs after four days incubation. Growth profiles were obtained by monitoring cells for 30 h with and without MMS treatment.

Saturated MTB cultures were diluted to 0.05 OD in 7H9 liquid medium supplemented with 10% ADC⁽¹⁰²⁾ and grown for 15 days. A₆₀₀ was measured every 48 h for 8 days. At day 8; 0.03% or 0.015% MMS or specific drug were added., Cell viability was evaluated at day 11, 13 and 15 by enumerating CFUs. Experiments were performed in triplicate. Cells detection was performed by Ziehl-Neelsen acid-fast staining⁽¹⁰³⁾. MIC measurements were performed with the help of Resazurin Microtiter Assay (REMA) as described earlier⁽¹⁰⁴⁾. Briefly, wells of a 96 well microtitre plate were filled with 50 µl of 7H9 media and serial dilutions of antibiotic were added. The last column was left untreated and used as a control. *M. smegmatis* strains were grown in replicates in 7H9 medium to an A₆₀₀ ~0.6; diluted 1000 times, and 50 µl of the diluted culture was added to each well. After 40 h of incubation, 30 µl of resazurin dye was added to all the well and incubated for 6 h under shaking and imaged. MICs were determined as the values of the first well showing no growth as indicated by resazurin dye staining.

Differential Gel Electrophoresis (DIGE)

Protein extracts from MMS treated *M. smegmatis* (MMS_SMEG) and untreated *M. smegmatis* (control_SMEG) cells were analyzed by DIGE procedure ^(105,106). Four independent gels were performed in order to obtain statistically significant data. The protein extracts were resuspended in buffer containing 0.03 M Tris-HCl pH 7.5, 7 M urea, 2 M thiourea and 4% chaps. Equal amounts of protein lysates from MMS treated and control cells were labeled *in vitro* using Cy3 and Cy5 cyanine minimal dyes respectively (GE Healthcare, Piscataway, NJ). A third cyanine dye (Cy2) was used to label a mixture of the two samples used as internal standard ^(107,108). The first dimension separation was performed using 18 cm IPG strips, 3-10NL pH range. Labeled proteins were loaded on the strips and electrofocused overnight (75kV/h) at 20°C. The focused proteins were reduced in equilibration buffer containing 0.5% dithiothreitol for 15 min and alkylated with 4.5% iodoacetamide for a further 15 min. SDS-PAGE was performed using 10% polyacrylamide gels (20 × 24 cm) onto Ettan Dalt Twelve system (GE Healthcare, Piscataway, NJ) overnight at 2W for each gel. The fluorescent images were acquired at excitation/emission values of 488/520, 532/580, 633/670 nm, at 100 μm resolution, using a Typhoon 9400 Variable Mode Imager (GE Healthcare, Piscataway, NJ). Images were processed by DeCyder v5.2 software (GE Healthcare) in Batch Processing mode performing the detection and quantification of protein spots in Differential In-Gel (DIA) module and spot matching in Biological Variation Analysis (BVA) module, as previously described ⁽¹⁰⁹⁾. According to DIGE procedure, the fluorescence intensity was associated to each selected spot. In order to reduce inter-gel variation, the spot biological fold change was expressed as a mean value of

the four biological samples. Finally, spot intensities were compared between MMS treated and control gels and the spot variation was evaluated by statistic *t-test*. We included protein spots with fold change >1.20 and $p < 0.05$ in the image analysis. The accepted spot matching was checked by manual inspection.

Proteomic analysis

Protein extract (500 µg) from four biological replicates of MMS_SMEG and from four biological replicates of control_SMEG were used to perform a preparative gel. Gel was stained using fluorescent dye Sypro Ruby (Molecular Probes Inc., Eugene, OR) ⁽¹¹⁰⁾. Selected spots were excised, hydrolyzed and processed by LC-MS/MS as described earlier ⁽¹¹¹⁾. The MS/MS spectra raw data were processed by in-house Mascot software (version 2.4) ⁽¹¹²⁾. The Mascot research parameters were the following: *M. smegmatis* protein database; trypsin as proteolytic enzyme; up to 1 missed cleavage; 200 ppm mass tolerance for precursor ions; 0.8 Da mass tolerance for fragment ions, S-carbamidomethylcysteine as fixed modification, pyro-Glu formation (from N-term Gln) and Met oxidation as variable modifications. Peptides, displaying an individual MASCOT score > 38 were considered significant for identification ^(113,114).

Clustering analysis

The ‘STRING: functional protein association networks’ 7.0 software (<http://string-db.org/>) was used to analyse identified protein dataset. The STRING database allowed us to define the physical (direct) and functional (indirect) protein interactions.

Identified proteins were assembled into significant canonical pathways or networks according to their associated score, defined as the negative logarithm of the p-value (115).

Generation of MsΔglmU gene replacement mutant

M. tuberculosis glmU gene was digested with NdeI-HindIII from pQE2-glmUMtb construct and sub-cloned into the corresponding sites on pST-KirT vector (94,95). *M. smegmatis* mc2155 (Ms) strain was electroporated with pST-glmUtet-off construct to generate a merodiploid strain Ms::glmU. Approximately 1 kb upstream and downstream flanking sequences of glmUMsm were amplified followed by the generation of AES, which was subsequently cloned into phAE159 to generate temperature sensitive phagemid (94,116). MsΔglmU conditional mutant was generated from Ms::glmU using specialized transduction (116). Genomic DNA was isolated from the wild type (Ms) and the potential mutant (MsΔglmU) and the recombination at the native locus was confirmed by PCR.

Generation of MspNitglmU overexpressing mutant

M. tuberculosis glmU from pQE2-glmUMtb construct was released with NdeI-HindIII and subcloned into the corresponding sites to modified pNit1 construct containing apramycin resistance gene. *M. smegmatis* was electroporated with pNit-Apra-glmU construct to generate Ms::pNit-glmU strain. In the presence of isovaleronitrile (IVN) the strain overexpresses GlmU.

Growth and scanning electron microscopy (SEM) analysis.

For monitoring growth on plates, cultures of *M. smegmatis* (Ms), *M. smegmatis* merodiploid (Ms::glmU) and MsΔglmU (ΔglmU) were grown in the absence of ATc till A600 of 0.8 and streaked on 7H11 agar plates with or without ATc. To evaluate the growth pattern, A600 ~0.8 cultures of Ms and ΔglmU grown in the absence of ATc were seeded at A600 ~0.02 and growth was monitored every 3 h for 30 h. For SEM analysis, cultures were grown for 9 or 12 h in the presence or absence of ATc and the samples were processed for SEM as described earlier ⁽¹¹⁶⁾.

Static biofilm assay

M. smegmatis (WT) and MsΔglmU(ΔglmU) conditional mutant strains were grown overnight in the absence of ATc. The cultures were seeded in triplicate for each experiment (Crystal Violet assay and CFU analysis) at A600~ 0.05 in Sauton's medium (200 µl) in a sterile 96 well plates. ATc was added to WT samples at 24 h and in control ΔglmU sample ATc was not added. In other ΔglmU samples ATc was added at different time points after starting the culture (24, 48, 72 and 96 h). All the samples were analyzed for biofilm formation and viability after 120 h (5 days) by both crystal violet and CFU analysis respectively.

M. smegmatis cultures were freshly streaked on 7H11 agar plates and grown for 24 h at 37°C. 2-3 colonies were inoculated in 7H9 medium + ADC for 16h at 37°C. Saturated *M. smegmatis* cultures were seeded in triplicate at A600 of 0.05 OD in Sauton's medium (200µl) in a sterile 96 well plates. Cultures were incubated at 30°C for 4 days and then treated with 0.03% or 0.05% (w/v) MMS in the absence and in the

presence of either 20 μ M iodoacetamide (IAA) or 20 mM N-acetylglucosamine-1-phosphate (GlcNAc1P) for 24 h. All the samples were analyzed for biofilm formation and the IAA treated sample was also monitored for cell growth.

Crystal violet assays were performed as follows: bacterial cells were removed and the biofilm containing wells were washed twice with sterile water. Wells were then dried at RT and 200 μ l 0.1% crystal violet was added and incubated at RT for 20-30 min. The dye was removed, wells were washed with sterile water and 200 μ l of destaining solution (80% ethanol-20% acetic acid) was added at room temperature and incubated for 20-30 min. The absorbance was measured at 590 nm.

Chapter 3

Functional proteomic approaches in the study of the mechanism of action of antimicrobial peptides

The complete description of the complex network of cellular mechanisms and the use of the network to predict the full range of cellular behaviors are the major goals of systems biology ⁽¹¹⁷⁾. In this respect, functional proteomics crucial role in modern biology research, as it is addressed towards two major targets: the elucidation of biological functions of unknown proteins and the definition of cellular mechanisms at the molecular level ⁽¹¹⁸⁾. Functional proteomics can describe the biological function of an unknown proteins through the identification of its protein partners belonging to protein complexes involved in a specific mechanism ⁽¹¹⁹⁾.

In this scenario, one of the in vitro methods exploited to define protein interactors consists in Pulldown experiments where the protein of interest is immobilised onto an insoluble support and incubated with the entire cellular extract ⁽¹²⁰⁾.

Marucci et al., identified GALNT2 as a novel modulator of insulin signaling and a potential target of novel treatments of insulin resistance and abnormal glucose homeostasis by RNA pull-down ⁽¹²¹⁾. Garzia et al., while studying the breast cancer progression and metastasis formation, identified the h-prune- nm23-H1 complex, which is involved in cancer metastasis, leading to new translational studies involved into the inhibition of cell migration ⁽¹²²⁾.

Functional Proteomic approaches using pull-down experiments were applied to the investigation of the mechanism of action of the antimicrobial peptide Temporin L (TL) a natural peptide secreted from the skin of the European frog *Rana temporaria* on *E. coli* cells.

The antimicrobial peptide Temporin L impairs *E. coli* cell division by interacting with FtsZ and the divisome complex

*The work presented in this chapter has under published as:
Di Somma A., Avitabile C., Cirillo A., Moretta A., Merlino A., Paduano L.,
Duilio A., and Romanelli A.
“The antimicrobial peptide Temporin L impairs E. coli cell division by
interacting with FtsZ and the divisome complex”.
Biochim Biophys Acta (2020)*

Effect of Temporin L on *E. coli* cell growth

The antimicrobial activity of Temporin L was evaluated by monitoring *E. coli* cells growth in the presence of different concentrations of Temporin L (20 and 50 μM). **Fig. 21A** shows that in the presence of 20 μM TL, cell growth decreased to about 50% whereas *E. coli* was unable to grow in the presence of higher peptide concentrations (50 μM). The MIC value was calculated to be 16 μM , in accordance with values already reported (**Fig. 21B**).

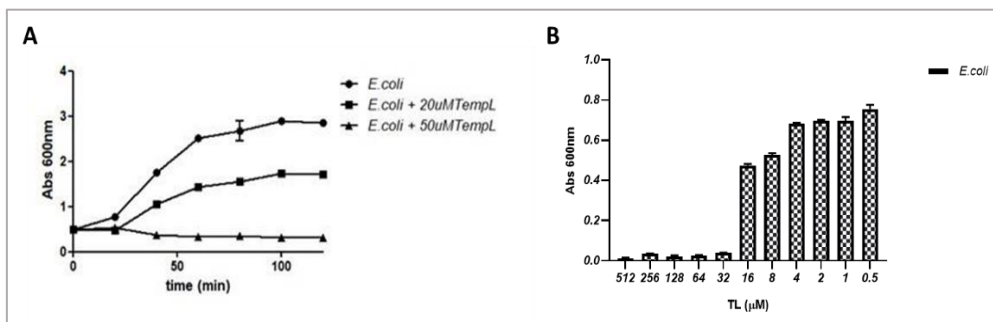


Figure 21. The antimicrobial activity of Temporin L. A) Growth profile in the presence and the absence of TL. B) MIC assay in the presence of increasing concentrations of peptide

Pull Down experiment

A detailed investigation of the mechanism of action of TL at the molecular level was pursued by functional proteomics approaches. Biotinylated Temporin L was immobilised onto streptavidin-conjugated agarose beads and used as a bait to identify specific *E. coli* putative protein interactors. Membrane proteins were isolated from *E. coli* cells and precleaned by incubation with free agarose beads to remove aspecific proteins. The unbound proteins were then incubated with the bait and putative protein interactors were recovered by competitive elution with a biotin excess and fractionated by SDS-PAGE. The eluate from the precleaning resin was also analysed as control. Both the sample and control lanes were cut in slices and protein bands were digested *in situ* with trypsin. The resulting peptide mixtures were directly analysed by LC-MS/MS and the mass spectral data used to search a protein database using an in-house version of the Mascot software leading to protein identification. Proteins that were identified both in the control and in the sample, lanes were discarded, whereas those solely occurring in the sample and absent in the control were considered as putative TL interactors (**Table 3**).

Fig. 22A shows the distribution of Temporin L putative protein partners according to their cellular localization and the biological processes they are involved into. A bioinformatic analysis was performed using the String software and the KEGG pathway showing that a large number of proteins gathered within a network involved

in cell division and the biosynthesis of peptidoglycan for the production of the division septum (**Fig. 22B**).

Proteins	Peptides	SwissProt Code
Bifunctional protein PutA	43	P09546
Chromosome partition P (MukB)	13	P22523
Gln synth Ado transferase (GlnE)	18	P30870
Protein translocase sub SecA (SecA)	6	P10408
Elongation factor Tu 1 (TufA)	5	P0CE47
Elongation factor 4 (LepA)	3	P60785
D-lactate dehydrogenase (Dld)	22	P06149
NADH-CoQ oxidoreduct C/D (NuoC)	11	P33599
Pyridine nucleotide transhydrog (SthA)	7	P27306
Malate quinone oxidoreductase (Mqo)	6	P33940
Biotin carboxylase (AccC)	5	P24182
Serine Protease DegP (DegP)	5	P0C0V0
D-amino acid DH (DadA)	7	P0A6J5
NADH-CoQ oxidoreduct sub F (NuoF)	3	P31979
Transcrip termination Fact Rho (Rho)	8	P0AG30
Cell division protein FtsZ (FtsZ)	11	P0A9A6
L-lactate dehydrogenase (LldD)	13	P33232

UbiF	8	P75728
UbiH	9	A0A069FV1
D-Ala-D-Ala C-peptidase DacA (DacA)	5	P0AEB2
Protein TolB (TolB)	3	P0A855
Rod shape-determ P MreB (MreB)	2	P0A9X4
Multidrug efflux pump AcrA (AcrA)	5	P0AE06
PTS system Mannose-spec EIIAB (ManX)	6	P69797
FKBP-type PPI isomerase (FkpA)	6	P45523
Epimerase family protein (YfcH)	4	P77775
ADP-Hept-LPS heptosyltransf 2 (RfaF)	5	P37692
MurG	4	P17443
Protein RecA (RecA)	3	P0A7G6
ArnC	2	P77757
Cell division protein FtsA (FtsA)	2	P0ABH0
Uncharacterized P YkgG (YkgG)	4	P77433
Stringent starvation P A (SspA)	4	P0ACA3
FKBP-type 22 kDa PPI isom (FklB)	2	P0A9L3

Table 3. Putative protein interactors of TL from membrane extracts from E. coli cells.

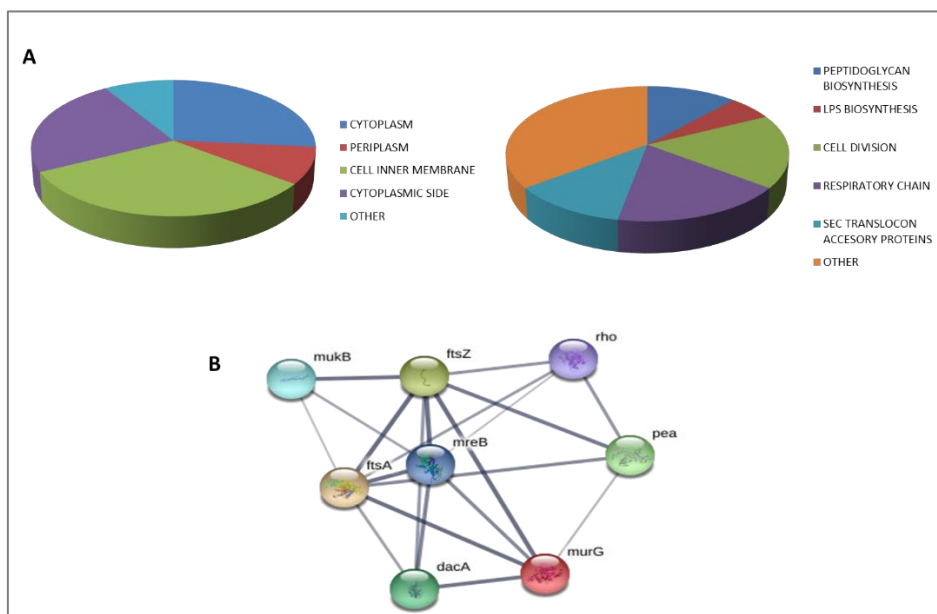


Figure 22. Bioinformatic analysis of TL proteins interactor. A) Distribution of TL putative protein partners identified in the pull-down experiment according to their cellular localization and biological functions. B) STRING analysis of the putative TL interactors belonging to the divisome complex showing the occurrence of a network including 8 proteins: FtsZ, FtsA, MurG, MukB, Rho, DacA, pea and MreB.

In particular, several proteins belonging to the divisome complex were identified including FtsZ, FtsA, MurG, MukB and MreB. Importantly, FtsZ is reported to be the target of two peptides, CRAMP (16-33) and MciZ, that show high sequence identity with TL (**Fig. 23A**). This result urged us to investigate the interaction of TL with FtsZ *in vitro* and *in vivo* and to develop a molecular model of the peptide-protein interaction by docking calculations.

Docking experiments

To reveal the structural basis of the binding of TL to FtsZ, a docking study has been performed (**Fig. 23B**). Calculations reveal that TL may bind the cavity that allows the accommodation of GDP in the structures of FtsZ from *B.subtilis* and *P.aeruginosa* (**Fig. 23C**), thus suggesting a possible competitive inhibition of the peptide for the GTPase activity of the protein. A detailed analysis of the interactions at the protein/peptide interface suggests the involvement of hydrophobic and coulombic interactions, with Phe and Trp residues of the peptide that pack against residues Gly20, Gly21, Gly71, Ala72, Gly105, Gly106, Gly107 and Phe182 of the protein and with the side chain of the peptide Arg that could make a salt bridge with the side chain of Glu138 of Ftsz (**Fig. 23D**).

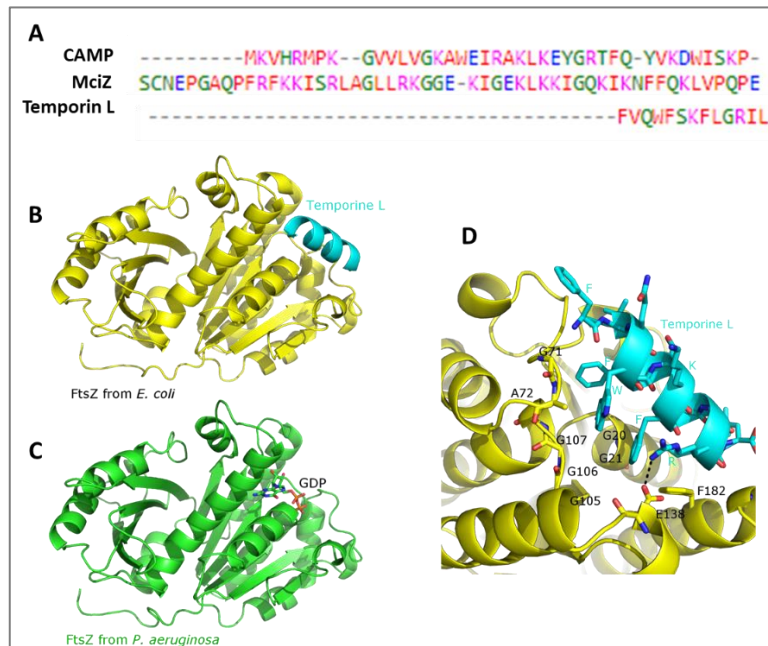


Figure 23. **A)** Sequence alignment of peptide temporin L, CRAMP 16-33 and MciZ. **B)** The predicted structure of the complex between FtsZ (yellow) and TL (cyan). **C)** Putative binding site well superimposes to that of GDP in the structures of *B. subtilis* and *P. aeruginosa* FtsZ. **D)** Predicted binding site of TL (cyan) on FtsZ structure (yellow).

Binding experiments

The binding of the peptide TL to the protein FtsZ was investigated by fluorescence, using the peptide labeled at the N-terminus with fluoresceine, incubated with

increasing concentrations of the protein (**Fig. 24**). The K_d value was calculated to be 17.4 ± 0.8 nM.

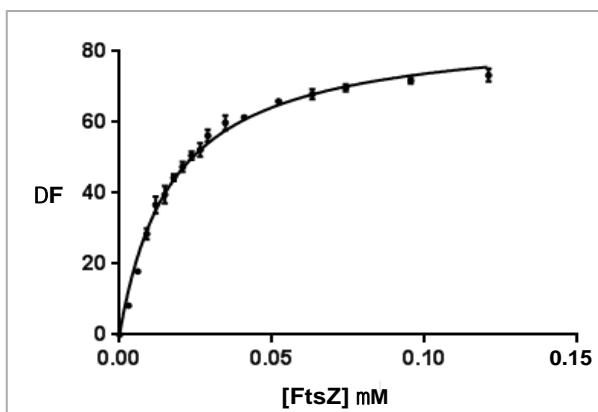


Figure 24. Binding of TL to FtsZ as determined by fluorescence experiments.

Enzymatic assays

To validate the docking predictions and to study the effect of TL on FtsZ, a recombinant form of the protein was produced and its GTPase activity was studied in the absence and in the presence of TL. The purified recombinant protein was incubated with GTP in the presence of the peptide (35 μ M) and the GTPase activity of FtsZ was monitored in comparison with the untreated protein at different GTP concentrations, reported in **Fig. 25**. In the presence of TL a decrease in the enzymatic activity of FtsZ was clearly observed. Kinetic parameters were calculated showing an increase of K_M by about 50% (112.0 μ M as compared to

56.6 μ M in the absence of the peptide) whereas V_{\max} remained unchanged, demonstrating the competitive inhibitory mechanism exerted by TL on FtsZ.

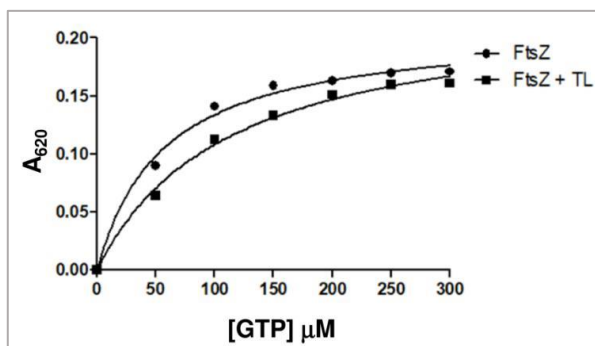


Figure 25. Enzymatic activity of recombinant FtsZ in the absence and in the presence of 35 μ M TL using GTP as substrate.

Optical microscopy and TEM analyses

The morphologic effect of FtsZ inhibition by TL on cell division was investigated *in vivo* by both optical microscopy measurements and TEM analyses on *E. coli* cell cultures grown in the presence and in the absence of the peptide. For optical microscopy, *E. coli* cells were inoculated in 10 mL of liquid LB and placed at 37°C for 16h under stirring. At the end of the incubation, bacterial cells grown to 0.5 OD/mL were incubated with 20 μ M TL and allowed to grow for a further 5h. A similar bacterial growth was prepared and used as control in the absence of the peptide. Samples of 100 μ L were observed by optical microscopy using a ZEISS optical

microscope for phase contrast and 50X magnifications. Images demonstrate that in the presence of TL (**Fig. 26B**) *E. coli* cells form long necklace-like structures containing a large number of *E. coli* cells originated by impairment in cell division that were absent in the control (**Fig. 26A**).

The TL effect on *E.coli* cell growth was also investigated by TEM. Bacterial cells were grown in the same conditions and incubated in presence of TL for 1h. TEM images further confirmed that in the presence of TL bacterial cells division was impaired as shown by several cells bound together and unable to divide (Figs. 26B e C) when compared to the control (**Fig. 26A**).

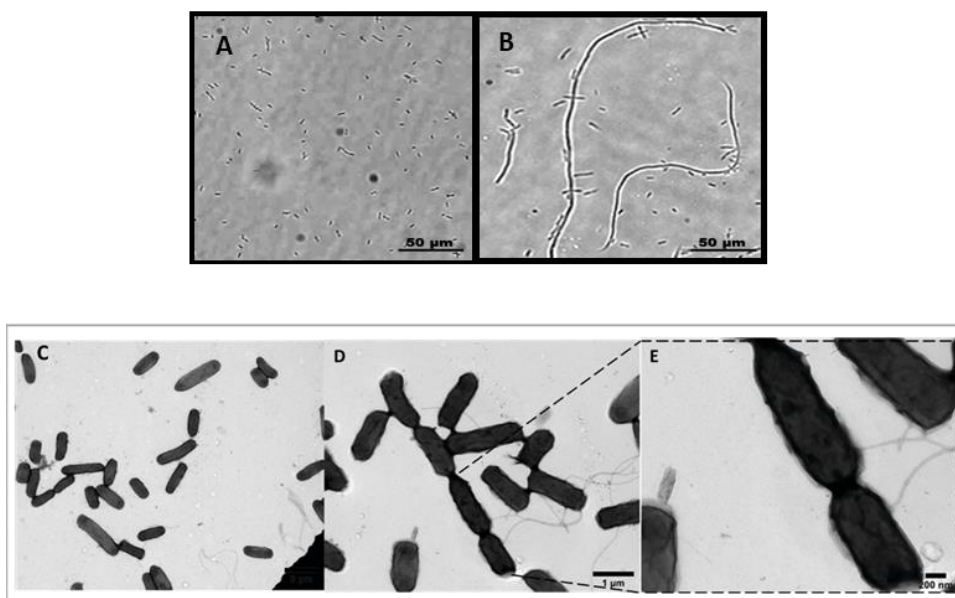


Figure 26. Optical and electron microscopy on *E.coli* with and without TL treatment. A) Optical microscopy and TEM analyses of *E. coli* cells grown in the absence (panel A) and in the presence (panel B) of 20 μM TL. Long necklace-like structures formed by *E. coli* cells were clearly detected in the presence of the peptide confirming the impairment of bacterial cell division. TEM investigations further confirmed the occurrence of bacterial cells unable to divide in the presence of TL (panel D) as compared to the control (panel C).

Scattering Measurements

The large structures formed by *E. coli* cells upon treatment with TL were further investigated by static light scattering experiments. *E. coli* cells were grown to 0.5 OD/mL in the presence and in the absence of 20 μM TL up to 1 OD at 600 nm and submitted to Dynamic Light Scattering (DLS) measurements in triplicate at fixed

scattering angle of 90° . As shown in **Fig. 27** small values of the scattering vector q , in the range probed by the LS, the scattering intensity profile decays with a q^{-1} power law for the sample of *E. coli* cells in the presence of TL, whereas it remains essentially constant for the pure bacteria, i.e for the cells in the absence of the peptide. This suggests that, in the presence of TL, large elongated structures are formed with a length larger than 6000 nm, the limit of LS instrument.

Furthermore, SANS analyses were exploited to investigate the effect of TL on *E. coli* cells, focusing on the structure formed in the range of 2 to 300 nm. SANS results revealed that a significant difference between untreated and treated *E. coli* cells occurs in the range between 20 nm and 60 nm. In such range, the profile of the scattering intensity of *E. coli* cells changes drastically upon TL addition suggesting a change in the spatial arrangement of the protein involved in the interaction with the peptide in agreement with the docking calculation.

Notably, in the range where structural changes on the membrane would be detectable, SANS analyses clearly showed no differences in the lamellar structure of *E.coli* cells, indicating the absence of a destabilization of the bacterial membrane.

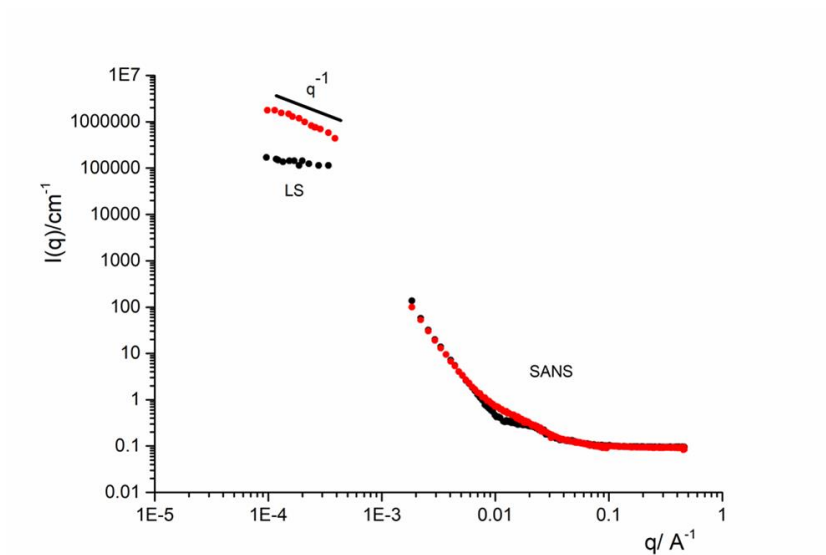


Figure 27. Dynamic Light Scattering (LS) and SANS analyses of *E. coli* cells in the absence (black points) and in the presence (red points) of $20 \mu\text{M}$ TL. LS measurements showed a decrease of the intensity with a q^{-1} power law for the treated sample, whereas this value remained essentially constant for the untreated sample.

Experimental section

Peptide Synthesis

Peptides were synthesized on solid phase by Fmoc chemistry on the MBHA (0.54 mmol/g) resin by consecutive deprotection, coupling and capping cycles ⁽¹²³⁾.

Biotin-conjugated TL was obtained by removing the amino terminal Fmoc group and coupling the peptide with N-(+)-Biotinyl-6-aminohexanoic acid in DMF employing the following conditions: 10 equivalents of N-(+)-Biotinyl-6-aminohexanoic acid + 9.8 equivalents of HATU (0.45 M in DMF)+ 14 equivalents of DIPEA; the solution was reacted with the peptide for 3 h at r.t. and double coupling was performed. Peptide was cleaved off the resin and deprotected by treatment with TFA/TIS/H₂O 95/2.5/2.5 v/v/v, 90 min. TFA was concentrated and peptides were precipitated in cold ethylic ether.

Purification of the peptides was performed by semi-preparative RP-HPLC using a gradient of acetonitrile (0.1% TFA) in water (0.1% TFA) from 30 to 85% in 30 min. Products were lyophilized three times and the peptides were characterized by MALDI tandem mass spectrometry (MALDI-MS/MS).

Bacterial cell growth and viability

The minimum inhibitory concentration (MIC) of TL was measured by broth microdilution. The cell strain of *E. coli* BL21 was incubated overnight in LB at 37°C. The culture was diluted to obtain a concentration of 0.08 OD₆₀₀ / mL in fresh medium and grown at 37°C for 90 minutes. At an OD/mL value of 0.5, 50 µl of bacterial suspension were added to ten wells and incubated with serial dilutions of the TL peptide from an initial concentration of 512 µM. The sterility control well contained

100 μ L of LB, while the growth control well contained 100 μ L of microbial suspension. *E. coli* cells were grown as previously described and the MIC was determined by the lowest concentration showing no visible growth after 24 h of incubation at 37°C by measuring the Abs at 600 nm. The assay was performed in triplicate.

Membrane proteins extraction.

E. coli cells were inoculated in 10 mL of liquid LB (*Luria-Bertani*) and placed at 37°C for 16 h under stirring. At the end of the incubation, bacterial cells were grown in 1L at 37°C under stirring for 3h. The pellet was recovered by centrifugation at 4°C for 15 minutes at 5000 rpm and stored at -80°C. The cell pellet was resuspended in 5 mL of *Cell Lysis Buffer* (20 mM Tris-HCl pH 8.0, 500 mM NaCl, 4 mM DTT, 1 mM PMSF) and subjected to mechanical lysis by French Press. The sample was then centrifuged at 4°C for 30 minutes at 10000 rpm in order to remove the cell debris and the supernatant recovered was ultracentrifuged for 2 hours at 4°C at 54,000 rpm. The obtained pellet was resuspended in solubilization buffer (50 mM Tris-HCl pH 8.0, 500 mM NaCl, 10% Glycerol, 4 mM DTT, 1 mM PMSF, 6 mM 3-[(3-Cholamidopropyl)dimethylammonio]-1-propanesulfonate (CHAPS)) under stirring at 4°C for 16 h. The sample was again ultracentrifuged for 2 hours at 4°C at 54,000 rpm. The supernatant containing cytosolic proteins was removed, while the membrane proteins were dissolved in solubilization buffer.

Pull Down experiments

The pull-down experiment was performed using 200 μL of dry avidin-conjugated agarose beads. The resin was divided in two portions, one portion was left unmodified and the second was incubated with a solution of 2 mg/mL of biotinylated TL for 30 minutes at 4°C under stirring. The supernatant was then removed by centrifugation at 4°C for 10 minutes at 3000 rpm and the resin equilibrated with 5 volumes of binding buffer at 4°C.

About 2.5 mg of membrane proteins were incubated on free agarose beads at 4°C for 2h under stirring to remove possible non-specific binding, according to the pre-cleaning procedure. The supernatant containing the unbound membrane proteins was recovered by centrifugation at 4°C for 10 minutes at 3000 rpm and then incubated on agarose beads with the immobilized peptide for 3h at 4°C under stirring. Beads were washed with 5 volumes of binding buffer and the peptide-interacting proteins were released by competitive elution with 500 μL of elution buffer containing an excess of biotin for 1h at 4°C under stirring.

TL putative protein interactors were fractionated by SDS-PAGE. Protein bands from sample and control lanes were excised from the gel and subjected to *in situ* hydrolysis with trypsin. The resulting peptide mixtures were analyzed by Liquid Chromatography/Tandem Mass Spectrometry (LC-MS/MS) using a LTQ Orbitrap XL Orbitrap mass spectrometer (Thermo Fisher Scientific, Bremen, Germany) and the data obtained were used to search for a non-redundant protein database using an in

house version of the Mascot software leading to identification of the putative AMP protein interactors. The putative peptide interactors were gathered within functional pathways by bioinformatic tools (DAVID, KEGG, STRING).

Docking calculations

The putative binding site of TL on FtsZ was determined using docking calculations. The structure of FtsZ has been modelled using SwissProt Model Server and the chain A of the structure of the protein from *P. aeruginosa* (2VAW, 60% sequence identity) as starting model^(124,125). The NMR structure of TL was kindly provided by Prof. Surajit Bhattacharyya. The peptide adopts an α -helix structure, in good agreement with CD spectra collected in solution⁽¹²⁶⁾. Interestingly, PEP-FOLD3 also predicts a helical structure for this peptide⁽¹²⁷⁾.

The model of the FtsZ-TL complex was obtained using FTDOCKs⁽¹²⁸⁾. The structure of the complex was then energy minimized and refined using Flexpeptdock⁽¹²⁹⁾. We have verified that the peptide binding site was predicted also by other docking programs and indeed the peptide binding site was predicted also by PEPDOCK and SWARMDOCK^(130,131). Analysis of the structure was done using Coot⁽¹³²⁾ figures were generated with PyMol (www.pymol.org).

Expression of Escherichia coli FtsZ and enzymatic assay

Untagged *E. coli* FtsZ was expressed from pET28a in BL21 cells. Cells were grown at 37 °C in 200 mL of LB culture media with 50 μ g/mL kanamycin and 0.4 mM isopropyl-beta-D-thiogalactopyranoside (IPTG) was added at an optical density of

~0.5 at 600 nm. The culture was grown for 90 min at 37°C for FtsZ production. Cells were harvested by centrifugation (5000 rpm during 15 min at 4 °C), and pellets were resuspended in Tris glycerol buffer (Tris glycerol buffer, 50 mM Tris-HCl, 50 mM KCl, 1 mM EDTA, 10% glycerol, pH 8.0) and were lysed on ice using a sonicator. The soluble fraction, containing the FtsZ protein, was separated from the cell debris by centrifugation (100,000 × g for 2 h at 4 °C).

The protein from the soluble fraction was precipitated with 30% ammonium sulfate for 16h. The sample was centrifuged (10000 rpm for 35 min at 4 °C), and the pellet was resuspended in 5 ml Tris glycerol buffer, pH 8.0 and dialyzed to remove the ammonium sulfate. The sample was purified by anion exchange chromatography using a Mono-Q HR 5/5 column equilibrated with Tris glycerol buffer, pH 8.0. FtsZ was retained on the column and was eluted with a 0–100% gradient of 1 M NaCl in the same buffer⁽¹³³⁾.

Protein concentration was estimated with Bradford reagent (Bio-Rad protein assay), protein purity was assessed by SDS- polyacrylamide gel electrophoresis (SDS-PAGE) and characterized by mass mapping using MALDI-MS/MS.

The activity of FtsZ on GTP substrate was determined with an enzymatic assay using BIOMOL® Green phosphate reagent (Biomol). Initially, FtsZ (6 µM) was incubated in 25 mM PIPES/NaOH, pH 6.8 for 30 minutes at 30°C. The enzyme was then treated with different concentrations of GTP, ranging from 0 µM to 250 µM, either in the absence or in the presence of 35 µM TL. The reaction was performed for 10 min and then stopped by addition of 100 µl BIOMOL® Green reagent and the increase in absorbance at 620 nm was measured following 25 min incubation. The experiment

was performed in duplicate. Kinetic parameters were fitted by non-linear regression with GraphPad Prism 4Project.

Binding experiment

Fluorescence experiments were performed at 25 °C in a 250 μ L quartz cuvettes (Hellma, Germany) on a VARIAN Cary Eclipse Fluorimeter. Titrations were carried out in 50 mM Tris-HCl buffer pH 7.2, 1M NaCl. Fluo-TL was excited at 440 nm (slit 5 nm) and the emission was monitored at 520 nm (slit 5 nm) without and in the presence of increasing concentrations of FtsZ protein (from 0.003 to 0.121 μ M) in a High Voltage mode. The peptide and the protein were dissolved at a 1.5 μ M concentration. All experiments were repeated in duplicate. The change in the fluorescence intensity of the reaction set was fit into “one site-specific binding” equation of GraphPad Prism 5 (GraphPad Software).

Optical Microscopy and TEM analyses

E. coli cells were inoculated in 10 mL of liquid LB and placed at 37°C for 16 h under stirring. At the end of the incubation, bacterial cells grown to 0.5 OD/mL were incubated with 20 μ M TL and allowed to grow for a further 5 h. A similar bacterial growth was prepared and used as control in the absence of the peptide. Samples of 100 μ L were observed by optical microscope using a ZEISS optical microscope for phase contrast and 50X magnifications.

TEM analyses were carried out on a JEOL JEM-1400 TEM with an accelerating voltage of 120kV. Digital images were collected with an EMSIS Xarosa digital camera with Radius software.

Scattering Measurements

E. coli cells were grown to 0.5 OD/mL in the presence and in the absence of 20 μ M TL up to 1 OD at 600 nm. Cells were then centrifuged at 5000 rpm for 15 min, treated with 0.4% paraformaldehyde for 10 min, washed with deuterated PBS1X for three times and the samples were finally resuspended in deuterated PBS1X.

Dynamic Light Scattering (DLS) measurements were performed by using a home-made instrument composed by a Photocor compact goniometer, a SMD 6000 Laser Quantum 50 mW light source operating at 532.5 nm, a photomultiplier (PMT-120-OP/B) and a correlator (Flex02-01D) from *Correlator.com* ^(134,135). All measurements were performed at 25 °C with the temperature controlled through the use of a thermostat bath.

All the measurements were performed in triplicate at fixed scattering angle of 90°. Small Angle Neutron Scattering (SANS) measurements were performed at 25 °C with the KWS-2 diffractometer operated by Julich Centre for Neutron Science at the FRMII source located at the Heinz Maier Leibnitz Centre, Garching (Germany). For all the samples, neutrons with a wavelength of 7 Å and $\Delta\lambda/\lambda \leq 0.2$ were used. A two-dimensional array detector at three different wavelength (W)/collimation (C)/sample-to-detector (D) distance combinations (W 7 Å/C 8 m/D 2 m, W 7 Å/C 8 m/D 8 m, and W 7 Å/C 20 m/ D 20 m) measured neutrons scattered from the samples. These

configurations allowed collecting data in a range of the scattering vector modulus q between 0.002 \AA^{-1} and 0.4 \AA^{-1} .

A deeper understanding of Magainin-2 mechanism of action

Pull-Down experiment

The second AMPs studied in this PhD project was Magainin-2 (Mag2). The mechanism of action of this peptide was investigated at the molecular level by preliminary functional proteomic experiments according to the procedure already used for Temporin L.

A biotinylated form of Mag2 was immobilized on avidin-conjugated agarose beads and incubated with a membrane protein extract from *E. coli* cells. The proteins specifically interacting with the peptide bait were eluted by competition, fractionated by SDS-PAGE and identified by LC-MS/MS analyses and database search. Proteins that were identified both in the control and in the sample were discarded, whereas those solely occurring in the sample and absent in the control were considered as putative Mag2 interactors. These putative protein interactors are listed in **Table 4**

Proteins	Peptides	SwissProt Code
Protein OmpA	13	P0A910
Protein OmpN	2	P77747
Protein OmpC	2	P06996
Protein OmpF	6	P02931
Porin NmpC	5	P21420
Porin PhoE	5	P02932
Prolipoprotein Lpp	2	P69776

Protein YhcB	4	P0ADW3
Protein TolC	6	P02930
Protein TolB	26	P0A855
Cell division coordinator CpoB	1	P45955
Maltoporin lamB	20	P02943
Multidrug efflux pump AcrA	12	P0AE06
Protein assembly factor BamA	5	P0A940
Protein assembly factor BamB	6	P77774
Protein assembly factor BamC	4	P0A903
Protein assembly factor BamD	7	P0AC02
Dehydratase FabZ	4	P0A6Q6
Modulator of FtsH protease HflK	10	P0ABC7
SecA	5	P0AFY8
FtsJ	1	P0C0R7
Cell division protein FtsZ	20	P0A9A6
Cell division protein FtsA	3	P0ABH0
Rod shape-determ P MreB	6	P0A9X4
MurG	4	P17443
MinD	9	P0AEZ3
Elongation factor Tu 1 (TufA)	32	P0CE48
Murein hydrolase activator NlpD	2	P0ADA3

LPS-Assembly protein LptD	2	P31554
Protein DnaA	4	P03004
Protein DnaJ	28	P08622
Transcrip termination Fact Rho (Rho)	5	P0AG30
Bifunctional protein PutA	4	P09546
Protein RecA	14	P0A7G6
LacI	4	P03023

Table 4. Putative protein interactors of Mag-2 from membrane extracts from E. coli cells.

Mag-2 putative interactors were then grouped according to their cellular localization and the biological processes they are involved into (**Fig. 27A**). A bioinformatic analysis using the STRING database was performed and the results are shown in **Fig. 27B**. A large number of protein interactors were involved in porin activity and protein insertion in membrane including Omp N/C/A and the BAM complex (ABCD).

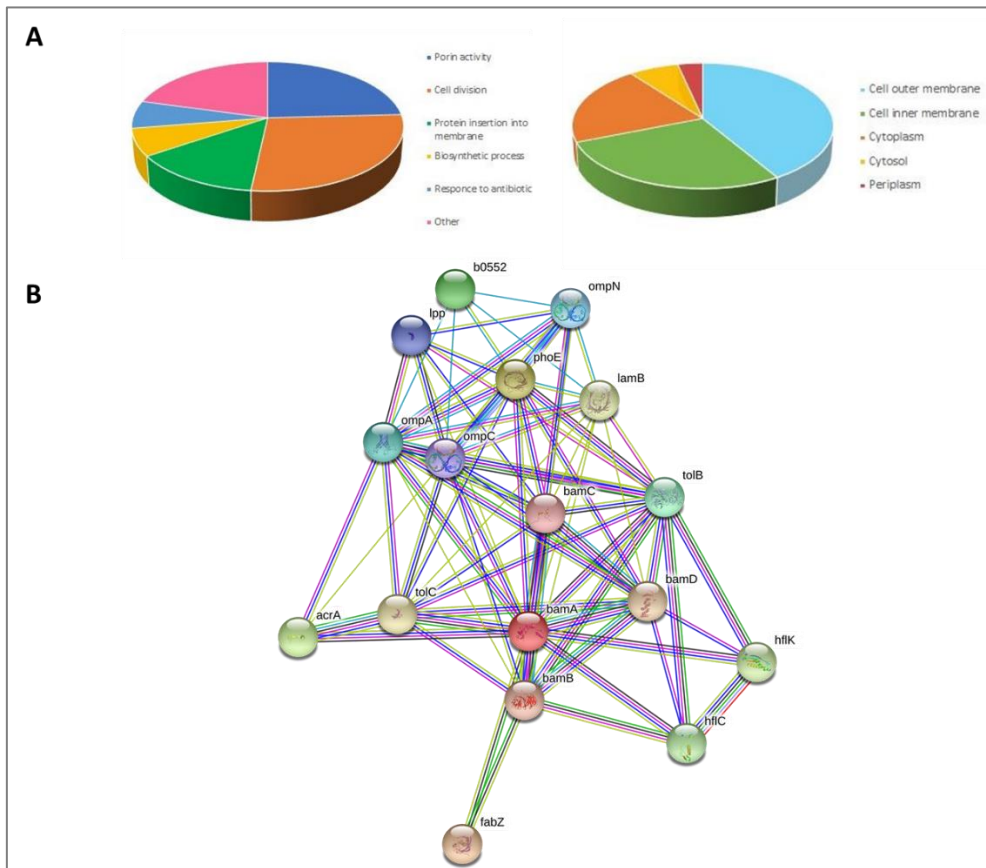


Figure 27. Bioinformatic analysis of Mag-2 proteins interactor. A) Distribution of Mag-2 putative protein partners identified in the pull-down experiment according to their cellular localization and biological functions. **B)** STRING analysis of the putative Mag-2 interactors belonging to the Omp N/C/A and the BAM complex (ABCD).

These results support literature data reporting the interaction of Mag-2 with the negatively charged membrane phospholipids. This interaction leads to the formation of transient pores that expand through the membrane and allow the translocation of the peptide into the inner membrane, leading to membrane disruption ⁽¹³⁶⁾.

Magainin-2 – BamA molecular docking

According to the pull-down experiment, BamA was identified as a putative Mag2 interactor. In order to support this hypothesis, a molecular docking analysis was performed in collaboration with Dr. Antonio Moretta, University of Basilicata at Potenza. All the interactions and the amino acids involved at the interface were determined using the PDBsum Server.

The results showed a favourable interaction between the peptide and the protein with the involvement of 193 non-bonded interactions and 7 hydrogen bonds as reported in **Fig. 28A** (schematic representation) and **Fig. 28B**. Moreover, in **Fig. 28C** are shown all the occurring interactions between the two molecules. The amino acid residues Thr359, Thr504, Lys610, Tyr649 and Asn666 from BamA were found to interact with Gly3, Asn22, Glu19, Asn22 and Ser23 of the Mag2 peptide respectively with Asn506 of BamA forming an interaction with both Met21 and Ser23 of Mag2. Residues involved in the hydrogen bonds belong to the β 6 and β 10 strands and to the L3 and L6 loops.

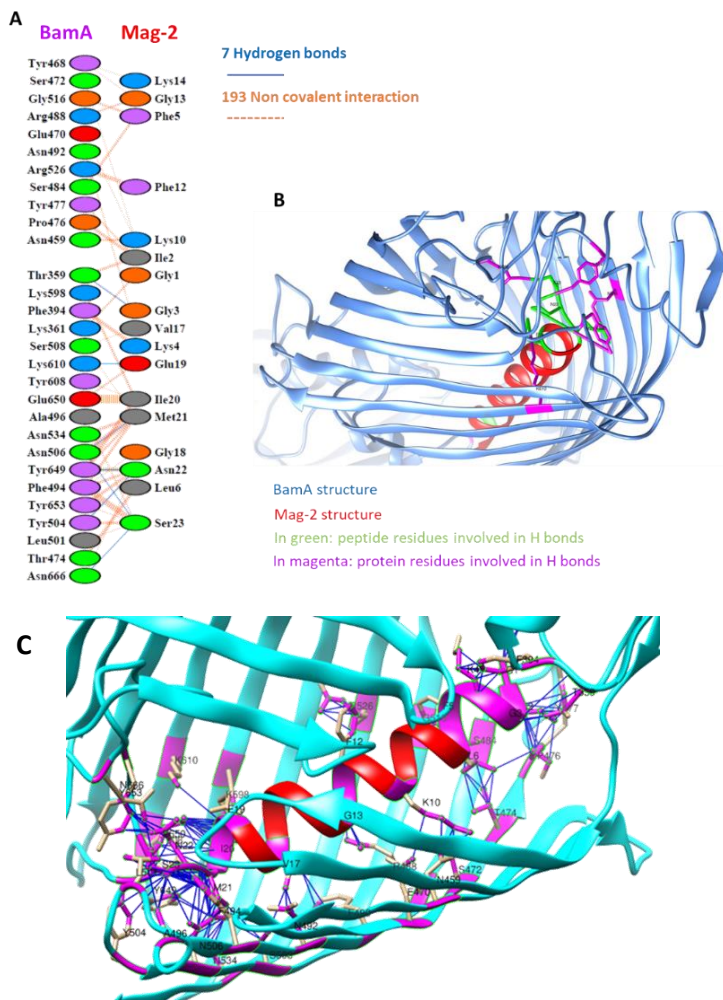


Figure 28. A) Schematic representation of the identified interactions. B) Protein-peptide docking. The image has been generated with CHIMERA. C) All residues (magenta) involved in the interaction (blue lines) between Mag2 peptide (red) and BamA protein (cyan).

Through the PRODIGY webserver, the Gibbs free energy, ΔG , and the dissociation constant, K_d , of the protein-peptide complex were predicted: $\Delta G = -14.6$ Kcal/mol; $K_d = 2.0E-11$ M (at 25 °C).

The BamA protein was already identified as a protein target for other peptides by Robinson, 2019⁽¹³⁷⁾. In particular, it was observed that the L6 loop of the BamA protein is involved in the interaction with the lectin-like bacteriocin LlpA, as we found for the Mag2 peptide. These results strongly support the interaction of Mag2 with the Bam complex that might be responsible for the stabilization of the membrane pore supporting the toroidal mechanism proposed in literature.

Experimental section

Peptide Synthesis

Peptides were synthesized on solid phase by Fmoc chemistry on the MBHA (0.54 mmol/g) resin by consecutive deprotection, coupling and capping cycles ⁽¹²³⁾.

Biotin-conjugated TL was obtained by removing the amino terminal Fmoc group and coupling the peptide with N-(+)-Biotinyl-6-aminohexanoic acid in DMF employing the following conditions: 10 equivalents of N-(+)-Biotinyl-6-aminohexanoic acid + 9.8 equivalents of HATU (0.45 M in DMF)+ 14 equivalents of DIPEA; the solution was reacted with the peptide for 3 h at r.t. and double coupling was performed. Peptide was cleaved off the resin and deprotected by treatment with TFA/TIS/H₂O 95/2.5/2.5 v/v/v, 90 min. TFA was concentrated and peptides were precipitated in cold ethylic ether.

Purification of the peptides was performed by semi-preparative RP-HPLC using a gradient of acetonitrile (0.1% TFA) in water (0.1% TFA) from 30 to 85% in 30 min. Products were lyophilized three times and the peptides were characterized by MALDI tandem mass spectrometry (MALDI-MS/MS).

Pull down

In order to performer the *pulldown* experiment with Mag-2 peptide, it was exploited the same protocol followed for TL peptide (pag 115).

Magainin-2 – BamA molecular docking

The putative binding sites of magainin-2 peptide on BamA protein were determined through molecular docking calculations. Both peptide and protein have

been modelled using I-TASSER Server^(138,139,140), while the Magainin-2-BamA complex model has been obtained using PatchDock Server⁽¹⁴¹⁾ and the structures have been refined with FireDock Server [5], which also gives the Global Energy, the Attractive and Repulsive Van der Waals (VdW) forces and the Atomic Contact Energy (ACE) values of the complex. Through the PDBsum Server^(142,143,144) all the interactions and the amino acids involved at the interface have been identified. The Gibbs free energy, ΔG , and the dissociation constant, K_d , of the protein-protein complex have been predicted using the PRODIGY webserver^(145,146,147). All the figures have been generated through UCSF CHIMERA software⁽¹⁴⁸⁾.

Investigation of the antimicrobial activity of Temporin-L and Magainin-2 on
different pathogenic strains

Determination of the Minimum Inhibit Concentration and Minimum Bactericidal Concentrations values on EUCAST reference strain of TL and Mag-2.

During my third year of PhD course I spend a period of time at the Department of Genetics and Genome Biology, University of Leicester, under the supervision of Prof. Marco Oggioni. In this period, I carried out a series of experiments to test the antimicrobial activity of Magainin-2 and Temporin-L against various wild type and multidrug-resistant bacterial strains including pathogenic species.

Different EUCAST (European Committee Antimicrobial Susceptibility Testing) strains were grown in the presence of serial dilution of the AMPs from 512 μM to 0.5 μM and the MIC values were determined as the lowest concentration showing no visible growth after 24h of incubation at 37°C.

In addition to the MIC values, the bactericidal activity of the AMPs was evaluated by determining the minimum bactericidal concentrations (MBCs). The MIC and MBC values of Mag2 and TL obtained in these experiments are summarized in **Table 5**.

The results demonstrated that Mag-2 does not exhibit a significant effect on almost all the strains, except for two Gram-negative bacteria *E.coli* and *H.influenzae* for which a weak bacteriostatic activity was monitored.

These data supported previous results obtained in the *Pull-down* experiment that identified Bam-A as a putative protein target of Mag-2. BamA is present only in Gram-negative bacteria thus explaining the absence of any antibacterial activity of the peptide on Gram-positive bacteria. However, Mag2 was ineffective also on some

Gram-negative strains. In order to understand this behaviour, the protein sequence of BamA from *E.coli* was aligned with the same protein from *P.aeruginosa* that was unaffected by Mag2. The result demonstrated that the sites predicted to be involved in the interaction with Mag-2 by the docking model are not conserved in BamA from *P.aeruginosa* suggesting that the peptide might be unable to interaction with the protein. This observation might explain at the molecular level the lack of antimicrobial activity of Mag2 on different bacterial strains.

On the contrary, TL showed a strong effect on both Gram-negative and Gram-positive bacteria. In particular on *E.coli*, *S.aureus* and *S. pneumonia* the peptide displayed bacteriostatic activity as indicated by the lower MIC values as compared to MBC values.

Strain	TL		Mag-2	
	MIC (µg/mL)	MBC (µg/mL)	MIC (µg/mL)	MBC (µg/mL)
<i>S. aureus</i> NCTC 12493	8	16	64	64
<i>E. coli</i> ATCC 25922	8	16	16	64
<i>E. coli</i> ATCC 35218	16	32	128	64
<i>K.Pneumoniae</i> ATCC 700603	> 512	512	> 512	>512
<i>P. aeruginosa</i> ATCC 27853	128	512	> 512	>512
<i>H. influenzae</i> ATCC49766	16	32	16	64
<i>S. pneumoniae</i> ATCC 49619	8	32	32	256
<i>E. feacalis</i> ATCC29212	> 512	> 512	>512	>512

Table5. MIC and MBC assay on different pathogenic strains.

Transmission electron microscopy

The effect of TL on *E.coli* (ATCC 25922), *S.aureus* (MRSA) (NCTC 12493) and *S.pneumonia* (NCTC 12977) strains was also investigated at the morphological level by TEM analyses. Bacterial strains were grown to 0.1OD in the presence of TL in sub-MIC concentration for 1h at 37°C. Cells were then centrifuged, washed with PBS and prepared for TEM microscopy.

Untreated cells of all bacteria species showed a classical cell morphology with undamaged structure (**Fig 29A, D, G**). Surprisingly, following treatment with sub-MIC concentration of TL, TEM investigations demonstrated that the peptide exerted different effects on each bacterial species. No damages were detected on *E. coli* cell membrane but the formation of long necklace-like structures indicated impairing of the cell division process caused by inhibition of the septation (**Fig 29 B and C**), confirming data obtained during my second year of PhD course.

In Gram-positive bacteria, a completely different effect was detected with possible alteration of cell membrane. In *S.pneumonia*, the sub-MIC concentration of TL showed the expected effect of membrane damages and leakage of the cytoplasmic content (**Fig 29 E and F**). On the contrary a completely different effect of the peptide was detected on *S.Aureus*. TEM images revealed the occurrence of several regularly distributed protrusions from the cell surface similar to bubbles or vesicles-like structures (**Fig 29 H and I**). However, these experiments did not provide data on the structure of these bubbles whether bilayer or monolayer and did not suggest their possible functions.

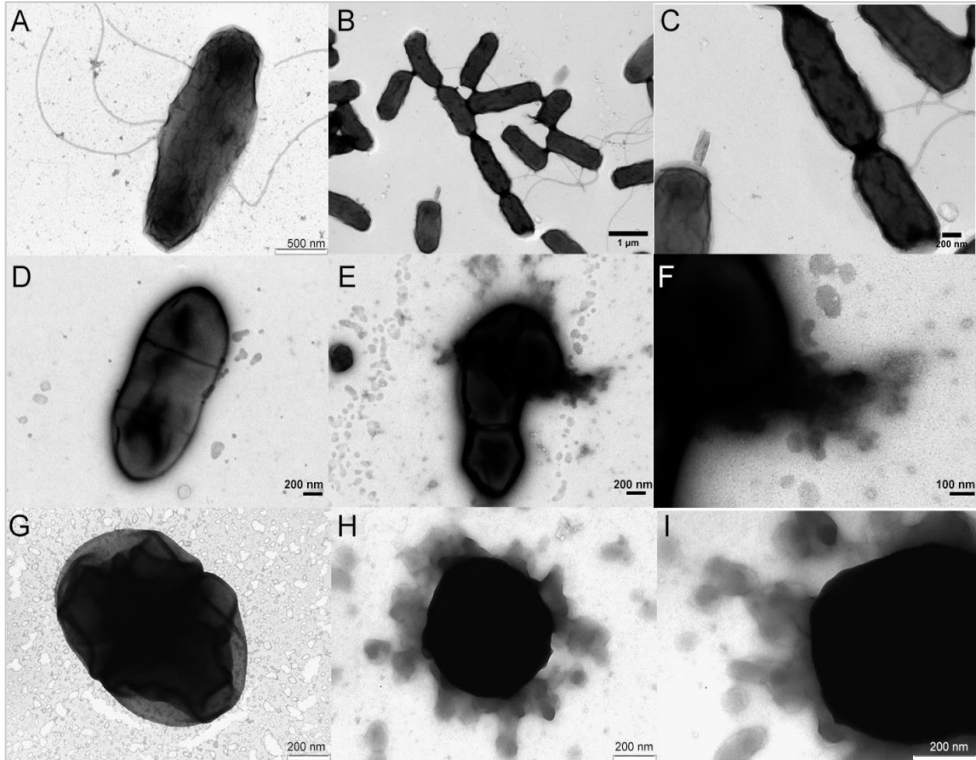


Figure 29 *E.coli* (A, B, C) *S.pneumonia* (D, E, F) and *S.aureus* (G, H, I) with and without treatment of TL.

Differential proteomic experiment

To analyse the effect of TL on *S.aureus* and elucidate the nature of the vesicle-like structures highlighted by TEM results, a differential proteomic experiment was designed according to the label-free procedure to compare the proteomic pattern on *S.aureus* before and after TL treatment.

S. aureus cells were grown in the same condition used for the TEM analysis, cells were lysed and the protein content digested with trypsin and analysed by nano LC-MS/MS procedures. Proteins were identified and their expression levels quantified for statistical significance using the MaXQuant software.

Preliminary data showed a total of 306 proteins identified, 68 down- and 238 up-regulated. In **Table 6** and **Table 7** were reported SwissProt code, protein name, gene, and FC for each proteins.

Swissprot Code	Proteins	Gene	FC
Q2FY73	Transcriptional regulator, putative	Fur, SAOUHSC_01592	0.31
Q2G2Q4	Ribosome-binding factor A	rbfA	0.31
Q2FWJ3	Serine-protein chinase RsbW	rbsW	0.34
P72360	Airon-sulfur cluster repaire proteine ScdA	scdA	0.34
Q2FXU0	Adenine phosphoribosyltransferase	apt	0.35
Q2G254	MazG domain-containing protein	SAOUHSC_01476	0.36
Q2G0R1	Hypoxanthine phosphoribosyltransferase	SAOUHSC_00485	0.37

Q2FW14	Ribosomal protein L29	rpmC	0.37
Q2G2F3	Signal transduction protein TRAP	traP	0.38
Q2FWE7	ATP synthase subunit delta	atpH	0.38
Q2FXG2	6,7-dimethyl-8-ribityllumazine synthase	ribH	0.39
Q2FXH9	Putative dipeptidase SAOUHSC_01868	SAOUHSC_01868	0.39
Q2G113	30S Ribosomal protein S6	rpsF	0.40
Q2FZX1	Uncharacterized protein	SAOUHSC_00864	0.40
Q2FZ53	3-oxoacyl-[acyl-carrier-protein] reductase	SAOUHSC_01199	0.40
Q2G0L4	Serine-aspartate repeat-containing protein D	sdrD	0.40
Q2FYLO	Phosphotransferase system enzyme II A, putative	SAOUHSC_01430	0.41
Q2FXE2	Aldo_ket_red domain-containing protein	SAOUHSC_01907	0.43
Q2FWB7	Ferritin domain containing protein	SAOUHSC_02381	0.43
Q2FXX8	5-methylthioadenosine/S-adenosylhomocysteine nucleosidase	mtnN	0.44
Q2G0T4	Nucleoid-associated protein SAOUHSC_00444	SAOUHSC_00444	0.46
Q2FXE8	Transaldolase	SAOUHSC_01901	0.48
Q2G0M7	Protein/nucleic acid declycase HchA	hchA	0.50
Q2G0L5	Serine-aspartate repeat-containing protein C	sdrC	0.50
Q2FY41	Elongation factor P	efp	0.50
Q2FXM0	Metal-dependent hydrolase SAOUHSC_01815	SAOUHSC_01815	0.50
P52078	Uncharacterized protein SAOUHSC_00997	SAOUHSC_00997	0.50
Q2G261	Superoxide dismutase [Mn/Fe]	sodM	0.52

Q2G0S5	Putative septation protein SpoVG	spoVG	0.52
Q2FYJ6	Extracellular matrix-binding protein ebh	ebh	0.52
Q2FZG5	Uncharacterized protein	SAOUHSC_01039	0.53
Q2FWX1	Uncharacterized protein	SAOUHSC_02150	0.53
Q2G1U6	Regulatory protein Spx	spxA	0.53
Q2G0S0	50S ribosomal protein L25	rplY	0.55
Q2FVA3	D-lactate dehydrogenase, putative	SAOUHSC_02830	0.56
Q2FZ83	Uncharacterized protein	SAOUHSC_01158	0.57
Q2FXY2	CRM domain-containing protein	SAOUHSC_01698	0.58
Q2FWJ5	S1 RNA binding domain protein	SAOUHSC_02297	0.59
Q2FUY2	Clumping factor B	clfB	0.61
Q2FYJ2	Alanine dehydrogenase 1	ald1	0.61
Q7BHL7	Regulatory protein MsrR	msrR	0.62
Q2FZE9	Iron-regulated surface determinant protein A	isdA	0.62
Q2G0D1	HTH-type transcriptional regulator SarX	sarX	0.64
Q2FZG6	Peptide deformylase	def	0.64
Q2G0R9	Peptidyl-tRNA hydrolase	ptH	0.64
Q2G224	Deoxyribose-phosphate aldolase	deoC	0.64
Q2FXG1	Riboflavin biosynthesis protein RibBA	ribBA	0.64
Q2G2U9	Transcriptional regulator SarA	sarA	0.65
Q2FXT0	50S ribosomal protein L27	rpmA	0.66
Q2FX98	HTH cro/C1-type domain-containing protein	SAOUHSC_01979	0.66
Q2FWN4	60kDa chaperonin	groL	0.67
Q2FW33	50S ribosomal protein L17	rplQ	0.67
Q2FW27	Adenylate kinase	adk	0.67
Q2G0Y9	Xanthine phosphoribosyltransferase	xpt	0.69

Q34090	Porphobilinogen deaminase	hemC	0.70
Q2FYI5	Cell cycle protein GpsB	gpsB	0.70
Q2FXI0	D-alanine aminotransferase	SAOUHSC_01867	0.72
Q2FW79	UPF0457 protein	SAOUHSC_02425	0.72
Q2FWZ8	Bacterial non-heme ferritin	ftnA	0.72
Q2G227	Phosphopentomutase	deoB	0.74
Q2FYG2	DNA-binding protein HU	SAOUHSC_01490	0.74
Q2FZ54	Malonyl CoA-acyl carrier protein transacylase	SAOUHSC_01198	0.74
Q2FZ70	Orotate phosphoribosyltransferase	pyrE	0.74
Q2G0Z2	Uncharacterized protein	SAOUHSC_00369	0.74
Q2FXA4	Ferrokelatase	hemH	0.75
Q2FXZ7	30S ribosomal protein S21	rpsU	0.76
Q2G030	Triosephosphate isomerase	tpiA	0.77

Table 6. S.aureus proteins down regulate after treatment with TL.

Swissprot Code	Proteins	Gene	FC
Q2FZY7	ABC transporter, ATP-binding protein, putative	SAOUSCH_00847	1,25
Q2G1U3	Oligoendopeptidase F	SAOUSCH_00937	1,25
Q2G1C0	Ribitol-5-phosphate cytidyltransferase 1	tarI	1,26
Q2G0L1	GTP cyclohydrolase FolE2	folE2	1,28
Q2FXW6	Uridine kinase	Udk	1,28
P95689	Serine--tRNA ligase	serS	1,3
Q2FV74	ATP-dependent Clp protease ATP-binding subunit ClpL	clpL	1,31
P48940	30S ribosomal protein S7	rpsG	1,32

Q2G0J0	Phosphate acetyltransferase	SAOUSCH_00574	1,34
Q2FW30	30S ribosomal protein S13	rpsM	1,36
Q2FY60	6-phosphogluconate dehydrogenase, decarboxylating	SAOUSCH_01605	1,36
Q2FZR9	3-oxoacyl-[acyl-carrier-protein] synthase 2	SAOUSCH_00921	1,38
P0A0B7	Alkyl hydroperoxide reductase C	ahpC	1,38
Q2G0M8	Aminotran_1_2 domain-containing protein	SAOUSCH_00532	1,39
Q2G2G7	UPF0637 protein SAOUHSC_01054	SAOUHSC_01054	1,39
Q2FZ46	Signal recognition particle protein	Ffh	1,39
P0A0H0	30S ribosomal protein S12	rpsL	1,41
Q2FW06	50S ribosomal protein L3	rplC	1,41
Q2G0Y6	GMP synthase [glutamine-hydrolyzing]	guaA	1,41
Q2FW10	30S ribosomal protein S19	rpsS	1,41
Q2G2G0	DM13 domain-containing protein	SAOUHSC_00717	1,42
Q2FXP7	Threonine--tRNA ligase	thrS	1,42
Q2G295	Catabolite control protein A	SAOUSCH_01850	1,42
Q2FVF5	Uncharacterized protein	SAOUSCH_02759	1,42
Q2G1G8	PTS system glucose-specific EIICBA component	ptsG	1,43
Q2FXM6	Acetyl-coenzyme A carboxylase carboxyl transferase	accD	1,43
Q2FVV8	Transcriptional regulator, putative	SAOUSCH_02583	1,44
Q2G0R0	ATP-dependent zinc metalloprotease FtsH	ftsH	1,45
Q2G0J1	Putative heme-dependent peroxidase SAOUHSC_00573	SAOUHSC_00573	1,45
Q2FXL4	N6_Mtase domain-containing protein	SAOUHSC_01821	1,45
Q2G247	UPF0478 protein SAOUHSC_01855	SAOUHSC_01855	1,46
Q2G1Z4	Proline--tRNA ligase	proS	1,47
Q2FY00	Uncharacterized protein	SAOUHSC_01675	1,47

Q2FW21	50S ribosomal protein L6	rplF	1,47
Q2FZ25	30S ribosomal protein S2	rpsB	1,47
Q2G2U1	Histidine protein kinase SaeS	saeS	1,47
Q2FYJ3	L-threonine dehydratase catabolic TdcB	tdcB	1,48
Q2FYI0	Penicillin-binding protein 2	SAOUHSC_01467	1,48
Q2G0Q9	33 kDa chaperonin	hslO	1,48
Q2FVK8	2,3-bisphosphoglycerate-dependent phosphoglycerate mutase	gpmA	1,49
Q2G2H4	Beta sliding clamp	SAOUHSC_00002	1,49
Q2FVT1	Lysostaphin resistance protein A	lyrA	1,5
Q2FW32	DNA-directed RNA polymerase subunit alpha	rpoA	1,5
Q2G115	Ribosome-binding ATPase YchF	ychF	1,51
P47768	DNA-directed RNA polymerase subunit beta	rpoB	1,51
Q2FZ59	Uncharacterized protein	SAOUHSC_01192	1,51
Q2FWZ0	Aspartyl/glutamyl-tRNA(Asn/Gln) amidotransferase subunit B	gatB	1,51
Q2FYF1	Elastin-binding protein EbpS	ebpS	1,53
Q2G1R9	Methionine--tRNA ligase	metG	1,53
Q2G029	2,3-bisphosphoglycerate-independent phosphoglycerate mutase	gpmI	1,53
Q2G0M4	Branched-chain-amino-acid aminotransferase	SAOUHSC_00536	1,53
Q2G2S0	Adenylosuccinate lyase	purB	1,54
Q2FZ27	GTP-sensing transcriptional pleiotropic repressor CodY	codY	1,55
Q2FW11	50S ribosomal protein L22	rplV	1,57
Q2FWD6	Putative aldehyde dehydrogenase	SAOUHSC_02363	1,57
Q2G0Q3	Lysine--tRNA ligase	lysS	1,57
Q2FXR3	Delta-aminolevulinic acid dehydratase	hemB	1,6
Q2FXS8	50S ribosomal protein L21	rplU	1,6

Q2FXL5	Acetate kinase	ackA	1,61
Q2FVW9	Fe/B12 periplasmic-binding domain-containing protein	SAOUHSC_02554	1,61
Q2G280	Thioredoxin domain-containing protein	SAOUHSC_01999	1,62
Q2FXZ3	Chaperone protein DnaJ	dnaJ	1,62
Q2FY36	Rhodanese domain-containing protein	SAOUHSC_01630	1,63
Q2FYT7	UPF0154 protein	SAOUHSC_01338	1,63
Q2FXQ1	50S ribosomal protein L20	rplT	1,63
Q2FWJ1	SigmaB regulation protein RsbU, putative	SAOUHSC_02301	1,64
Q2FZJ9	Probable quinol oxidase subunit 2	qoxA	1,64
P0C0V7	Phosphoglucosamine mutase	glmM	1,64
Q2FZS0	3-oxoacyl-[acyl-carrier-protein] synthase 3	fabH	1,65
Q2G248	Chorismate mutase domain-containing protein	SAOUHSC_01852	1,65
Q2FWA8	Lytic regulatory protein, putative	SAOUHSC_02390	1,66
Q2FWJ0	SigmaB regulation protein RsbU, putative	SAOUHSC_02302	1,66
Q2FWB8	Purine nucleoside phosphorylase DeoD-type	deoD	1,66
Q2FWE9	ATP synthase gamma chain	atpG	1,68
Q2G0P9	Uncharacterized protein	SAOUHSC_00501	1,68
Q2FZT4	Uncharacterized protein	SAOUHSC_00906	1,68
Q2FYT8	Transketolase	SAOUHSC_01337	1,68
Q2G0Q8	Cysteine synthase	SAOUHSC_00488	1,69
Q2FY42	Biotin carboxyl carrier protein of acetyl-CoA carboxylase	SAOUHSC_01624	1,69
Q2FYF5	Cytidylate kinase	SAOUHSC_01496	1,7
Q2G257	Uncharacterized protein	SAOUHSC_01477	1,7
Q2FY66	Glucose-6-phosphate 1-dehydrogenase	zwf	1,7
Q2FVL2	Uncharacterized protein	SAOUHSC_02699	1,7

Q2FW31	30S ribosomal protein S11	rpsK	1,71
Q2FZL5	1,4-dihydroxy-2-naphthoyl-CoA synthase	menB	1,71
Q2FZP9	Putative phosphoesterase SAOUHSC_00951	SAOUHSC_00951	1,71
Q2FZ72	Carbamoyl-phosphate synthase large chain	carB	1,71
Q2G2S6	Foldase protein PrsA	prsA	1,71
Q2FXP9	Translation initiation factor IF-3	infC	1,71
Q2FW23	30S ribosomal protein S5	rpsE	1,72
Q2FWF1	ATP synthase epsilon chain	atpC	1,73
Q2FWD4	UDP-N-acetylglucosamine carboxyvinyltransferase	1- murA	1,73
Q2FW38	50S ribosomal protein L13	rplM	1,73
Q2FZD8	Phenylalanine--tRNA ligase beta subunit	pheT	1,74
Q2FW75	ABC transporter periplasmic binding protein, putative	SAOUHSC_02430	1,75
Q2G2D2	Transcription termination/antitermination protein NusA	nusA	1,75
Q2FZY6	Uncharacterized protein	SAOUHSC_00848	1,75
Q2FWE5	Serine hydroxymethyltransferase	glyA	1,76
Q2G031	Phosphoglycerate kinase	pgk	1,76
Q2G0Y7	Inosine-5-monophosphate dehydrogenase	guaB	1,76
Q2FZT7	Signal peptidase I	SAOUHSC_00903	1,77
Q2G0N5	DNA-directed RNA polymerase subunit beta	rpoC	1,78
Q2FZ82	Isoleucine--tRNA ligase	ileS	1,79
Q2FW16	50S ribosomal protein L14	rplN	1,79
Q2FWY1	Probable manganese-dependent inorganic pyrophosphatase	ppaC	1,79
Q2FZK0	Probable quinol oxidase subunit 1	qoxB	1,8
Q2FV77	3-hydroxy-3-methylglutaryl coenzyme A reductase	SAOUHSC_02859	1,8
Q2G0L8	Uncharacterized protein	SAOUHSC_00542	1,8

Q2FXM8	ATP-dependent 6-phosphofructokinase	pfkA	1,82
Q2FY79	Transcriptional regulatory protein SrrA	srrA	1,82
Q2FVZ4	Lipid II:glycine glycytransferase	femX	1,82
Q2G2Q0	DNA gyrase subunit A	gyrA	1,83
P0A0J0	RNA polymerase sigma factor SigA	sigA	1,83
Q2FZU0	Glucose-6-phosphate isomerase	pgi	1,83
Q2FVD5	Uncharacterized oxidoreductase SAOUHSC_02778	SAOUHSC_02778	1,84
Q2FV87	PTS system glucoside-specific EIICBA component	glcB	1,85
Q2FXQ7	ATP-dependent Clp protease ATP- binding subunit ClpX	clpX	1,85
Q2FXI9	FtsK domain-containing protein	SAOUHSC_01857	1,85
O07325	Cell division protein FtsA	ftsA	1,85
P0A0F8	50S ribosomal protein L15	rplO	1,85
Q2FVX4	Molybdenum ABC transporter, periplasmic molybdate-binding protein	SAOUHSC_02549	1,86
Q2G1W5	NERD domain-containing protein	SAOUHSC_01908	1,86
Q2G2H5	Chromosomal replication initiator protein DnaA	dnaA	1,86
Q2FWD1	CTP synthase	pyrG	1,87
Q2FUQ3	tRNA uridine 5- carboxymethylaminomethyl modification enzyme MnmG	mnmG	1,88
Q2FYY6	Glutamine synthetase	SAOUHSC_01287	1,89
Q2FXM1	Usp domain-containing protein	SAOUHSC_01814	1,9
Q2G218	L-lactate dehydrogenase 1	ldh1	1,9
Q2G041	Thioredoxin reductase	SAOUHSC_00785	1,9
Q2FY08	Glycine--tRNA ligase	glyQS	1,9
O05204	Alkyl hydroperoxide reductase subunit F	ahpF	1,9
Q2FXA7	Uncharacterized protein	SAOUHSC_01958	1,91

Q2FXU5	Aspartate--tRNA ligase	aspS	1,92
Q2FWY9	Glutamyl-tRNA(Gln) amidotransferase subunit A	gatA	1,93
Q2FY55	DNA topoisomerase 4 subunit B	parE	1,93
Q2FXK6	30S ribosomal protein S4	rpsD	1,93
Q2G0N1	Elongation factor G	fusA	1,95
Q2G2W5	Biotin_lipoyl_2 domain-containing protein	SAOUHSC_02630	1,97
Q2G0P2	Transcription termination/antitermination protein NusG	nusG	1,97
Q2G1W0	Octopine_DH domain-containing protein	SAOUHSC_02574	1,97
Q2G1Y5	L-lactate dehydrogenase 2	ldh2	1,97
Q2FYR2	Aminoacyltransferase FemA	femA	1,97
Q2G2D0	Translation initiation factor IF-2	infB	1,99
Q2FVL4	Amino acid ABC transporter, ATP-binding protein, putative	SAOUHSC_02697	1,99
Q2FZ06	Uncharacterized protein	SAOUHSC_01265	2,02
Q2FWF0	ATP synthase subunit beta	atpD	2,02
Q2FYV7	Uncharacterized protein	SAOUHSC_01317	2,02
Q2FVN4	Uncharacterized protein	SAOUHSC_02668	2,02
Q2G2A4	Dihydrolipoamide acetyltransferase component of pyruvate dehydrogenase complex	SAOUHSC_01042	2,03
Q2FYP2	ABC transporter, ATP-binding protein, putative	SAOUHSC_01392	2,03
Q2FWE8	ATP synthase subunit alpha	atpA	2,03
Q2FZ22	Uridylate kinase	pyrH	2,04
Q2G111	30S ribosomal protein S18	rpsR	2,05
Q2G1W2	Phosphoenolpyruvate carboxykinase (ATP)	pckA	2,05
Q2FZ19	Ribonuclease J 2	rnj2	2,07
Q2FYF9	30S ribosomal protein S1, putative	SAOUHSC_01493	2,07

Q2FZV7	NADH dehydrogenase-like protein	SAOUHSC_00878	2,08
Q2G028	Enolase	eno	2,1
Q2FVB4	ABC transporter domain-containing protein	SAOUHSC_02820	2,1
Q2G235	Nicotinate phosphoribosyltransferase	SAOUHSC_02133	2,11
Q2FZ58	Uncharacterized protein	SAOUHSC_01193	2,12
Q2G0T9	Alpha amylase family protein, putative	SAOUHSC_00438	2,14
Q2FYT0	Glycine betaine transporter, putative	SAOUHSC_01346	2,15
Q2FXM9	Pyruvate kinase	pyk	2,16
Q2FYZ5	Glycerol kinase	glpK	2,17
Q2FZ42	50S ribosomal protein L19	rplS	2,17
Q2FZC7	Iron-sulphur subunit of succinate dehydrogenase, putative	SAOUHSC_01105	2,18
Q2FXM7	Acetyl-coenzyme A carboxylase carboxyl transferase subunit alpha	accA	2,18
Q2FXT8	Multifunctional fusion protein	secD	2,19
Q2G2P2	Globin domain protein	SAOUHSC_00204	2,2
Q2FZ20	Polyribonucleotide nucleotidyltransferase	pnp	2,21
Q2G064	Peptidase T	pepT	2,22
Q2FY54	Dihydrolipoamide acetyltransferase component of pyruvate dehydrogenase complex	SAOUHSC_01611	2,23
O06446	Protein translocase subunit SecA 1	secA1	2,23
Q2FZW3	Protein DltD	dltD	2,29
Q2FW12	30S ribosomal protein S3	rpsC	2,29
Q2FXK8	Septation ring formation regulator EzrA	ezrA	2,29
Q2G078	Ribonucleoside-diphosphate reductase	SAOUHSC_00742	2,31
Q2FZ75	Aspartate carbamoyltransferase	pyrB	2,33
Q2FX94	Fumarate hydratase class II	fumC	2,34

Q2FZY3	UPF0051 protein SAOUHSC_00851	SAOUHSC_00851	2,35
Q2G1W4	S-adenosylmethionine synthase	metK	2,36
Q2FZX4	Lipoyl synthase	lipA	2,36
Q2FVW4	Putative 2-hydroxyacid dehydrogenase SAOUHSC_02577	SAOUHSC_02577	2,37
Q2FXJ7	1-acyl-sn-glycerol-3-phosphate acyltransferases domain protein	SAOUHSC_01837	2,38
Q2FXZ6	Uncharacterized protein	SAOUHSC_01679	2,39
Q2FYS9	Aconitate hydratase	SAOUHSC_01347	2,39
Q2FWE6	Uracil phosphoribosyltransferase	upp	2,41
Q2FV16	Probable malate:quinone oxidoreductase	mqqo	2,44
Q2FVW3	FAD_binding_3 domain-containing protein	SAOUHSC_02579	2,44
Q2G2A3	Dihydrolipoyl dehydrogenase	SAOUHSC_01043	2,49
Q2FWA0	Glutamine--fructose-6-phosphate aminotransferase [isomerizing]	glmS	2,49
Q2G124	Probable acetyl-CoA acyltransferase	SAOUHSC_00336	2,5
Q2G274	DNA gyrase subunit B	gyrB	2,51
Q2FZ08	Ribonuclease Y	rny	2,51
Q2G2A5	Pyruvate dehydrogenase complex, E1 component, pyruvate dehydrogenase beta subunit, putative	SAOUHSC_01041	2,52
P60393	Ribosomal RNA small subunit methyltransferase H	rsmH	2,53
Q2FY78	8 Pseudouridine synthase	SAOUHSC_01587	2,56
Q2FWB5	EVE domain-containing protein	SAOUHSC_02383	2,56
Q2G1D8	Formate acetyltransferase	pflB	2,56
Q2FYH6	Asparagine--tRNA ligase	asnS	2,57
Q2FXJ6	PDZ domain-containing protein	SAOUHSC_01838	2,58
Q2FXZ9	UPF0365 protein SAOUHSC_01676	SAOUHSC_01676	2,59
Q2G1D7	Pyruvate formate-lyase-activating enzyme	pflA	2,61

Q2G032	Glyceraldehyde-3-phosphate dehydrogenase	SAOUHSC_00795	2,63
Q2G0G1	Alcohol dehydrogenase	adh	2,64
Q2FXL6	Putative universal stress protein SAOUHSC_01819	SAOUHSC_01819	2,67
Q2FZ89	Cell division protein FtsZ	ftsZ	2,7
Q2FZG4	Pyruvate dehydrogenase E1 component subunit alpha	pdhA	2,73
Q2G0N0	Elongation factor Tu	tuf	2,74
Q2FZS8	Chaperone protein ClpB	clpB	2,74
Q2FY53	2-oxoisovalerate dehydrogenase, E1 component, beta subunit, putative	SAOUHSC_01612	2,74
Q2FY15	DEAD-box ATP-dependent RNA helicase CshB	cshB	2,76
Q2G296	Formate--tetrahydrofolate ligase	fhs	2,8
Q2FZW0	Pyr_redox_2 domain-containing protein	SAOUHSC_00875	2,83
Q2FWG4	Membrane protein insertase YidC	yidC	2,85
Q2FZ37	Succinate--CoA ligase [ADP-forming] subunit beta	sucC	2,86
Q2G045	HPr kinase/phosphorylase	hprK	2,87
Q2FZP4	Peptide chain release factor 3	prfC	2,9
Q2FWF4	UDP-N-acetylglucosamine 1-carboxyvinyltransferase	murA	2,92
Q2FZU5	Glutamate dehydrogenase	SAOUHSC_00895	2,95
Q2FXI5	Uncharacterized protein	SAOUHSC_01861	2,96
Q2FZ36	Succinate--CoA ligase [ADP-forming] subunit alpha	sucD	2,98
Q2FZP2	Serine protease HtrA-like	SAOUHSC_00958	2,98
Q2FZ09	Protein RecA	recA	2,98
Q2G283	Glutamate-1-semialdehyde 2,1-aminomutase 2	hemL2	2,98
P60430	50S ribosomal protein L2	rplB	3

Q2G2S7	Metallophos domain-containing protein	SAOUHSC_01975	3,01
Q2FXT1	GTPase Obg	obg	3,04
Q2FWC1	Pyrimidine-nucleoside phosphorylase	pdp	3,1
Q2FY27	Glucokinase, putative	SAOUHSC_01646	3,16
Q2FW93	Uncharacterized protein	SAOUHSC_02406	3,19
Q2FY52	2-oxoisovalerate dehydrogenase, E1 component, alpha subunit, putative	SAOUHSC_01613	3,2
Q2G0S2	Ribose-phosphate pyrophosphokinase	prs	3,28
Q2FZ86	Cell division protein SepF	sepF	3,31
Q2G268	Coenzyme A biosynthesis bifunctional protein CoaBC	SAOUHSC_01178	3,32
Q2FXJ0	UDP-N-acetylmuramate--L-alanine ligase	murC	3,38

Table 7. S.aureus proteins up regulate after treatment with TL.

Most of the up regulated proteins belonged to pathways involved in synthesis of cell wall components, cell division, metabolic processes and response to antibiotic. In particular, proteins involved in the synthesis of cell wall components including MurA, GlmS, MurC and cell division including FtsA, FtsK, SecA, YidC, SepF suggested the hypothesis that TL treatment stimulated the bilayer formation inducing membrane extroflexion thus originating the vesicles-like structures observed in TEM analyses. Moreover, TL treatment might also affect *S.aureus* pathogenicity as several proteins involved in pathogenicity and adhesion cell were down-regulated following incubation with the peptide.

The most important were SarA, SarX, MrsR^(150, 151) involved in virulence regulation and cell adhesion including SdrD and SdrC proteins⁽¹⁵²⁾.

Experimental section

EUCAST reference strains

A collection of EUCAST reference strains was used in this work.

Gram-negative bacteria *Escherichia coli* (ATCC 25922), *Escherichia coli* TEM-1 β -lactamase (ATCC 35218), *Pseudomonas aeruginosa* (ATCC 27853), *Klebsiella pneumoniae* (ATCC 700603) were cultured on Luria Bertani agar and broth; *Haemophilus influenzae* (NCTC 12975) was cultured on Chocolate agar plate and Luria Bertani broth.

Gram-positive methicillin-resistant bacteria *Staphylococcus aureus* (MRSA) (NCTC 12493) and *Enterococcus faecalis* (NTCC 12697) were cultured respectively on Luria Bertani agar and broth while *Streptococcus pneumoniae* (NCTC 12977) on Blood plate and in BHI broth.

All bacteria were incubated aerobically at 37°C for 18 h except *Streptococcus pneumoniae*, which was incubated in CO₂-enriched atmosphere.

Bacterial susceptibility testing

The minimum inhibitory concentration (MIC) of TL and Mag-2 was calculated by broth microdilution. The bacterial strains were incubated overnight in LB at 37°C. The cultures were diluted approximately to 5X10⁵ CFU/mL and 50 μ L of bacterial suspension was added to ten wells and incubated with serial dilutions of peptides from an initial concentration of 512 μ M. The sterility control well contained 100 μ L of LB, while the growth control well contained 100 μ L of microbial suspension. The plates were incubated at 37°C for 16/ 20h grown and the MIC was determined by the lowest concentration showing no visible growth by measuring the absorbance at 600 nm. For

the minimum bactericidal concentration (MBC), the MIC well and the wells with concentration higher than MIC value were plated on agar plate and incubated at 37°C for 16/ 20h. The MBC value was determined as the amount of AMPs allowing no colony growth from the directly plated content of the wells. All MIC and MBC determinations of all assays were performed in triplicate.

TEM analysis

Escherichia coli (ATCC 25922), *Staphylococcus aureus* (MRSA) (NCTC 12493) and *Streptococcus pneumoniae* (NCTC 12977) cells were grown to 0.2OD/mL600nm and treated with MIC and Sub-MIC concentration of TL for 1h at 37°C. After the incubation, bacterial cells were centrifuged at 3000 rpm for 15 min, washed with PBS and resuspended in PBS and 2.5% glutaraldehyde to fix the samples. 10 µL of sample were applied to a glow discharged formvar/carbon film copper mesh grid and leave to adsorb for 2 minutes. The liquid excess was removed by water washes, stained with 1% uranyl acetate, applied and the grids were dried before TEM analyses.

TEM analyses were carried out on a JEOL JEM-1400 TEM with an accelerating voltage of 120kV. Digital images were collected with an EMSIS Xarosa digital camera with Radius software.

Proteomic analysis.

Differential proteomic analysis was carried out on *S.aureus* incubated with and without TL for 60 min. Cells were harvested by centrifugation of 5 mL of bacterial culture. After triple washing with PBS, the bacterial pellet was resuspended in lysis

buffer (100 mM Tris HCl, 2% SDS, 100 mM DTT, and 100 μ L of a cocktail of proteinase inhibitors; pH 7.6), and incubated for 5 min at 95°C. The solution was then sonicated for 30 min on ice (with 200 W power). After, the suspension was centrifuged (16,100 rpm, 10 min) to obtain the supernatant, which was used for the measurement of protein concentration with a Bradford Assay⁽¹⁴⁹⁾.

Protein extracts for each condition were digested by trypsin onto S-Trap filters, following the standard protein digestion protocol of the manufacturer (Protifi, Huntington, NY). The biological replicates analysed were two for untreated cells, three for 60 min treated cells. Each biological replicate was analyzed in duplicate by nano LC-MS/MS using the chromatographic system Easy-nLC II coupled with a LTQ Orbitrap XL mass spectrometer (ThermoFisher Scientific, Waltham, MA). Peptide mixtures were separated on a C18 capillary column (5 μ m biosphere, 75 μ m ID, 200 mm length) using a non-linear 5% to 50% gradient of eluent B (95% acetonitrile, 0.2% formic acid) over 260 min.

The mass analyses were performed in Data Dependent Acquisition (DDA) mode by fragmenting the 10 most intense ions in CID modality. Protein identification and quantification were carried out by MaxQuant software (v.1.5.2.8) using UniProt *S.aureus* as database for Andromeda search. Parameters used for protein identification were: a minimum of 2 peptides, including at least 1 unique one; variable modifications allowed were methionine oxidation and pyroglutamate formation on N-terminal glutamine; accuracy for first search was set to 10 ppm, then lowered to 5 ppm in the main search; 0.01 FDR was used with a reverse database for decoy; retention time alignment and second peptides search functions were allowed. For protein

quantification, a minimum of 2 unique peptides were required and no modifications were allowed. The fold changes (FCs) were calculated according to LFQ values.

Chapter 4

Discussion

Microorganisms have the extraordinary ability to live in almost any environment and to protect themselves from external agents through sophisticated survival mechanisms such as biofilm formation. Biofilms consist of a complex microbial community adhering to biotic or abiotic surfaces and enclosed within a protein/polysaccharide self-produced matrix. Formation of this structure represents the most important adaptive mechanism that leads to antibacterial resistance and therefore closely connected to pathogenicity.

Identification of key proteins involved in biofilm production is the first step to define new compounds capable of affecting biofilm formation in bacteria, leaving the pathogen exposed to antibiotics and avoiding the development of resistance.

The effect of alkylating stress in biofilm formation in *E.coli* and *M.smegmatis* was investigated by differential proteomic approaches using the Differential in Gel Electrophoresis procedure (DIGE). Besides the down regulation of various proteins belonging to metabolic processes, the most intriguing result in *E.coli* was the strong decrease in the expression of the N-acetylneuraminase lyase (NanA), an enzyme involved in sialic acid metabolism. Since sialic acid was widely recognized as a signaling molecule in biofilm formation and cell-cell interactions, we then investigated the biological role of NanA in biofilm formation.

When the *E.coli* cells were treated with 0,04% MMS, biofilm formation was drastically decreased. To investigate whether this event was related to the decrease of NanA expression, a null NanA mutant, $\Delta nanA$, was produced and used in biofilm formation experiments. $\Delta nanA$ showed a phenotype nearly superimposable to wild type *E.coli* under methylation stress conditions. Moreover, complementation assays

demonstrated that re-integration of the lyase NanA restored the ability of the mutant strain to adhere to abiotic surface with a concomitant great increase in biofilm formation. Finally, inhibition of NanA enzymatic activity with a sialic acid analogue (DANA) resulted in a clear decrease in biofilm production supporting by the pivotal role of NanA in this process.

Surprisingly, a completely different results was observed in *M.smeg* under methylation stress conditions with a large increase in biofilm formation in the presence of MMS. Quantitative analysis of proteomic profiles showed that most of the up-regulated proteins gathered within cell wall biosynthesis, energy metabolic processes and biofilm formation. These data suggested that *M.smeg* response to damaging events led to an increase in the expression of proteins involved in cellular defence mechanisms.

Among the up-regulated proteins, we focused our attention on the Bifunctional protein GlmU, an enzyme involved in the de novo biosynthetic pathway for UDP-N-acetylglucosamine (UDP-GlcNAc) that was reported to play a key role in biofilm production. Biofilm levels in *M.smegmatis* were then measured in the presence of two different GlmU inhibitors, iodoacetamide (IAA) and N-Acetylglucosamine-1-phosphate (GlcNAc-1P), demonstrating that inhibition of GlmU led to a strong decrease in biofilm formation.

The pivotal role of this enzyme in the defence mechanisms elicited by *M. smegmatis* upon alkylation stress was confirmed by using a conditional GlmU deletion mutant in collaboration with Prof. Nandikoori from “National Institute of

Immunology” at New Delhi. A drastic reduction of biofilm formation was observed in the mutant thus demonstrating a critical role for GlmU in this process.

Altogether these data demonstrated that differential proteomic approaches are instrumental to evaluate the global effect of biofilm formation conditions on bacterial cells and have the ability to identify specific proteins involved in the process of biofilm production. Interestingly, NanA and GlmU, the two enzymes playing key role in the mechanism of biofilm generation in *E.coli* and *M.smegmatis* respectively, belong to two strictly related pathways that connect sialic acid metabolism and the amino sugars biosynthesis.

Moreover, NanA and GlmU proteins occur within the proteome of well known opportunistic pathogens such as *S.Aureus* (both NanA and GlmU), *K.pneumoniae* (GlmU) and *P.aeruginosa* (GlmU) and **are exclusive to prokaryotes being absent in humans**. This observation opens up the way to the development of compounds that can effectively target these enzymes, that are essential for the biosynthesis and assembly of the pathogens cell wall and involved in the formation of biofilm protective architecture.

These results address this project to the development of new procedures and compounds as antimicrobial peptide that can effectively and specifically impair biofilm formation in opportunistic bacteria with slight effects on cell survival. In this respect AMPs are attractive candidates for the design of new antibiotics because of their natural antimicrobial properties and a low propensity for the development of resistance.

AMPs represent an interesting class of molecules with large possible applications in the biomedical field. In this project I evaluated the antimicrobial activity of Magainin-2 and Temporin-L against various wild type and multidrug-resistant bacterial strains including pathogen species.

Magainin-2 showed a low activity on pathogenic bacteria strains, except form *E.coli*. The mechanism of action was investigated by functional proteomic experiments showing that Mag2 might interact with proteins involved in porin activity and protein insertion in membrane including Omp N/C/A and BAM complex (ABCD). Preliminary docking experiments confirmed the interaction with BamA suggesting that Magainin-2 might stabilize the pore structure supporting the toroidal mechanism proposed in literature.

On the contrary, Temporin-L showed significant and surprisingly different effects on Gram-negative and Gram-positive bacteria. Pull down experiments suggested that the peptide might interact with proteins belonging to the divisome complex including FtsZ, FtsA, MurG, MukB and MreB. Docking studies, enzymatic assays and fluorescence experiments demonstrated a direct interaction of TL with the FtsZ protein leading to the inhibition of its GTPase activity with a competitive mechanisms. FtsZ is the protein responsible for the correct formation of the Z disk during bacterial cell division. Inhibition of FtsZ might then result in impairing cell division. DLS measurements and SANS analyses supported this hypothesis clearly demonstrating that in the presence of TL *E.coli* cells generated a very much larger structure showing no damages in the cell membran.e Finally, morphologic investigations of *E. coli* cells in the presence of TL by both optical microscopy measurements and TEM analyses

revealed the formation of largely elongated “necklace-like” structures originated by a multitude of bacterial cells, demonstrating that the presence of the peptide hinders *E. coli* cells division.

Since FtsZ is responsible for a crucial biological event of bacterial life and it is absent in humans, this protein might represent a good target for the rational design of new antibiotics.

A different effect of TL was observed in *S. pneumonia*, where a predominant disruption of cell membrane causing the release of cytoplasmic material occurred. Finally, in *S. aureus*, TL treatment a peculiar effect on cell membrane inducing the formation of numerous regularly distributed protrusions from the cell surface. Differential proteomic experiments carried out on *S. aureus* before and after TL treatment indicated the up-regulation of several proteins belonged to pathways involved in the synthesis of cell wall components, cell division, metabolic processes and response to antibiotic. These preliminary data suggested the hypothesis that TL treatment stimulated the bilayer formation inducing membrane extroflexion that originated the vesicles-like structures observed in TEM analyses. Moreover, TL treatment might also affect *S. aureus* pathogenicity several proteins involved in pathogenicity and adhesion cell were down-regulated following TL incubation.

Bibliography

1. Rodney M. Donlan. "Biofilms: Microbial Life on Surfaces". *Emerging Infectious Diseases* (2002) pp 881 – 890.
2. Hans-Curt Flemming, Thomas R. Neu, and Daniel J. Wozniak.. "The EPS Matrix: The "House of Biofilm Cells". *JOURNAL OF BACTERIOLOGY* (2007), pp 7945–7947
3. C. Dobell "Antony van Leeuwenhoek and his "Little animals." Being Some Account of the Father of Protozoology and Bacteriology and his Multifarious Discoveries in these Disciplines. Collected, Translated, and Edited, from his Printed Works, Unpublished Manuscripts, and Contemporary Records. Published on the 300th Anniversary of his Birth." New York: Dover Publications INC, (1960), 239–55).
4. H. Heukelekian, A. Heller "Relation between Food Concentration and Surface for Bacterial Growth" *J. Bacteriol*, 40 (1940), 547–558.
5. Henrici A.T. "Studies of Freshwater Bacteria: I. A Direct Microscopic Technique.) *J Bacteriol.* (1933), 277-87.
6. C. E. Zobell, "The Effect of Solid Surfaces upon Bacterial Activity" *J. Bacteriol*, 46 (1943), 39-56.
7. N. Rabin, Y. Zheng, C. Opoku-Temeng, Y. Du, H. O. Sintim "Biofilm formation mechanisms and targets for developing antibiofilm agents" *Future Med. Chem.* 74 (2015), 493-512.

8. Montanaro L., Poggi A., Visai L., Ravaioli S., Campoccia D., Speziale P., Arciola C. "Extracellular DNA in biofilms". *Int J Artif Organs* (2011), pp 824-831.
9. HC. Flemming, TR. Neu, DJ. Wozniak "The EPS Matrix: The "House of Biofilm Cells" *J. Bacteriol.*, 189 (2007), 7945–7947.
10. D. López, H. Vlamakis, R. Kolter "Biofilms" *Cold Spring Harb Perspect Biol.*, 2 (2010), 1-11.
11. Davey M. and George A. O'toole.. "Microbial Biofilms: from Ecology to Molecular Genetics". *MICROB. AND MOLECULAR BIOLOGY REVIEWS* (2000) pp 847–867.
12. JP. O’Gara "Ica and beyond: biofilm mechanisms and regulation in *Staphylococcus epidermidis* and *Staphylococcus aureus*" *FEMS Microbiol Lett.*, 270 (2007), 179–188.
13. Ryder C1, Byrd M, Wozniak DJ "Role of polysaccharides in *Pseudomonas aeruginosa* biofilm development" *Curr Opin Microbiol.* (2007) 644-8.
14. AH. Tart, DJ Wozniak "Shifting Paradigms in *Pseudomonas aeruginosa* Biofilm Research" *Bacterial Biofilms*, 322 (2008), 193-206.
15. JNC. Fong, FH Yildizi "Biofilm Matrix Proteins" *American Society for Microbiology* (2015).
16. L. Montanaro, A. Poggi, L. Visai, S. Ravaioli, D. Campoccia, P. Speziale, CR. Arciola "Extracellular DNA in Biofilms" *Int J Artif Organs*, 34 (2011), 824-31.

17. "Secreted single-stranded DNA is involved in the initial phase of biofilm formation by *Neisseria gonorrhoeae*" *Environmental Microbiology*, 16 (2014), 1040-1052.
18. ME. Davey, GA. O'toole. "Microbial biofilms: from ecology to molecular genetics" *Microbiol. Mol. Biol. Rev.*, 64.4 (2000), 847-867.
19. P. Thomen, J. Robert, A. Monmeyran, AF. Bitbol, C. Douarche, N. Henry. "Bacterial biofilm under flow: First a physical struggle to stay, then a matter of breathing" *Plos One*, 12 (2017)
20. WM. Weaver, V. Milisavljevic, JF. Miller, D. Di Carlo "Fluid Flow Induces Biofilm Formation in *Staphylococcus epidermidis* Polysaccharide Intracellular Adhesin-Positive Clinical Isolates" *Applied and Environmental Microbiology*, 78 (2012), 5890-5896.
21. R. Rusconi, M. Garren, R. Stocker "Microfluidics expanding the frontiers of microbial ecology, Bacterial biofilm under flow: First a physical struggle to stay, then a matter of breathing" *Annual Review of Biophysics*, 43 (2014), 65-91.
22. Y. Yawata, J. Nguyen, R. Stocker, R. Rusconi "Microfluidic Studies of Biofilm Formation in Dynamic Environments" *J. Bacteriol*, 198 (2016), 2589-2595.
23. Y. Liu, JH Tay "Metabolic response of biofilm to shear stress in fixed-film culture". *J. Appl. Microbiol*, 90 (2001), 337-342.

24. P. Stoodley, K. Sauer, DG. Davies, JW Costerton “Biofilm sas complex differentiated communities” *Annual Review of Microbiology*, 56 (2002), 187-209.
25. N. Liu, T. Skauge, DL. Marban, B. Hovland, B. Thorbjornsen, FA. Radu, BF. Vik, T. Baumann, G. Bodtker “Microfluidic study of effects of flow velocity and nutrient concentration on biofilm accumulation and adhesive strength in the fowing and no-fowing microchannels” *Journal of Industrial Microbiology & Biotechnology*, 46 (2019) 855–868.
26. V. Cepas, Y. López, E. Muñoz, D. Rolo, C. Ardanuy, S. Martí, M. Xercavins, JP. Horcajada, J. Bosch, SM. Soto “Relationship Between Biofilm Formation and Antimicrobial Resistance in Gram-Negative Bacteria” *Microbial Drug Resistance*, 25 (2019), 72-79.
27. JM. Munita, CA. Arias “Mechanisms of Antibiotic Resistance” *American Society for Microbiology*, 17 (2016)
28. J. Davies “Inactivation of antibiotics and the dissemination of resistance genes.” *Science*, 264 (1994), 375-382.
29. H. Nikaido “Antibiotic resistance caused by gram-negative multidrug efflux pumps.” *Clin. Infect. Dis.*, 27 (1998), S32-S41.
30. Costerton JW1, Stewart PS, Greenberg EP. “Bacterial biofilms: a common cause of persistent infections”.*Science*. (1999),1318-22.

31. Schierle CF1, De la Garza M, Mustoe TA, Galiano RD. "Staphylococcal biofilms impair wound healing by delaying reepithelialization in a murine cutaneous wound model". *Wound Repair Regen* (2009), 354-9.
32. JC. Nickel, I. Ruseska, JB. Wright, JW. Costerton "Tobramycin resistance of *Pseudomonas aeruginosa* cells growing as a biofilm on urinary catheter material" *Antimicrob. Agents Chemother*, 27 (1985), 619-624.
33. SB. I. Luppens, MW. Reij, RW. L. van der Heijden, FM. Rombouts, T. Abee "Development of a standard test to assess the resistance of *Staphylococcus aureus* biofilm cells to disinfectants" *Appl. Environ. Microbiol.*, 68 (2002), 4194-4200.
34. R. Patel "Biofilms and Antimicrobial Resistance" *Clinical Orthopaedics and Related Research*, 437 (2005), 41-47.
35. RM. Donlan "Role of Biofilms in Antimicrobial Resistance" *ASAIO*, 46 (2000), S47-S52.
36. CL. Ventola, MS "The Antibiotic Resistance Crisis Part 1: Causes and Threats" *Pharmacy and Therapeutics*, 40 (2015), 277-283.
37. RJ. Dubos "Studies on a bactericidal agent extracted from a soil *Bacillus*: I. Preparation of the agent. Its Activity in Vitro" *J Exp Med*, 70 (1939), 1-10.
38. HL. Van Epps "René Dubos: unearthing antibiotics" *J Exp Med* 203, (2006), 259.
39. Wang G, Li X, Wang Z (2017) The antimicrobial peptide database. <http://apsunmcedu/AP/mainphp> Accessed 20 March 2017).

40. HS. Joo, CI. Fu, M. Otto "Bacterial strategies of resistance to antimicrobial peptides" *Phil. Trans. R. Soc. B*, 371(2016), 1-11.
41. S. Ray, HPS. Dhaked, D. Panda "Antimicrobial peptide CRAMP (16-33) Stalls Bacterial Cytokinesis by Inhibiting FtsZ Assembly" *Biochemistry*, 53,41 (2014), 6426-6429.
42. A. Boto, JM. Pérez de la Lastra, CC. González "The Road from Host-Defense Peptides to a New Generation of Antimicrobial Drugs" *Molecules*, 23 (2018), 311.
43. NJ. Lakshmaiah, JY. Chen "Antimicrobial peptides: Possible anti-infective agents" *Peptides*, 72 (2015), 88-94.
44. F. Guilhelmelli, N. Vilela, P. Albuquerque, L. da S. Derengowski, IS. Pereira, CM. Kyaw "Antibiotic development challenges: the various mechanisms of action of antimicrobial peptides and of bacterial resistance" *Front. Microbiol.*, 4 (2013), 1-2.
45. MR. Yeaman, NY. Yount "Mechanisms of antimicrobial peptide action and resistance" *Pharmacol. Rev.*, 55 (2003), 27-55.
46. KA. Brogden "Antimicrobial peptides: Pore formers or metabolic inhibitors in bacteria?" *Nat. Rev. Microbiol.*, 3 (2005), 238-250.
47. WC. Wimley "Describing the Mechanism of Antimicrobial Peptide Action with the Interfacial Activity Model" *ACS Chem Biol*, 5, 10 (2015), 905-917.

48. Z. Yang, J.C. Weisshaar “HaloTag Assay Suggests Common Mechanism of *E. coli* Membrane Permeabilization Induced by Cationic Peptides” *ACS chemical biology*, 13 (2018), 2161-2169.
49. C.F. Le, C.M. Fang, S.D. Sekaranc. “Intracellular Targeting Mechanisms by Antimicrobial Peptides” *Antimicrob Agents and Chem.*, 61 (2017), 1-16.
50. G. Batoni, G. Maisetta, S. Eisin “Antimicrobial peptides and their interaction with biofilms of medically relevant bacteria” *BBA- Biomembranes*, 1858 (2016), 1044-1060.
51. M. Yasir, MDP. Willcox, D. Dutta “Action of Antimicrobial Peptides against Bacterial Biofilms” *MDPI* 11 (2018), 2468.
52. A. Algburi, N. Comito, D. Kashtanov, LMT. Dicks, ML. Chikindas “Control of Biofilm Formation: Antibiotics and Beyond” *Applied and Environmental Microbiology*, 83 (2017), e02508-16.
53. M.B. Miller, B.L. Bassler “Quorum sensing in bacteria” *Annu. Rev. Microbiol.*, 55 (2001), 165-199.
54. D. Pletzer, S.R. Coleman, R.W. Hancock “Anti-biofilm peptides as a new weapon in antimicrobial warfare” *Elsevier*, 33 (2016), 35-40.
55. A. Giacometti, O. Cirioni, M.S. Del Prete, F. Barchiesi, M. Fortuna, D. Drenaggi, G. Scalise “In vitro activities of membrane-active peptides alone and in combination

with clinically used antimicrobial agents against *Stenotrophomonas maltophilia*” *Antimicrob. Agents Chemother.*, 44 (2000), 1716-1719.

56. MS. Zharkova¹, DS. Orlov, O. Yu. Golubeva, OB. Chakchir, IE. Eliseev, TM. Grinchuk, OV. Shamova “Application of Antimicrobial Peptides of the Innate Immune System in Combination with Conventional Antibiotics—A Novel Way to Combat Antibiotic Resistance?” *Front. Cell. Infect. Microbiol.*, 9 (2019), 1-23.

57. A. Lewies, JF. Wentzela, A. Jordaan, C. Bezuidenhout, LH. Du Plessisa “Interactions of the antimicrobial peptide nisin Z with conventional antibiotics and the use of nanostructured lipid carriers to enhance antimicrobial activity” *International Journal of Pharmaceutics*, 526 (2017), 244-253.

58. R. Geitani, CA. Moubareck, L. Touqui, DK. Sarkis “Cationic antimicrobial peptides: alternatives and/or adjuvants to antibiotics active against methicillin-resistant *Staphylococcus aureus* and multidrug-resistant *Pseudomonas aeruginosa*” *BMC Microbiology*, 54 (2019), 1-12.

59. GYC. Cheung, EL. Fisher, JW. McCausland, J. Choi, JWM. Collins, SW. Dickey, M. Otto “Antimicrobial Peptide Resistance Mechanism Contributes to *Staphylococcus aureus* Infection” *The Journal of Infectious Diseases*, 217 (2018), 1153–1159.

60. MS. Lupa, P. Mydel, K. Krawczyk, K. Wójcik, M. Puklo, B. Lupa, P. Suder, J. Silberring, M. Reed, J. Pohl, W. Shafer, F. McAleese, T. Foster, J. Travis, J. Potempa

“Degradation of human antimicrobial peptide LL-37 by *Staphylococcus aureus*-derived proteinases” *Antimicrob. Agents Chemother.*, 48 (2004), 4673-4679.

61. P. Teufel, F. Götz “Characterization of an extracellular metalloprotease with elastase activity from *Staphylococcus epidermidis*” *J. Bacteriol.*, 175 (1993), 4218-4224.

62. A. Peschel, M. Otto, RW. Jack, H. Kalbacherl, G. Jung and Friedrich Götz “Inactivation of the *dlt* operon in *Staphylococcus aureus* confers sensitivity to defensins, protegrins, and other antimicrobial peptides” *The Journal of Biological Chemistry*, 274 (1999), 8405–8410.

63. SM. McBride, AL. Sonenshein “The *dlt* operon confers resistance to cationic antimicrobial peptides in *Clostridium difficile*” *Microbiology*, 157 (2011), 1457-1465.

64. B. Bechinger, SU. Gorr “Antimicrobial Peptides Mechanisms of Action and Resistance” *VEDI RIVISTA* 96 (2016), 254-260.

65. SM. Moskowitz, RK. Ernst, SI. Miller “PmrAB, a two-component regulatory system of *Pseudomonas aeruginosa* that modulates resistance to cationic antimicrobial peptides and addition of aminoarabinose to lipid A” *J. Bacteriol.*, 186 (2004), 575-579.

66. LA. Rollins-Smith, LK. Reinert, CJ. O’Leary, LE. Houston, DC. Woodhams “Antimicrobial Peptide Defenses in Amphibian Skin” *Integrative and Comparative Biology*, 45 (2005), 137–142.

67. A. Bhunia, R. Saravanan, H. Mohanram, ML. Mangoni, S. Bhattacharjya “NMR structures and interactions of temporin-1Tl and temporin-1Tb with lipopolysaccharide micelles: mechanistic insights into outer membrane permeabilization and synergistic activity” *J Biol Chem.*, 286 (2011), 24394-24406.
68. C. Avitabile, L. D. D'Andrea, M. Saviano, A. Romanelli “Determination of the secondary structure of peptides in the presence of Gram positive bacterium *S. epidermidis* cells” *Rsc Adv.*, 6 (2016), 51407-51410.
69. C. Avitabile, LD. D'Andrea, A. Romanelli “Studying the Interaction of Magainin 2 and Cecropin A with *E. coli* Bacterial Cells Using Circular Dichroism” *Antimicrobial Peptides*, 1548 (2006) 247-253.
70. Caterino M., Chandler R., Sloan J. L, Dorko K, Cusmano-Ozog K., Ingenito L, Strom S. C., Imperlini E., Scolamiero E., Venditti C.P., Ruoppolo M. “The proteome of methylmalonic acidemia (MMA): the elucidation of altered pathways in patient livers”. *Molecular Biosystems*. 12 (2016), 566-574.
71. Vertommen D., Ruiz N., Leverrier P., Silhavy J.T, and Collet JF. “Characterization of the role of the *Escherichia coli* periplasmic chaperone SurA using differential proteomics” *Proteomics* 9. (2009) 2432–2443.
72. Rippa V., Duilio, A., di Pasquale, P., Amoresano, A., Landini, P., Volkert, M.R. “Preferential DNA damage prevention by the *E. coli* AidB gene: A new mechanism for the protection of specific genes”. *DNA repair* 10 (2011), 934-941

73. Vimr, E.R. “Unified Theory of Bacterial Sialometabolism: How and Why Bacteria Metabolize Host Sialic Acids”. *ISRN Microbiol* 2013 (2013), 816713.
74. Trappetti C., Kadioglu A, Carter M, Hayre J, Iannelli, F, Pozzi, G. Andrew PW, Oggioni MR. “Sialic acid: a preventable signal for pneumococcal biofilm formation, colonization and invasion of the host. *J.Infect.Dis.* 199, (2009) 1497–1505.
75. Boudeau J., Glasser, A.L., Masseret, E., Joly B., Darfeuille-Michaud, A. “Invasive ability of an *Escherichia coli* strain isolated from the ileal mucosa of a patient with Crohn's disease”. *Infect. Immun* 67 (1999), 4499-509.
76. Bringer, M.A., Billard, E., Glasser, A.L., Colombel, J.F., Darfeuille-Michaud, A. “Replication of Crohn's disease-associated AIEC within macrophages is dependent on TNF- α secretion”. *Lab. Invest* 92 (2012), 411-9.
77. Datsenko, K.A., Wanner, B.L.” One-step inactivation of chromosomal genes in *Escherichia coli* K-12 using PCR products”. *Proc. Natl. Acad. Sci. USA* 97 (2000), 6640-5.
78. Caterino, M., Ruoppolo, M., Fulcoli, G., Huynh, T., Orrù, S., Baldini, A., Salvatore, F. “Transcription factor TBX1 overexpression induces downregulation of proteins involved in retinoic acid metabolism: a comparative proteomic analysis”. *J. Proteome Res* 8 (2009), 1515-26.
79. Cella, L., Conson, M., Caterino, M., De Rosa, N., Liuzzi, R., Picardi, M., Grimaldi, F., Solla, R., Farella, A., Salvatore, M., Pacelli, R. “Thyroid V30 predicts radiation-induced hypothyroidism in patients treated with sequential chemo-

radiotherapy for Hodgkin's lymphoma". *Int. J. Radiat. Oncol. Biol. Phys* 82 (2012), 1802-8.

80. Livak, K.J., Schmittgen, T.D. "Analysis of Relative Gene Expression Data Using RealTime Quantitative PCR and the 22DDCT Method". *Methods* 25 (2001), 402-408.

81. Darfeuille-Michaud, A., Boudeau, J., Bulois, P., Neut, C., Glasser, A.L., Barnich, N., Bringer, M.A., Swidsinski, A., Beaugerie, L., Colombel, J.F. "High prevalence of adherent-invasive *Escherichia coli* associated with ileal mucosa in Crohn's disease". *Gastroenterology* 127(2014), 412-421.

82. Agrawal, P., Miryala, S. and Varshney, U. "Use of *Mycobacterium smegmatis* deficient in ADP ribosyltransferase as surrogate for *Mycobacterium tuberculosis* in drug testing and mutation analysis". *PLoS One* 13(2015), e0122076.

83. Caterino, M., Ruoppolo, M., Fulcoli, G., Huynh, T., Orrù, S., Baldini, A., Salvatore, F. "Transcription factor TBX1 overexpression induces downregulation of proteins involved in retinoic acid metabolism: a comparative proteomic analysis". *J Proteome Res.* 8 (2009), 1515-1526.

84. Arita-Morioka, K., Yamanaka, K., Mizunoe, Y., Ogura, T. and Sugimoto, S. "Novel strategy for biofilm inhibition by using small molecules targeting molecular chaperone DnaK". *Antimicrob. Agents Chemother.* 59 (2015), 633-641.

85. Ojha, A., Anand, M., Bhatt, A., Kremer, L., Jacobs, W.R. Jr., and Hatfull, G.F. "GroEL1: a dedicated chaperone involved in mycolic acid biosynthesis during biofilm formation in mycobacteria". *Cell* 123 (2005), 861-873.

86. Jiao X, Sherman BT, Stephens R, Baseler MW, Lane HC, Lempicki RA. "DAVID-WS: a stateful web service to facilitate gene/protein list analysis". *Bioinformatics* 28 (2012), 1805-1806.
87. Burton, E., Gawande, P.V., Yakandawala, N., LoVetri, K., Zhanel, G.G., Romeo, T., Friesen, A.D. and Madhyastha, S. "Antibiofilm activity of GlmU enzyme inhibitors against catheter-associated uropathogens". *Antimicrob Agents Chemother.* 50 (2006), 1835-1840.
88. Sharma, R., Rao Lambu, M., Jamwa, U., Rani, C.2, Chib, R., Wazir, P., Mukherjee, D., Chaubey, A. and Ali Khan, I. "Escherichia coli N-Acetylglucosamine-1-Phosphate-Uridyltransferase/ Glucosamine-1-Phosphate-Acetyltransferase (GlmU) Inhibitory Activity of Terreic Acid Isolated from *Aspergillus terreus*". *J. Biomol. Screening* 21 (2016), 342-353.
89. Itoh Y, Wang X, Hinnebusch B J, Preston J F 3rd, Romeo T. "Depolymerization of beta-1,6-N-acetyl-D-glucosamine disrupts the integrity of diverse bacterial biofilm". *J. Bacteriol* 187 (2005), 382-387.
90. Chen, J.W, Scaria, J, Chang, YF. "Phenotypic and transcriptomic response of auxotrophic *Mycobacterium avium* subsp. *paratuberculosis* leuD mutant under environmental stress". *PLoS One* 7, (2012) e37884.
91. Lessard, I.A., Walsh, C.T. "VanX, a bacterial D-alanyl-D-alanine dipeptidase: resistance, immunity, or survival function?" *Proc Natl Acad Sci U S A.* 96(1999), 11028-11032.

92. Di Pasquale, P., Caterino, M., Di Somma, A., Squillace, M., Rossi, E., Landini, P., Iebba, V., Schippa, S., Papa, R., Selan, L., Artini, M., Palamara, A. T., and Duilio, A. "Exposure of *E. coli* to DNA-Methylating Agents Impairs Biofilm Formation and Invasion of Eukaryotic Cells via Down Regulation of the N-Acetylneuraminase Lyase NanA". *Frontiers in Microbiology* 7 (2016), 147.
93. Suman E, D'souza SJ, Jacob P, Sushruth MR, Kotian MS. "Anti-biofilm and anti-adherence activity of Glm-U inhibitors". *Indian J Med Sci.* 65(2011), 387-92.
94. Soni, V., Upadhyay, S., Suryadevara, P., Samla, G., Singh, A., Yogeewari, P., Sriram, D., Nandicoori, V. K. "Depletion of *M.tuberculosis* GlmU from Infected Murine Lungs Effects the Clearance of the Pathogen". *PLoS Pathog.* 11 (2015), e1005235.
95. Parikh, A., Kumar, D., Chawla, Y., Kurthkoti, K., Khan, S., Varshney, U. and Nandicoori, V.K. "Development of a new generation of vectors for gene expression, gene replacement, and protein-protein interaction studies in mycobacteria". *Appl Environ Microbiol.* 79 (2013), 1718-1729.
96. Pandey, A.K., Raman, S., Proff, R., Joshi, S., Kang, C.M., Rubin, E.J., Husson, R.N. and Sassetti, C.M. "Nitrile-inducible gene expression in mycobacteria". *Tuberculosis (Edinb).* **89** (2009), 12-16.
97. Pompeo, F., van Heijenoort, J., Mengin-Lecreulx, D. "Probing the role of cysteine residues in glucosamine-1-phosphate acetyltransferase activity of the

- bifunctional glmU protein from *Escherichia coli*: Site-directed mutagenesis and characterization of the mutant enzymes". *J. Bacteriol.* 180 (1998), 4799–4803.
98. Zhang Z, Bulloch E M.M, Bunker R.D, Baker E.N, Squire C J. "Structure and function of GlmU from *Mycobacterium tuberculosis*". *Acta Crystallogr D Biol Crystallogr.* 65(2009), 275–283.
99. Mengin-Lecreulx, D. & van Heijenoort, J. *J. Bacteriol.* 175(1993), 6150–6157.
100. Buurman ET, Andrews B, Gao N, Hu J, Keating TA, Lahiri S, Otterbein LR, Patten AD, Stokes SS, Shapiro AB "In Vitro Validation of Acetyltransferase Activity of GlmU as an Antibacterial Target in *Haemophilus influenzae*". *J boil chem.* 286(2011), 40734-40742.
101. Stokes SS, Albert R, Buurman ET, Andrews B, Shapiro AB, Green M, McKenzie AR, Otterbeinb LR. "Inhibitors of the acetyltransferase domain of N-acetylglucosamine-1-phosphate-uridylyltransferase/glucosamine-1-phosphate-acetyltransferase (GlmU). Part 2: Optimization of physical properties leading to antibacterial aryl sulfonamides". *Bioorg Med Chem Lett.* Vol22. (2012), 1510-1519.
102. Sharma, R., Rani, C., Mehra, R., Nargotra, A., Chib, R., Rajput, VS., Kumar, S., Singh, S., Sharm,a P.R. and Khan I.A. "Identification and characterization of novel small molecule inhibitors of the acetyltransferase activity of *Escherichia coli* N-acetylglucosamine-1-phosphate-uridylyltransferase/glucosamine-1-phosphate acetyltransferase (GlmU)". *Appl Microbiol Biotechnol.* 100, (2016) 3071-3085.

103. Chen, J.W, Scaria, J, Chang, YF. “Phenotypic and transcriptomic response of auxotrophic *Mycobacterium avium* subsp. paratuberculosis leuD mutant under environmental stress”. *PLoS One* 7(2012), e37884.
104. Agrawal, P., Miryala, S. and Varshney, U. “Use of *Mycobacterium smegmatis* deficient in ADP ribosyltransferase as surrogate for *Mycobacterium tuberculosis* in drug testing and mutation analysis”. *PLoS One* 13 (2015), e0122076.
105. Imperlini, E., Santorelli, L., Orru', S., Scolamiero, E., Ruoppolo, M., Caterino, M. “Mass Spectrometry-Based Metabolomic and Proteomic Strategies in Organic Acidemias”. *Biomed Res Int.* 2016, (2016) 9210408.
106. Chandler, R.J., Caterino, M., Sloan, J.L., Dorko, K., Cusmano-Ozog, K., Ingenito, L., Strom, S.C., Imperlini, E., Scolamiero, E., Venditti, C.P. and Ruoppolo, M. “The hepatic proteome of methylmalonic acidemia (MMA): elucidation of altered cellular pathway in humans”. *Mol Biosyst.* 12, (2016) 566-574.
107. Caterino, M., Pastore, A., Strozziro, M.G., Di Giovamberardino, G., Imperlini, E., Scolamiero, E., Ingenito, L., Boenzi, S., Ceravolo, F., Martinelli, D., Dionisi-Vici, C. and Ruoppolo, M. “The proteome of cblC defect: in vivo elucidation of altered cellular pathways in humans”. *J Inherit Metab Dis.* 38(2015), 969-977.
108. Capobianco, V., Caterino, M., Iaffaldano, L., Nardelli, C., Sirico, A., Del Vecchio, L., Martinelli, P., Pastore, L., Pucci, P, Sacchetti, L. “Proteome analysis of human amniotic mesenchymal stem cells (hA-MSCs) reveals impaired antioxidant

ability, cytoskeleton and metabolic functionality in maternal obesity”. *Sci Rep.* 6 (2016), 25270.

109. Barbarani, G., Ronchi, A., Ruoppolo, M., Santorelli, L., Steinfeld, R., Elangovan, S., Fugazza, C., Caterino, M. “Unravelling pathways downstream Sox6 induction in K562 erythroid cells by proteomic analysis”. *Sci Rep.* 7(2017), 14088.

110. Spaziani, S., Imperlini, E., Mancini, A., Caterino, M., Buono, P. and Orrù, S. “Insulin-like growth factor 1 receptor signaling induced by supraphysiological doses of IGF-1 in human peripheral blood lymphocytes”. *Proteomics* 14(2014), 1623-1629.

111. Caterino, M., Aspesi, A., Pavesi, E., Imperlini, E., Pagnozzi, D., Ingenito, L., Santoro, C., Dianzani, I., Ruoppolo, M. “Analysis of the interactome of ribosomal protein S19 mutants”. *Proteomics* 14(2014), 2286-96.

112. Imperlini, E., Spaziani, S., Mancini, A., Caterino, M., Buono, P. and Orrù, S. “Synergistic effect of DHT and IGF-1 hyperstimulation in human peripheral blood lymphocytes”. *Proteomics* 15(2015), 1813-1818.

113. Caterino, M., Zacchia, M., Costanzo, M., Bruno, G., Arcaniolo, D., Trepiccione, F., Siciliano, R.A., Mazzeo, M.F., Ruoppolo, M., Capasso, G. Urine “Proteomics Revealed a Significant Correlation Between Urine-Fibronectin Abundance and Estimated-GFR Decline in Patients with Bardet-Biedl Syndrome”. *Kidney Blood Press Res.* 43(2018), 89-405.

114. Alberio, T., Pieroni, L., Ronci, M., Banfi, C., Bongarzone, I., Bottoni, P., Brioschi, M., Caterino, M., Chinello, C., Cormio, A., Cozzolino, F., Cunsolo, V.,

Fontana, S., Garavaglia, B., Giusti, L., Greco, V., Lucacchini, A., Maffioli, E., Magni, F., Monteleone, F., Monti, M., Monti, V., Musicco, C., Petrosillo, G., Porcelli, V., Saletti, R., Scatena, R., Soggiu, A., Tedeschi, G., Zilocchi, M., Roncada, P., Urbani, A., Fasano, M. "Toward the Standardization of Mitochondrial Proteomics: The Italian Mitochondrial Human Proteome Project Initiative". *J Proteome Res.* 16(2017), 4319-4329.

115. Caterino, M., Ruoppolo, M., Mandola, A., Costanzo, M., Orrù, S., Imperlini, E. "Protein-protein interaction networks as a new perspective to evaluate distinct functional roles of voltage-dependent anion channel isoforms". *Mol Biosyst.* 13(2017), 2466-2476.

116. Jain, P., Hsu, T., Arai, M., Biermann, K., Thaler, D.S., Nguyen, A., González, P.A., Tufariello, J.M., Kriakov, J., Chen, B., Larsen, M.H. and Jacobs, W.R. Jr. "Specialized transduction designed for precise high-throughput unmarked deletions in *Mycobacterium tuberculosis*". *M Bio* 5(2014), e01245-14.

117. Monti M, Cozzolino M, Cozzolino F, Vitiello G, Tedesco R, Flagiello A, Pucci P. "Puzzle of protein complexes in vivo: a present and future challenge for functional proteomics". *Expert Rev Proteomics.* (2009) 159-169.

118. Monti M., Orrù S., Pagnozzi D., Pucci P. "Functional proteomics". *Clinica Chimica Acta* (2005), 140–150.

119. Monti M., Orrù S., Pagnozzi D., Pucci P. "Interaction Proteomics" *Bioscience Reports* Vol 25(2005), 45-56.

120. Monti M, Cozzolino M, Cozzolino F, Tedesco R, Pucci P. "Functional proteomics: protein-protein interactions in vivo". *Ital J Biochem.* (2007), 310-4.
121. Marucci A, Cozzolino F, Dimatteo C, Monti M, Pucci P, Trischitta V, Di Paola R. "Role of GALNT2 in the modulation of ENPP1 expression, and insulin signaling and action: GALNT2: a novel modulator of insulin signaling". *Biochim Biophys Acta* (2013), 1388-95.
122. GarziaL., Roma C., Tata N., Pagnozzi D., Pucci P., Zollo M. "H-prune-nm23-H1 protein complex and correlation to pathways in cancer metastasis. *Journal of Bioenergetics and Biomembranes* (2006), 205-213.
123. Piras, L., Avitabile, C., D'Andrea, L. D., Saviano, M., and Romanelli, A. "Detection of oligonucleotides by PNA-peptide conjugates recognizing the biarsenical fluorescein complex FIAsh-EDT2." *Biochem Bioph Res Co* 493(2017), 126-131.
124. Waterhouse, A., Bertoni, M., Bienert, S., Studer, G., Tauriello, G., Gumienny, R., Heer, F. T., de Beer, T. A. P., Rempfer, C., Bordoli, L., Lepore, R., and Schwede, T. "SWISS-MODEL: homology modelling of protein structures and complexes". *Nucleic Acids Res* 46(2018), W296-W303.
125. Oliva, M. A., Trambaiolo, D., and Lowe, J. "Structural insights into the conformational variability of FtsZ." *J Mol Biol* 373(2007), 1229-1242.

126. Avitabile, C., D'Andrea, L. D., Saviano, M., and Romanelli, A. "Determination of the secondary structure of peptides in the presence of Gram positive bacterium *S. epidermidis* cells" *Rsc Adv* 6 (2016), 51407-51410.
127. Shen, Y. M., Maupetit, J., Derreumaux, P., and Tuffery, P. J "Improved PEP-FOLD Approach for Peptide and Miniprotein Structure Prediction" *Chem Theory Comput* 10(2014), 4745-4758.
128. Gabb, H. A., Jackson, R. M., and Sternberg, M. J. J "Modelling protein docking using shape complementarity, electrostatics and biochemical information". *Mol Biol* 272 (1997), 106-120.
129. Raveh, B., London, N., and Schueler-Furman, O. "Sub-angstrom modeling of complexes between flexible peptides and globular proteins." *Proteins* 78 (2010), 2029-2040.
130. Lee, H., Heo, L., Lee, M. S., and Seok, C. "Protein-peptide docking tool based on interaction similarity and energy optimization" *Nucleic Acids Res* 43 (2015), W431-435.
131. Torchala, M., Moal, I. H., Chaleil, R. A., Fernandez-Recio, J., and Bates, P. A. "SwarmDock: a server for flexible protein-protein docking." *Bioinformatics* 29 (2013), 807-809.
132. Emsley, P., Lohkamp, B., Scott, W. G., and Cowtan, K. "Features and development of Coot." *Acta Crystallogr D Biol Crystallogr* 66 (2010), 486-501.

133. Rivas, G., Lopez, A., Mingorance, J., Ferrandiz, M. J., Zorrilla, S., Minton, A. P., Vicente, M., and Andreu, J. M. "Magnesium-induced linear self-association of the FtsZ bacterial cell division protein monomer. The primary steps for FtsZ assembly." *J Biol Chem* 275(2000), 11740-11749.
134. Della Vecchia, N. F., Luchini, A., Napolitano, A., D'Errico, G., Vitiello, G., Szekely, N., d'Ischia, M., and Paduano, L. "Tris buffer modulates polydopamine growth, aggregation, and paramagnetic properties." *Langmuir* 30(2014), 9811-9818.
135. Luchini, A., Irace, C., Santamaria, R., Montesarchio, D., Heenan, R. K., Szekely, N., Flori, A., Menichetti, L., and Paduano, L. "Phosphocholine-decorated superparamagnetic iron oxide nanoparticles: defining the structure and probing in vivo applications" *Nanoscale* 8 (2016), 10078-10086.
136. Wakamatsu K, Takeda A, Tachi T, Matsuzaki K. "Dimer structure of magainin 2 bound to phospholipid vesicles". *Biopolymers* 64 (2002), 314-327.
137. Robinson J.A. "Folded Synthetic Peptides and Other Molecules Targeting Outer Membrane Protein Complexes in Gram-Negative Bacteria" *Front Chem* 7 (2019).
138. Roy, A., Kucukural, A., & Zhang, Y. "I-TASSER: a unified platform for automated protein structure and function prediction". *Nature protocols*, 5(2010), 725.
139. Yang, J., Yan, R., Roy, A., Xu, D., Poisson, J., & Zhang, Y. "The I-TASSER Suite: protein structure and function prediction". *Nature methods*, 12(2015), 7.
140. Yang, J., & Zhang, Y.. "I-TASSER server: new development for protein structure and function predictions". *Nucleic acids research*, 43(2015), 174-W181.

141. Schneidman-Duhovny, D., Inbar, Y., Nussinov, R., & Wolfson, H. J. “PatchDock and SymmDock: servers for rigid and symmetric docking”. *Nucleic acids research*, 33(suppl_2) . (2005), W363-W367.
142. Mashiach, E., Schneidman-Duhovny, D., Andrusier, N., Nussinov, R., & Wolfson, H. J. “FireDock: a web server for fast interaction refinement in molecular docking”. *Nucleic acids research*, 36(suppl_2) (2008), 229-W232.
143. Laskowski, R. A. PDBsum new things. *Nucleic acids research*, 37(suppl_1) (2008), 355-359.
144. De Beer, T. A., Berka, K., Thornton, J. M., & Laskowski, R. A.. PDBsum additions. *Nucleic acids research*, 42(D1) (2013), 292-296.
145. Laskowski, R. A. PDBsum: summaries and analyses of PDB structures. *Nucleic acids research*, 29(2001), 221-222.
146. Vangone, A., & Bonvin, A. M. (2015). Contacts-based prediction of binding affinity in protein–protein complexes. *Elife*, 4, e07454.
147. Xue, L. C., Rodrigues, J. P., Kastitis, P. L., Bonvin, A. M., & Vangone, A.. PRODIGY: a web server for predicting the binding affinity of protein–protein complexes. *Bioinformatics*, 32(2016), 3676-3678.
148. Pettersen, E. F., Goddard, T. D., Huang, C. C., Couch, G. S., Greenblatt, D. M., Meng, E. C., & Ferrin, T. E. UCSF Chimera—a visualization system for exploratory research and analysis. *Journal of computational chemistry*, 25(2004), 1605-1612.

149. Suo B, Yang H, Wang Y, Lv H, Li Z, Xu C, Ai Z. “Comparative Proteomic and Morphological Change Analyses of *Staphylococcus aureus* During Resuscitation From Prolonged Freezing”. *Front Microbiol.* (2018).
150. Ambrose L. Cheung, Koren A. Nishina, Maria Pilar Trotonda Pous, and Sandeep Tamber. “The SarA protein family of *Staphylococcus aureus*”. *Int J Biochem Cell Biol* 40. 2008; 355–361.
151. Bronner S., Monteil H, Prévost G. “Regulation of virulence determinants in *Staphylococcus aureus*: complexity and applications “. *FEMS Microbiology Reviews*, Vol 28 (200), 183–200.
152. Askarian F, Ajayi C, Hanssen AM, van Sorge NM, Pettersen I, Diep DB, Sollid JU, Johannessen M. “The interaction between *Staphylococcus aureus* SdrD and desmoglein 1 is important for adhesion to host cells”. *Sci Rep.* (2016) 22134.